U.S. Department
of Transportation
**Federal Railroad
Administration**

# Evaluation of Damaged Tank Car Structural Integrity

Office of Research and
Development
Washington, D.C. 20590

Walter G. Reuter
Joey D. Mudlin
Bob L. Harris
Fahmy M. Haggag
William L. Server
Jonathan S. Epstein

EG&G Idaho, Inc.
P.O. Box 1625
Idaho Falls, Idaho 83415

DOT/FRA/ORD-88/02

January 1988
Final Report

NOTICE

This document is disseminated under the sponsorship of the Department of Transportation in the interest of information exchange. The United States Government assumes no liability for its contents or use thereof.

NOTICE

The United States Government does not endorse products or manufacturers. Trade or manufacturers' names appear herein solely because they are considered essential to the object of this report.

Technical Report Documentation Page

| 1. Report No. | 2. Government Accession No. | 3. Recipient's Catalog No. |
|---|---|---|
| DOT/FRA/ORD-88/02 | | |

| 4. Title and Subtitle | 5. Report Date |
|---|---|
| Evaluation of Damaged Tank Car Structural Integrity | January 1988 |
| | 6. Performing Organization Code |
| 7. Author(s) | 8. Performing Organization Report No. |
| W. G. Reuter, J. D. Mudlin, B. L. Harris, et al. | EGG-MS-7570 |
| 9. Performing Organization Name and Address | 10. Work Unit No. (TRAIS) |
| EG&G Idaho, Incorporated<br>P. O. Box 1625<br>Idaho Falls, ID 83415 | 11. Contract or Grant No.<br>DTFR53-84-X-00026 |
| | 13. Type of Report and Period Covered<br>August 1984-December 1986<br>Technical |
| 12. Sponsoring Agency Name and Address<br>U.S. Department of Transportation<br>Federal Railroad Administration<br>Office of Research and Development<br>Washington, D.C. 20590 | 14. Sponsoring Agency Code<br>RRS-32 |

15. Supplementary Notes

16. Abstract

The Federal Railroad Administration of the U.S. Department of Transportation is concerned with the safety of the public and the crews clearing wrecked tank cars containing hazardous materials. To assess the safety of moving a damaged tank car, it is necessary to know the sizes and shapes of cracks, the stresses associated with moving the tank car, and the fracture toughness of the material used to fabricate the tank car. This report provides the results and recommendations for the following research related to the above needs: (1) examination of nondestructive evaluation techniques and measurements of the mechanical properties of deformed steel plate; (2) evaluation of computer codes to identify those capable of performing a large displacement inelastic analysis; (3) two 1/5-scale-model tank cars, representing damaged tank cars, were hydroburst to failure; and (4) preliminary tests were conducted using moire interferometry for determining residual stresses of rail components.

| 17. Key Words | 18. Distribution Statement |
|---|---|
| Tank Car<br>Structural Integrity<br>Hazardous Material | National Technical Information Service<br>Springfield, VA 22161 |

| 19. Security Classif. (of this report) | 20. Security Classif. (of this page) | 21. No. of Pages | 22. Price |
|---|---|---|---|
| Unclassified | Unclassified | 115 | |

Form DOT F 1700.7 (8-72) Reproduction of completed page authorized

# METRIC CONVERSION FACTORS

## Approximate Conversions to Metric Measures

| Symbol | When You Know | Multiply by | To Find | Symbol |
|---|---|---|---|---|
| **LENGTH** | | | | |
| in | inches | *2.5 | centimeters | cm |
| ft | feet | 30 | centimeters | cm |
| yd | yards | 0.9 | meters | m |
| mi | miles | 1.6 | kilometers | km |
| **AREA** | | | | |
| $in^2$ | square inches | 6.5 | square centimeters | $cm^2$ |
| $ft^2$ | square feet | 0.09 | square meters | $m^2$ |
| $yd^2$ | square yards | 0.8 | square meters | $m^2$ |
| $mi^2$ | square miles | 2.6 | square kilometers | $km^2$ |
| | acres | 0.4 | hectares | ha |
| **MASS (weight)** | | | | |
| oz | ounces | 28 | grams | g |
| lb | pounds | 0.45 | kilograms | kg |
| | short tons (2000 lb) | 0.9 | tonnes | t |
| **VOLUME** | | | | |
| tsp | teaspoons | 5 | milliliters | ml |
| Tbsp | tablespoons | 15 | milliliters | ml |
| fl oz | fluid ounces | 30 | milliliters | ml |
| c | cups | 0.24 | liters | l |
| pt | pints | 0.47 | liters | l |
| qt | quarts | 0.95 | liters | l |
| gal | gallons | 3.8 | liters | l |
| $ft^3$ | cubic feet | 0.03 | cubic meters | $m^3$ |
| $yd^3$ | cubic yards | 0.76 | cubic meters | $m^3$ |
| **TEMPERATURE (exact)** | | | | |
| °F | Fahrenheit temperature | 5/9 (after subtracting 32) | Celsius temperature | °C |

*1 in. = 2.54 cm (exactly). For other exact conversions and more detail tables see NBS Misc. Publ. 286, Units of Weight and Measures. Price $2.25 SD Catalog No. C13 10 286.

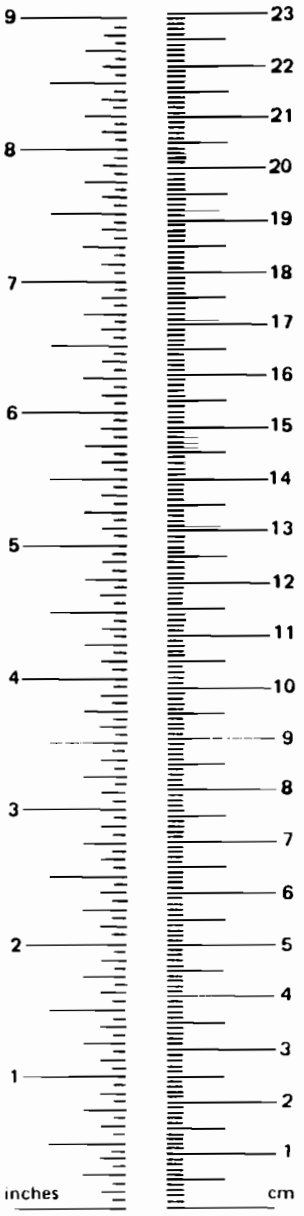


## Approximate Conversions from Metric Measures

| Symbol | When You Know | Multiply by | To Find | Symbol |
|---|---|---|---|---|
| **LENGTH** | | | | |
| mm | millimeters | 0.04 | inches | in |
| cm | centimeters | 0.4 | inches | in |
| m | meters | 3.3 | feet | ft |
| m | meters | 1.1 | yards | yd |
| km | kilometers | 0.6 | miles | mi |
| **AREA** | | | | |
| $cm^2$ | square centimeters | 0.16 | square inches | $in^2$ |
| $m^2$ | square meters | 1.2 | square yards | $yd^2$ |
| $km^2$ | square kilometers | 0.4 | square miles | $mi^2$ |
| ha | hectares (10,000 $m^2$) | 2.5 | acres | |
| **MASS (weight)** | | | | |
| g | grams | 0.035 | ounces | oz |
| kg | kilograms | 2.2 | pounds | lb |
| t | tonnes (1000 kg) | 1.1 | short tons | |
| **VOLUME** | | | | |
| ml | milliliters | 0.03 | fluid ounces | fl oz |
| l | liters | 2.1 | pints | pt |
| l | liters | 1.06 | quarts | qt |
| l | liters | 0.26 | gallons | gal |
| $m^3$ | cubic meters | 36 | cubic feet | $ft^3$ |
| $m^3$ | cubic meters | 1.3 | cubic yards | $yd^3$ |
| **TEMPERATURE (exact)** | | | | |
| °C | Celsius temperature | 9/5 (then add 32) | Fahrenheit temperature | °F |

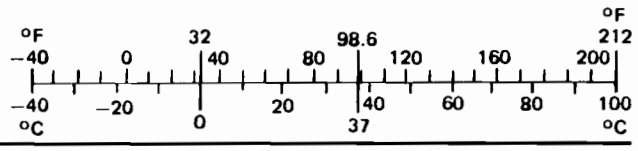

CONTENTS

FIGURES

TABLES

# EXECUTIVE SUMMARY

The Federal Railroad Administration (FRA) of the U.S. Department of Transportation is concerned with the safety of the public and the crews clearing wrecked tank cars containing hazardous materials. To assess the safety of moving a tank car, it is necessary to nondestructively detect, locate, and size cracks, as well as measure the wall thickness, to determine the extent of damage. It is also necessary to be able to estimate the mechanical properties, especially fracture toughness, in the damaged region and to estimate the stress conditions for the damaged region when the tank car is being put back on to the track. The combination of applied stress, crack size, and fracture toughness are the primary parameters needed to predict safety.

The Idaho National Engineering Laboratory (INEL) was initially asked to perform a preliminary evaluation[1] of the technology required to assess the safety of moving a damaged tank car. The recommendations from that evaluation are summarized in Table 1. FRA subsequently contracted with INEL to perform the four tasks described in this report: Task 1, NDE/Fracture Correlation Study (of damaged material); Task 2, Structural Mechanics Analysis (identifies potential codes for predicting stresses); Task 3, Hydrostatic Burst Testing of Damaged Tanks (to simulate behavior of a damaged tank car); and Task 4, Application of Moire Interferometry (a tool for measuring displacements).

This Executive Summary summarizes the results of the four tasks completed and recommends future work.

TABLE 1. RECOMMENDATIONS FROM PRELIMINARY EVALUATION

1. Develop NDE techniques to (a) measure the extent of identations in the damaged tank car which may be related to wall thinning, (b) measure the wall thickness, and (c) locate and characterize cracks.

2. Develop a data base relating the change in tensile strength and fracture toughness with the percent reduction in wall thickness. Develop techniques to predict the stress associated with the deformation and contents of the car. Develop techniques to predict the stresses associated with moving a damaged tank car. (These latter results could be used to specify the method for moving the damaged tank car that would develop the lowest stresses in the damaged region.)

   The materials accepted for fabricating tank cars consist of the following:[2]

   ASTM A515-70, Grades 55, 60, 65 and 70
   ASTM A285-70a, Grades A, B*, and C*
   ASTM A516-70a, Grades 55*, 60*, 65*, and 70
   ASTM A537-701 Grade A*
   ASTM 302-70a, Grade B
   AAR TC 128-70 Grades A and B

   Of these materials, those with an asterisk are included in Table 16 of ASTM A-20, Reference 3, which identifies the minimum temperature at which a minimum Charpy V-notch impact (CVN) energy has to be obtained. These requirements are not included in Reference 2 but since they exist in Reference 3 there should be substantial data available. One problem will be to estimate $K_{Ic}$ based on CVN data.

3. Develop a correlation between the reduction in wall thickness, with attendant decrease in fracture toughness, and the extent of cracking associated with real accident conditions.

4. Develop acoustic emission systems to locate the source of cracking if any crack growth occurs. (This would be a real-time monitoring system that is attached to the damaged region until the car has been moved to a safe place and unloaded. It is necessary to develop techniques for separating acoustic emission generated by a growing crack from noise associated with moving the tank car.)

5. Conduct tests of subscale and full-scale tank cars to verify predictive models. Instrument a car and conduct a test simulating the damage associated with a typical accident, then move the car by different methods and measure the stresses for comparison with estimated values. (Both of the above tests would be used to verify the stress predictions for "typical" accidents.)

6. Conduct tests to quantify the conservatism of the total approach.

## Summary of Work Completed

### Task 1, NDE/Fracture Correlation Study

Task 1 consisted of evaluating nondestructive examination (NDE) techniques and measuring mechanical properties of deformed steel plates. The purpose of this task was to establish a data base for crack detection and characterization and measures of deformation, and to correlate these with metallurgical measures of damage and remaining structural strength of deformed specimens that represented damaged areas on railroad tank cars. The evaluations used plates deformed by the Ballistic Research Laboratory (BRL) as well as a plate removed from a damaged railroad tank car by the National Bureau of Standards (NBS). Sixty-eight flat plate specimens, all from a single heat of ASTM A515 Grade 70 were dynamically deformed at BRL using several tup and die combinations to obtain different damage geometries.

Because the plate specimens were so badly corroded, it was necessary to clean the surfaces by lightly glass-bead blasting. Ultrasonic testing (UT) techniques were then successfully used to measure the wall thickness and to detect and characterize cracks (length and type of defect, but not depth).

The mechanical property tests showed the changes in yield strength, ultimate tensile strength, plane strain fracture toughness ($K_{Ic}$), and the tearing modulus as a function of prior deformation.

The National Bureau of Standards has studied damaged tanks cars for FRA, and these reports were examined by INEL both to obtain information pertinent to determining the safety of moving a damaged railroad tank car and to select a representative plate from an actual tank car for NDE studies and measurements of residual mechanical properties. The review of the reports suggested that many of the failures occurred by brittle fracture, but there was insufficient information to distinguish between cleavage or low upper shelf fracture toughness and/or low tearing modulus. The NDE examination and measurement of mechanical properties on the NBS plate showed results very similar to those obtained with the plates deformed by BRL.

The tests on the sixty-eight BRL plates and one NBS plate showed the adequacy of UT techniques for measuring wall thickness and for detecting and characterizing defects in a damaged railroad tank car. Tests of deformed material showed that yield strength increased and both fracture toughness and the tearing modulus decreased with increased deformation. These results provide the baseline needed to understand the problem, but are insufficient to predict the behavior of other materials damaged in accidents because of the substantial material-to-material differences.

Task 2, Structural Mechanics

A special purpose, large displacement, large strain computer code is required to perform the inelastic stress analysis of a damaged tank car since a large amount of permanent deformation of the tank may occur during an accident. It is desirable to model the residual stresses resulting from an accident and then predict the stresses resulting from moving the tank car back into position. A survey of computer codes was performed to identify those capable of performing a large displacement inelastic analysis of a 3-dimensional problem. Of 800 codes evaluated, six were identified as having a high probability of successfully performing the tank car analysis. An evaluation of the economies associated with each code was conducted. Two large deflection sample problems were identified and run on the 1978 version of the computer code ADINA. The problem simulating the ends of the tank car was run successfully; the second problem, which simulated the cylindrical portion of the car, was not as successful and discussions with the authors of ADINA could not identify any reason for this. The authors of ADINA felt that the 1984 version should provide an accurate solution to the second problem.

Another problem, a cylinder with opposing concentrated loads, was solved by an outside vendor using ABAQUS. This problem simulates a point load on a cylindrical tank, which is directly applicable to the tank car analysis. Three cases were run consisting of (1) an elastic analysis, (2) an inelastic analysis using small displacement theory, and (3) an inelastic analysis using large displacement theory. There is no known solution to this problem, and the only ways to verify the results of the ABAQUS solution

are to (1) use other codes, but if different solutions are obtained there is no way to identify which solution is correct; (2) perform experiments; and (3) continue the search for another problem with a verified solution.

It was concluded that the methodology evaluated could provide a catalog of solutions of the stresses as a function of damage configuration, but it is necessary to verify the adequacy of the solutions.

Task 3, Hydrostatic Burst Testing of Damaged Tanks

Twelve 1/5-scale-model tank cars were impacted by BRL to simulate damage done to an actual tank car during a derailment. The damage in the tanks was confined to the heads, which had dents of varying severity, and in some cases the damaged end had been penetrated. Visual, liquid penetrant, and ultrasonic examinations were conducted on both surfaces of the damaged head to determine the extent of damage. On those heads that had not been penetrated, no surface cracks were found. The amount of wall thinning was less than 5% of the wall thickness.

At least one end of each tank had been penetrated; therefore, it was necessary to remove the penetrated ends and weld unpenetrated ends together to form a new tank. There were sufficient unpenetrated ends to fabricate four tanks for the burst tests. The damaged area of a tank was instrumented with strain gages and acoustic emission sensors. The latter were used to detect the location of crack growth. A pressure transducer was used to monitor the pressure as it was applied during the burst tests.

Two tanks were tested. Both tanks failed in regions other than the damaged area or the new weldments. Because of this, and because the wall thicknesses were insufficient to provide the behavior simulating an actual damaged railroad tank car, only the two tanks were tested. The walls of the scale models tested acted like a membrane, there was no appreciable bending stress because of the thin wall, which is not represenative of an actual railroad tank car. Cracking was detected by the acoustic emission sensors, but the source was not located since the failure occurred outside the area instrumented by the four sensors.

## Task 4, Application of Moire Interferometry

Moire interferometry was used as a novel alternative method for determining residual stresses of rail components, such as wheels and rails, subject to time elapsed wear. Unlike traditional strain gage measuring technologies which are by nature discrete and average over their gage length, moire interferometry yields full-field in-plane displacement on the free surface of the specimen. The sensitivity to in-plane displacement in this study was approximately 33 $\mu$m; the in-plane displacement sensitivity can be as great as 0.2 $\mu$m if desired. The 33 $\mu$m sensitivity was chosen because a large amount of residual displacement was expected from sectioning the wheel components (roughly 5.1 mm closure after a saw blade cut on a 838 mm diameter wheel). Moire interferometry (diffraction) gratings were applied to a test wheel at the FRA Transportation Test Center in Pueblo, CO. The grating was protected and the wheel was sectioned. The moire gratings were put on the 0 degree and 90 degree portion of the ring. The sectioned pieces were then sent back to the INEL where the moire grating could be interpreted.

Of the three displacement components for the 0 and 90 degree sectioned pieces, only the hoop strain was determined accurately. But, this one component illustrated the advantages of obtaining a full-field displacement field, using moire interferometry, as opposed to the local strain measurement from a strain gage.

Moire interferometry could be useful in providing experimental data for stressed and/or damaged railway components for use in evaluating the adequacy of computer codes. In addition, the technique has been used, at the INEL, to obtain experimental data under dynamic loading. This technique could be used to obtain experimental data of the displacement fields that occur during an accident.

## Present Status and Recommendations

Knowledge is required in three areas before a useful prediction of structural integrity may be made. These areas, the nature of the defect

(crack size and wall thinning), fracture mechanics (analytical models and data), and applied stress, are outlined in the Recommendations Section. The research on characterization of defects has shown the capability of ultrasonic (UT) techniques to detect, locate, and size defects on the back surface of a flat plate and to measure wall thickness. It is recommended that preliminary evaluations of existing UT techniques be conducted to determine their ability to measure thickness and detect and characterize defects in actual damaged tank cars and in plates containing insulation. At the present time, it is evident that acoustic emission techniques could be used to increase the safety of working around damaged tank cars. Therefore, it is recommended that the technique be adapted to the problems specific to damaged railroad tank cars.

Fracture mechanics concepts are presently available for predicting structural integrity if it is assumed that failure is controlled by the fracture toughness at the lower shelf. It is recommended that predictions of the safety of moving a damaged railroad tank car use $K_{Ic}$ associated with the lower shelf. Once it has been identified if cleavage and/or low fracture toughness plus a low tearing modulus is primarily responsible for past failures, it will then be possible to identify criteria that may be used for procurement of materials with increased resistance to failure. These criteria could reduce failures that occur during an accident as well as failures that occur when damaged railroad tank cars are moved.

The stress analysis research has identified potential codes capable of predicting the stresses associated with large displacement. Because of the difficulties in verifying the accuracy of these solutions and the cost of using these codes, it is recommended that a 3-D elastic analysis be conducted because of the substantial cost savings that would occur if the technique is shown to be adequate. If shown to be adequate, the elastic solutions are cheaper and faster. But, if shown to be inadequate, the results will still provide useful qualitative information for efficient utilization of the large-deformation models. Completion of 3-D elastic analyses of typical accident configurations should include preliminary verification by experiments which simulate damage in heads, cylinders, and

junctions, as well as large deflection analyses. These results will provide estimates of the sensitivity of stress, in a damage zone, as a function of lifting technique. (These results could be used to determine if there is a need for large-scale deflection analysis.)

It will be necessary to conduct tests of full size and scaled versions of tank cars to verify predictive models. For future tests, if scaled versions of tank cars are used, it is recommended that the wall thickness not be reduced. This change in thickness relative to tank geometry can be treated by analytical methods. Also, more areas of the tanks should be instrumented, including the use of additional strain gauges and acoustic emission detectors. Additional information that would be useful in performing future burst tests includes a complete design description of the vessels, fabrication history, and deformation procedures along with the supporting test results.

It has been shown that moire interferometry techniques will provide considerably more displacement data with increased accuracy than existing techniques. It is recommended that tests be conducted in a laboratory environment with emphasis on the information being produced. Controlled specimens with known strain and deformations should be used to exactly calibrate the moire interferometry results. The data in this study reflected a complicated residual stress state; it would be helpful to have comparable data from a simple stress state to identify any problems encountered in interpreting the moire interferometry results.

# EVALUATION OF DAMAGED TANK CAR STRUCTURAL INTEGRITY

## 1. NDE/FRACTURE CORRELATION STUDY

### 1.1 Introduction

This task consisted of an evaluation of NDE techniques and measurements of mechanical properties of the deformed material. The evaluations were made on plates deformed by the Ballistic Research Laboratory (BRL) under a previous FRA program. The deformation consisted of creating controlled damage to flat plates fabricated from ASTM A515 Grade 70, one of the materials used to fabricate railroad tank cars.

A piece of steel obtained from an actual damaged tank car was also included in the evaluation to correlate the adequacy of data developed from the BRL plates with the real problem of damaged tank cars. The National Bureau of Standards (NBS) performed analyses of damaged tank cars for FRA and stored the pieces of the damaged railroad tank cars.

The following discussion is separated into two sections, with the first describing the results obtained from the BRL plates while the second describes the results for the NBS plates.

### 1.2 FRA/BRL Plates

Sixty-eight flat plate specimens fabricated from ASTM A515 Grade 70 were deformed and furnished to INEL for nondestructive and fracture mechanics evaluations. These plates had been impacted by the Ballistic Research Laboratory (BRL) for the purpose of achieving dents, under controlled conditions from a single heat and plate of material, which could be used to verify that available NDE techniques could detect cracks and other types of flaws in specimens that represented areas of tank cars damaged in accidents. The specimens ranged from those which were slightly deformed to those which had fractures and through-thickness tears.

The ASTM A515 Grade 70 plates were impacted using several tup and die combinations to obtain the different damage geometries. Each plate was placed on a die and a drop hammer was used to drive the tup into the plate. The plates were 1.59 cm (5/8 inch) thick and were 61 cm (24 inches) square. Four tup geometries were used to impact the plates. Three tups were hemispherical in shape and were 5.1 cm (2.0 inches), 9.6 cm (3.75 inches), and 14 cm (5.5 inches) in diameter, and one was flat in shape and was 14 cm (5.5 inches) in diameter. Four different die diameters were used: 15.2 cm (6.0 inches), 21 cm (8.25 inches), 28 cm (11.0 inches), and 35 cm (13.75 inches) in diameter.

### 1.2.1 Nondestructive Evaluation (NDE)

Nondestructive evaluation was used to establish a data base for crack detection, crack characterization, and measures of deformation, and to assess the ability to correlate these data with metallurgical measures of damage and remaining structural strength of the deformed specimens.

The surfaces of the sixty-eight plate specimens were badly corroded from exposure to the weather. Because the presence of rust and scale prohibits the use of some NDE techniques (e.g. liquid penetrant and ultrasonic examinations), it was necessary to remove the corrosion products from the plate surfaces. Several methods were investigated for removal of rust and scale from the damaged BRL plates. Chemical processes were ruled out for fear that residue from the cleaning process would affect the liquid penetrant surface examinations. Mechanical methods for removing the corrosion product using steel wool and wire brushes were tried but were ineffective. Experiments were performed with two other cleaning methods: sandblasting and lightly glass-bead blasting. While sandblasting actually damaged the material and closed cracks, glass-bead blasting caused no adverse effects. Since lightly glass-bead blasting the dented areas did not mask the surface cracks, the results of liquid penetrant examinations of the damaged area would be valid. Therefore, both surfaces (convex and concave) of the dented area of each plate were lightly glass-bead blasted to remove the rust and scale so that various NDE examinations could be performed.

A variety of nondestructive techniques was used, including mechanical measurement, visual inspection, liquid penetrant inspection, and various ultrasonic techniques, under conditions where each was appropriate.

Surface Inspection. Both surfaces (convex and concave) of the dent in each BRL plate were examined for surface cracks using a liquid penetrant. A Magnaflux Dual-Purpose Penetrant Test System was used for the examinations. This is a specialty penetrant system which combines the flaw detection capabilities of both the color contrast and fluorescent penetrant systems. This system gave the best resolution of the several penetrant systems tested. The liquid penetrant examination procedure used is included in Appendix A.

The plate specimens showed no signs of cracking on the concave sides of the dents except when tears completely penetrated the thickness. Approximately half of the plates had some surface cracking on the convex sides. The surface cracks were observed to occur parallel to the rolling direction of the steel. The surface crack indications were measured and documented with photographs. Measurements of the surface cracks (e.g. length of cracks, and number of surface cracks) were tabulated to see if there was a correlation between surface cracking and measurements of deformation such as depth of dent or percent reduction in thickness.

Dimensional Measurements. A Krautkramer-Branson Model CL204 ultrasonic thickness gauge was used with a contact, delay-line, 6.3 mm (0.25 inch) diameter, 15 MHz transducer to measure the thickness at one centimeter intervals across two directions of the deformed areas of the plates. Ultragel II was used for the transducer couplant. The UT unit was calibrated using a reference block made from a section of one of the plates. This contact ultrasonic testing unit was able to measure the thickness to within 0.13 mm (0.005 inches) on the cleaned surfaces (no significant rust or scale and no insulation). The accuracy of the ultrasonic testing unit was verified by use of thickness measurements made with micrometers.

Plots were prepared, for each plate, of thickness as a function of position across the dent, see Figure 1. From these plots, a calculation of

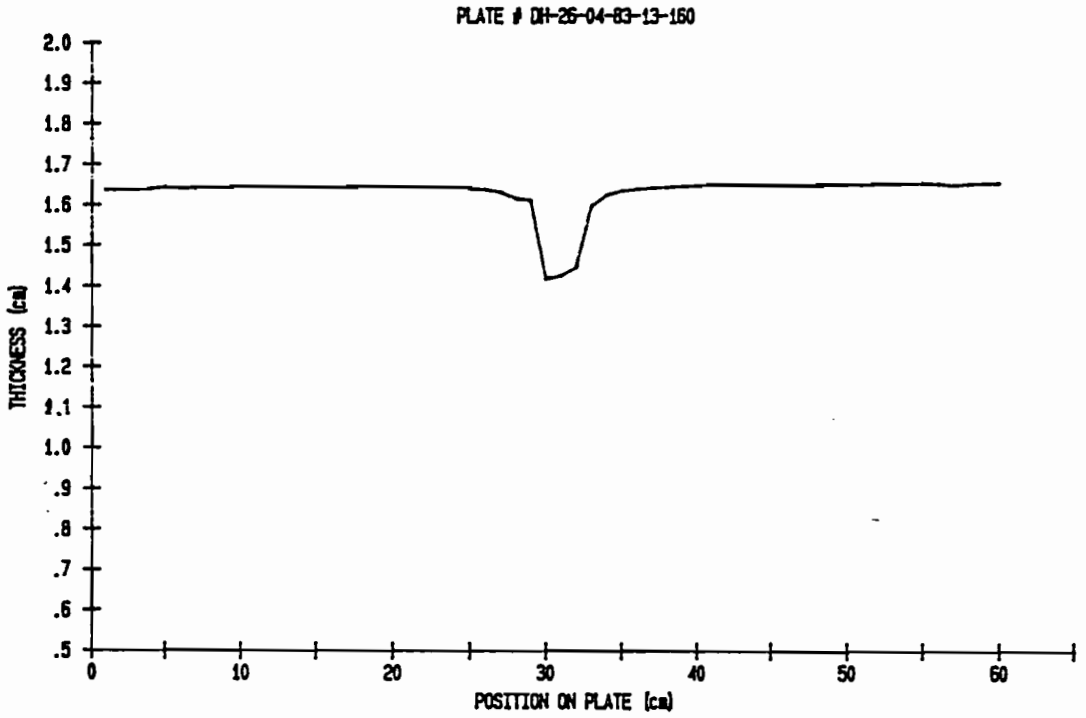


(a) Slightly damaged (dent depth of 2.78 cm).

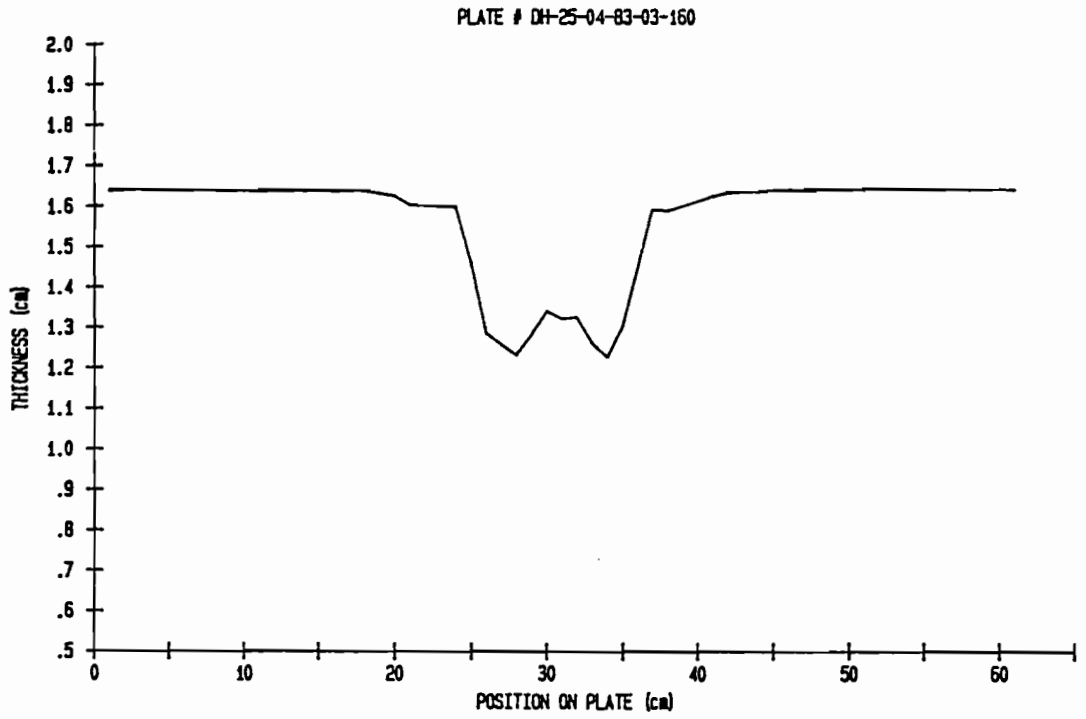


(b) Dent depth of 4.28 cm.

Figure 1. Typical measurement of thickness vs. position, obtained by use of ultrasonic thickness gauge, for 3 BRL plates.

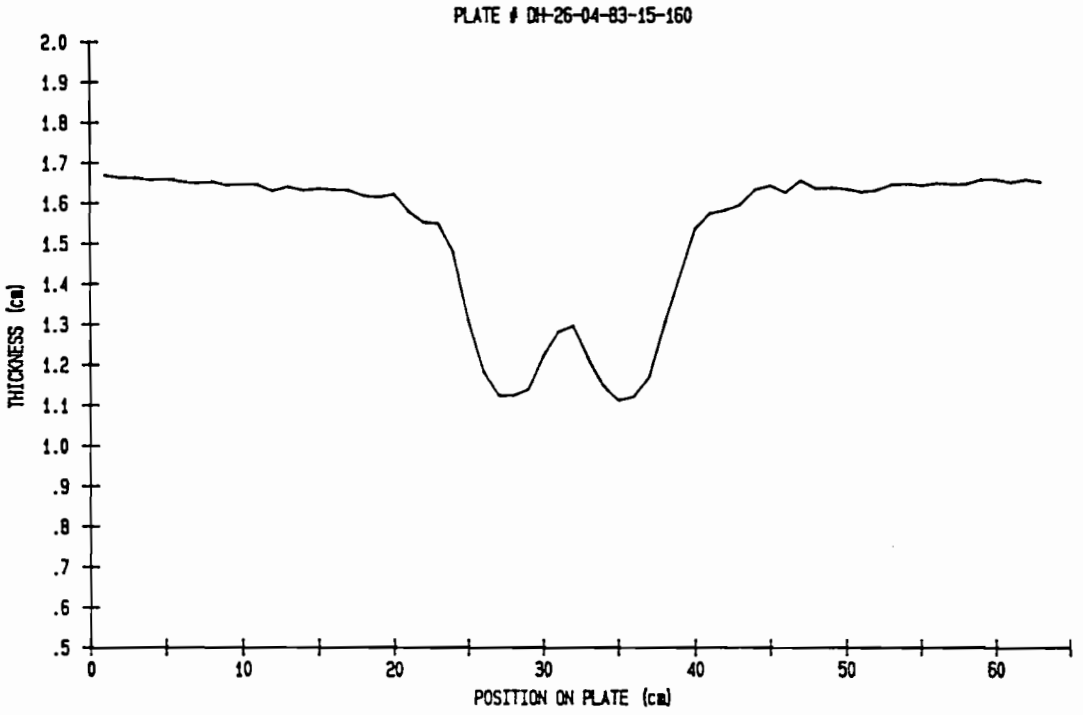


(c) Deeply dented (dent depth of 9.98 cm). The two lobes on this plot represent the areas of greatest thinning.

Figure 1. (continued).

percent reduction in thickness was made for each plate. These calculated values were then compared to the data obtained by the other NDE examinations and fracture mechanics evaluations to determine if correlations existed. The fractures and tears that were found visually and the surface cracks, found with liquid penetrant examinations, were observed to be located in the areas with the greatest degree of thinning. Reduction of plate thickness by as much as 37% was observed in some samples. Figure 1(c) shows an example of typical areas of greatest thinning, which consists of the two lobes on the thickness plot of the plate specimen. These areas of greatest thinning constitute the points where the residual strength is in question. As suggested in Figure 1(a) and (b), the greatest reduction in thickness did not occur at the maximum depths but along the sides where the tup and die interacted to create more of a shear stress than a bending stress. This part of the BRL tests is not expected to simulate the type of deformation generally encountered in damaged railroad tank cars.

Earlier it had been noted that all of the plates had been glass-bead blasted to remove rust and scale. This cleaning operation suggests that the accuracy of thickness measurements obtained with the UT thickness gauge is not totally representative of that obtainable from an actual damaged tank car; with scale and rust on the back surface of the plate, a decrease in the level of the UT signal was observed. The corrosion layer could cause an impedance mismatch and/or scattering of the signal which would reduce the amplitude of the return signal making it more difficult to detect. It is expected that the inner surface of tank cars would be relatively clean, although rust does occur. These tests show the applicability of using the UT thickness gage on damaged, railroad tank cars where the surfaces are relatively clean. No measurements were made of damaged components covered with insulation.

Various mechanical techniques were also used to measure deformation on the 68 specimens. These measurements were restricted to methods that could easily be used in the field and consisted of measuring the depth and radius of curvature of each deformed area. Figure 2 is an example of plots that were made previously[1] of dent depth versus position.

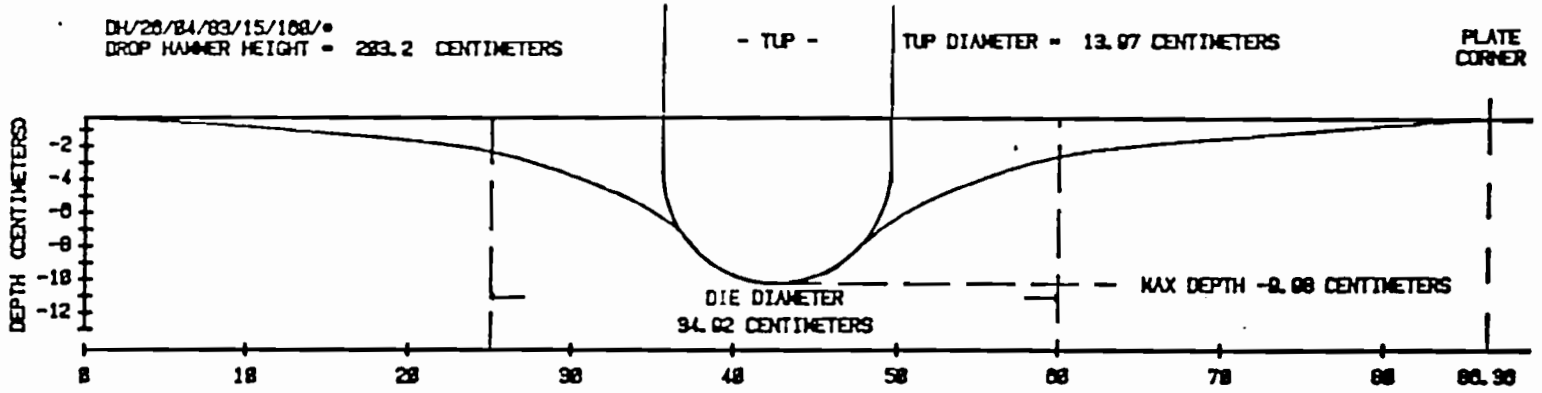


Figure 2. Dial micrometer measurement of dent depth.

UT Inspection for Internal and Surface Flaws. A computer-controlled ultrasonic imaging system was used for immersed testing of the plates to detect internal flaws and image the cracks. The immersion test was used since it is the most sensitive of ultrasonic techniques and if this was unsuccessful then the concept would not be pursued. Previous work[1] using immersed ultrasonics on a small number of plates indicated that it may be possible to locate areas of distressed metal, which were assumed to have the following properties: (1) be near known tears, (2) be in otherwise "sound metal" (middle third of thickness), (3) have relatively stronger echo signals at high frequencies than at low frequencies, and (4) have same orientation as known cracks (which indicate stress directions). It was theorized that the deformation, plastic flow, and/or formation of incipient shear bands would change the metallurgical characteristics and acoustic impedance in such a way that partial reflections could be obtained. During the previous study,[1] targets meeting the above postulated conditions were found in various areas evaluated in the plates. Small point-like targets, and some of slightly extended areas, were found in moderately deformed areas. Such targets were entirely absent in areas of little or no deformation, thus indicating that the targets in question are associated with high deformation.

An attempt was made to confirm the above interpretation of the observed targets as representing severe and moderate damage preceding the formation of a crack. Ultrasonic measurements were made by scanning with an immersed, 6.3 mm (0.25 in.) diameter, 45 degree shear-wave angle-beam, 10 MHz transducer in conjunction with computer-generated imaging for interpretation. No definite targets meeting the postulated conditions were found, therefore, a confirmation of the previous interpretations of observed targets could not be made.

Cracks that are open to the convex surface were imaged by the computer-controlled ultrasonic imaging system. The UT system was also mounted on the convex surface for ease in test setup. There is no difference in flaw detection and characterization capabilities between this system and the one in which the UT sensors would have been mounted on the concave surface. Figure 3 shows contour plots, generated by this ultrasonic

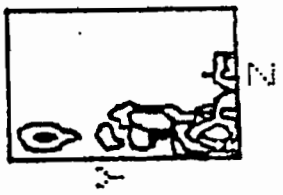


(b)

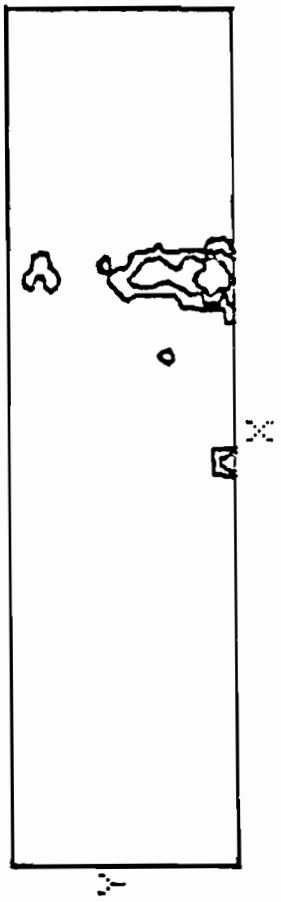


(a)

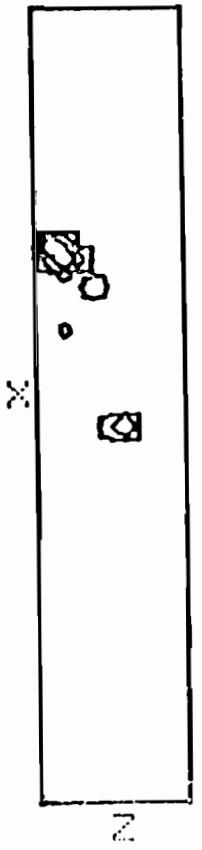


(c)

Figure 3. Typical contour plots generated by a computer-controlled ultrasonic imaging system showing images of cracks in the metal (three dimensions): (a) plan view, (b) cross-sectional view parallel to rolling direction, and (c) cross-sectional view transverse to rolling direction. (Plate #DH-25-04-83-18-160)

imaging system, of cracks that are open to the surface. The system produces maps of the part in which the contours are lines of equal reflected sonic intensity. These maps are read much like a standard topographic map; the patterns made by the reflected sound are the "hills" of the topographic map giving a sonic picture of the flaw. The x-y plane is the top view of a small area of a plate specimen. The x-z and the y-z planes are different views of the thickness of the same area. The above demonstrates that ultrasonic scanning systems can effectively image the cracks that are open to the convex inside surfaces of the damaged areas in derailed tank cars. These images suggest that measurements of the crack depth are possible but they are not accurate. The system used was able to characterize the signal to the extent it could provide a good estimate of crack length and could distinguish between a crack and an inclusion. The equipment/technique used were unable to provide an accurate estimate of crack depth. This can be done but requires development for the specific problem of a dented railroad tank car.

The UT technique was evaluated and found acceptable for detecting and characterizing defects in structures that simulated damaged railroad tank cars. The surface cleanliness required for application of this UT technique has not been quantified. A qualitative assessment may be made which identifies two boundaries, which are probably adjustable: the UT technique was not useful for the as-received surface but was used successfully after glass-bead blasting, and, as will be shown later, the UT system was used successfully on a piece removed from a damaged railroad tank car and stored by NBS. This illustrates that UT techniques has a good probability for being used successfully on railroad tank cars. But, these tests were conducted for assessment purposes and it would be necessary to develop the system for the specific surface conditions encountered in the field before a final UT system could be identified. Once the stress conditions are available, it will be possible to calculate the nominal critical crack sizes that will be used to specify detection capabilities required of the NDE system. Future activities will have to be concerned with the effects of insulation, which is often attached to tank cars.

### 1.2.2 Mechanical Property Testing

This section describes the results of an approach for evaluating changes in flow properties and fracture toughness of the ASTM A515 Grade 70 steel as a result of deformation. These data enable a correlation of the NDE results with the mechanical properties of the plate when subjected to representative equivalent damage conditions, thereby establishing a data base to permit an assessment of the residual mechanical properties. An adequate data base would provide information relative to safety considerations regarding movement of a damaged tank car when clearing an accident site.

Tensile Test Results. In order to verify the applicability of this technique to estimating the properties in localized areas of dented steel plates, specimens were obtained from unstrained plate as well as from plates that had been subjected to 4, 8 and 12% strain by uniaxial tension and by biaxial (dented area of a BRL plate) deformation conditions. Testing temperatures between -45 and +75°C were considered as representative of what may be encountered in the field. The results from testing conventional specimens were compared to the results obtained from miniature shear punch specimens.

Eight small and three large tensile specimens, for uniaxial tension tests, were machined from A515 Grade 70 steel plate (61 x 61 cm x 1.63 cm thick), with their axes aligned with the transverse direction of the plate. The small specimens were round (0.64 cm diameter, 2.54 cm gage section) while the large specimens were flat (1.63 cm thick, 7.7 cm wide, and 12.2 cm gage section). The small specimens were tested according to American Society for Testing and Materials (ASTM) Standard E-8-82 over the temperature range -45 to +75°C to determine the tensile properties of the material in the as-received condition. The three flat tensile specimens were strained at room temperature until their gage sections reached 4, 8, and 12% strains, respectively. After straining, smaller round tensile specimens, precracked three-point bend specimens, and 0.5 mm thick slabs (taken from the plane perpendicular to the longitudinal axis of the flat specimen) were machined from the prestrained reduced sections.

The tensile test results for the as-received material are shown in Figure 4. The flow stress curve shown in this figure is obtained by averaging the measured yield and ultimate stresses. The effect of prior strain on the yield stress, ultimate stress, and uniform elongation is shown in Figure 5. Both the yield and ultimate stresses increased with increased prior strain, although the increase for the latter was less pronounced. The uniform elongation decreased with increased prior strain.

Shear Punch Tests. Miniaturized shear punch specimens were utilized in this work because substantial mechanical property variations could possibly occur in localized areas in the dented plate. Obtaining conventional specimens from such areas is sometimes not possible and the results obtained from such specimens would likely give average properties over a larger region than the specific damaged area of interest. A shear punch test has been devised to meet the requirement for determining the mechanical properties of very small areas within a sample. The miniaturized shear punch test was originally developed to extract strength and ductility information from very small sheet samples, and punches as small as 1 mm in diameter have been used successfully. This test is similar to a common blanking operation used during sheet metal fabrication. By performing the punching operation with an instrumented load frame, the punch load may be monitored as a function of displacement using a load cell. The punching operation is performed on a clamped sheet as illustrated in Figure 6. Additional detail on the characteristics of this technique may be found in Reference 4 where it has found application in the nuclear industry. The punch diameter used in these shear punch tests was 3 mm. Shear punch tests were conducted on 0.5 mm thick slabs in the as-received (i.e. prior strain of 0%), 4, 8, and 12% prestrained conditions.

Shear punch test results on the as-received material with punch locations near the plate middle indicated good agreement with tensile test data for the yield and ultimate stresses, as shown in Figure 7. However, shear punch data obtained on plate surface material showed a difference in tensile results. By performing transverse punching sequences, the through-thickness variation in properties was mapped for the as-received and prior-strained conditions. Figure 8 is a plot of yield stress determined

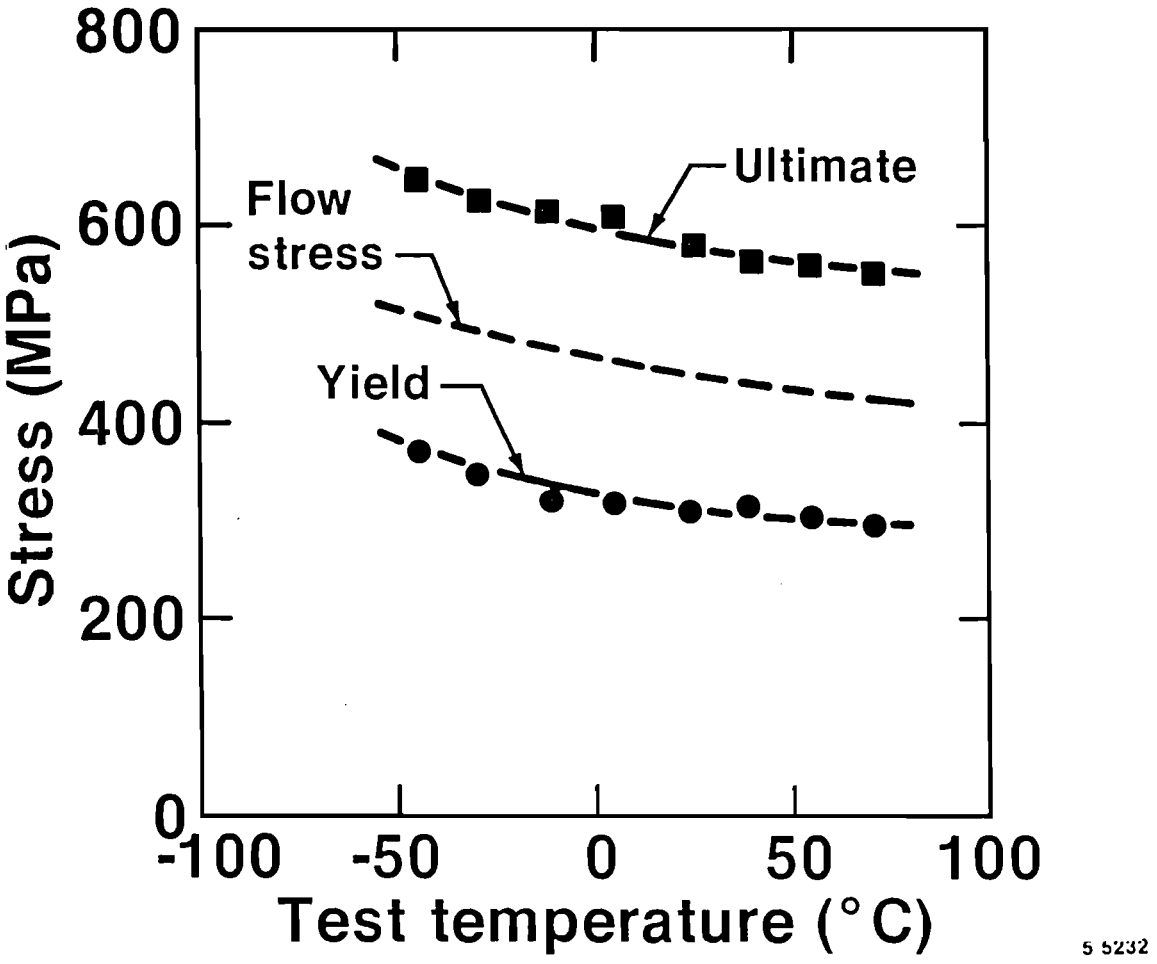


Figure 4. Uniaxial tensile stress vs. test temperature for A515 steel.

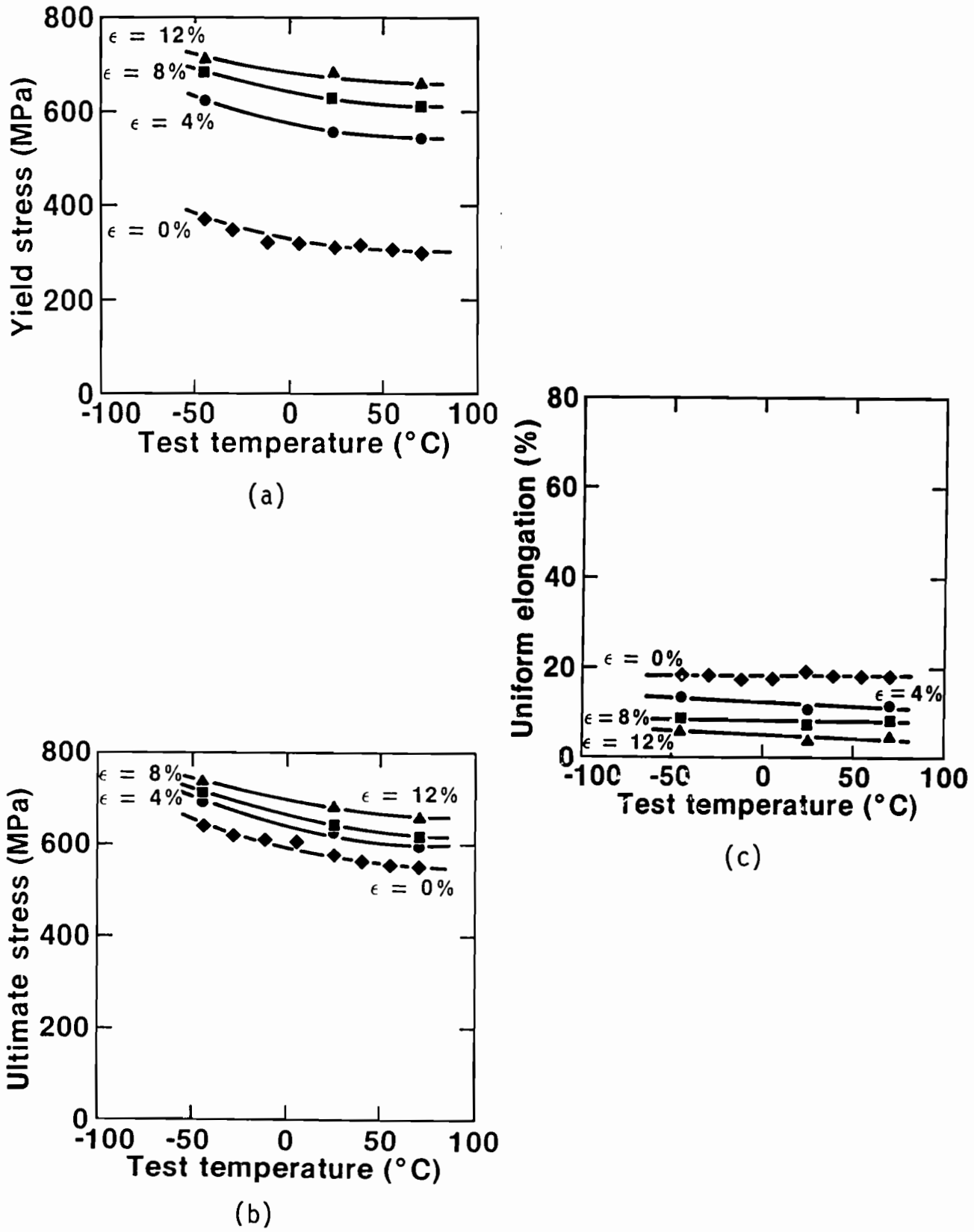


Figure 5. Effect of prior strain on uniaxial tensile properties of A515 steel: (a) yield stress, (b) ultimate tensile stength, and (c) uniform elongation.

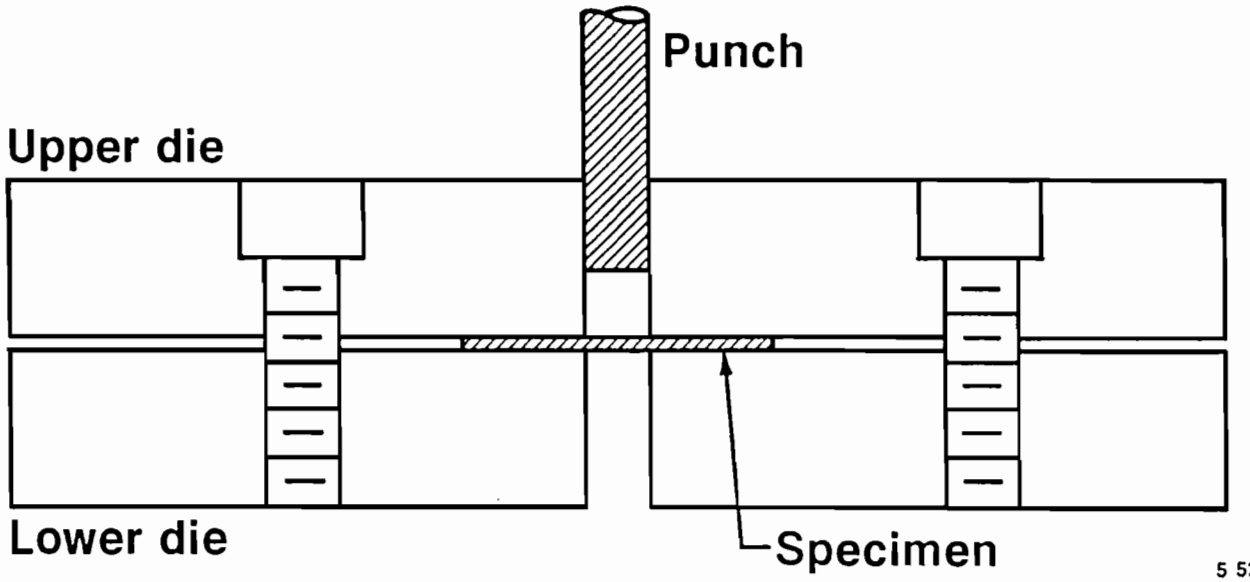


Figure 6. Schematic illustration of the shear punch apparatus.

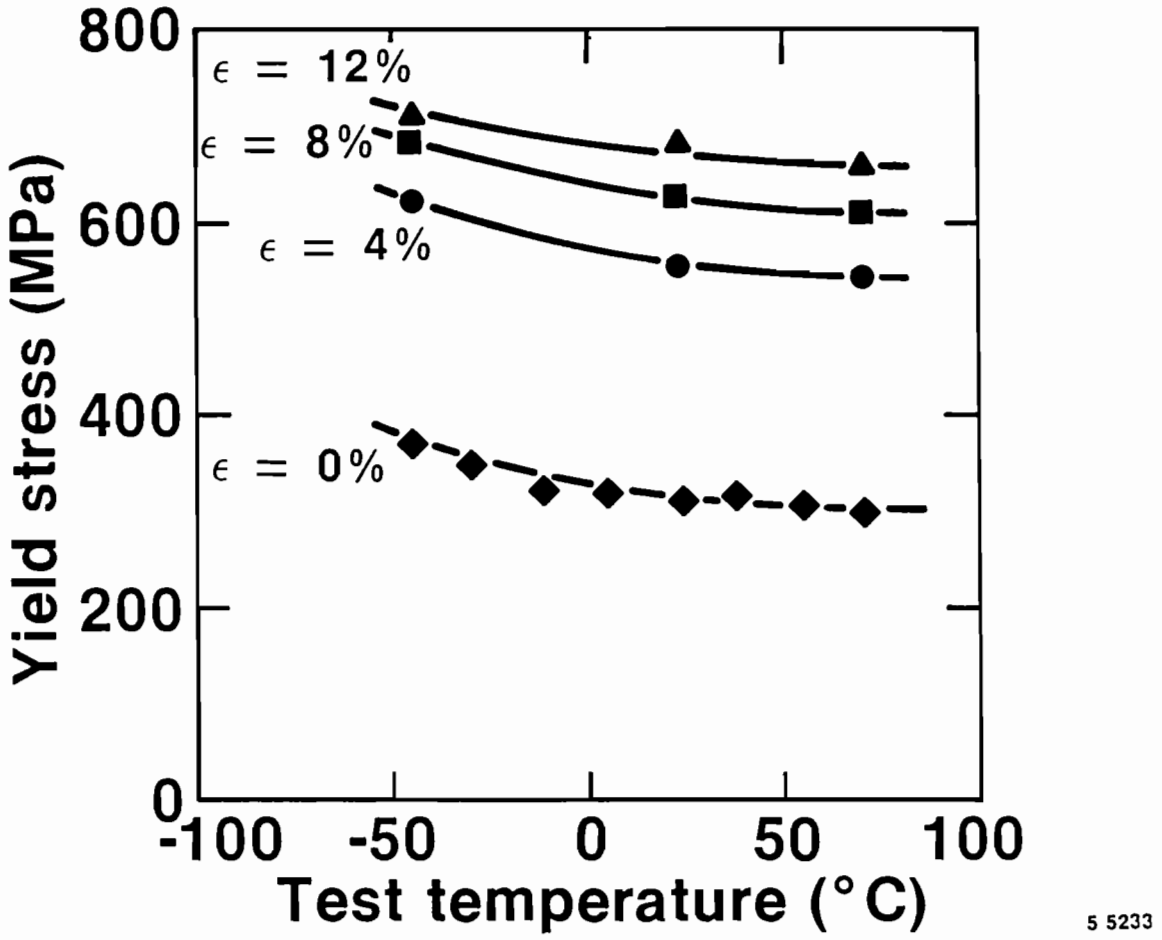


Figure 7. Comparison of uniaxial tensile and shear punch data for A515 steel unstrained specimens.

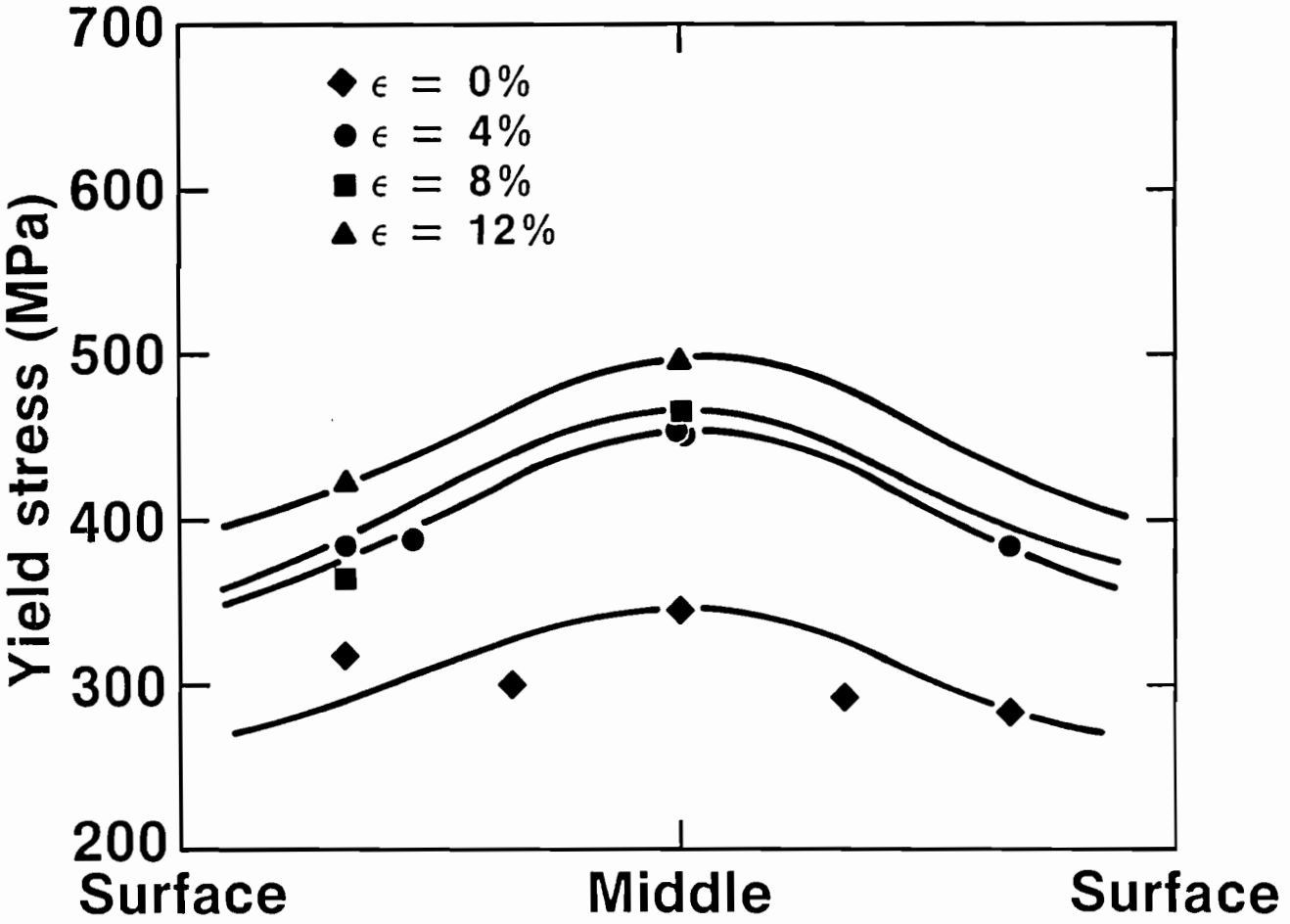


Figure 8. Comparison of through-thickness yield stress (shear punch data) at various prior strain levels.

from shear punch tests at room temperature as a function of thickness position. This figure shows that the variation through the thickness is significant. Since tensile sample gage sections corresponded to the centerline of the plate, agreement between the two test techniques is best here, as shown by Figure 9. It should be noted also that the through-thickness variation was largely retained in the strained specimens, with a significant peak in yield stress at the centerline, see Figure 8. The peaks in ultimate tensile stress were less pronounced, and there were no corresponding valleys in the reduction in area (RA) or strain hardening exponent (n).

Figure 9 provides plots of shear punch data for strained material; both through-thickness average and peak values are shown. The peak values were obtained from tests performed at the middle of the plate. As shown in Figure 9(a), the values of ultimate stress determined in shear punch and tensile tests on strained material are in good agreement. However, a discrepancy developed between the two techniques for yield stress measurements on specimens with increasing prior strain [Figure 9(b)]. Because n is determined from a ratio of yield to ultimate stress,[4] this discrepancy was propagated to estimates of n as well, and this is shown in Figure 9(c). The discrepancy in yield stress may arise largely from the difficulty in determining the yield load in shear punch tests from the point of deviation from linearity in the load-displacement curve. As the material becomes harder with prior strain, this point becomes more difficult to discern. It might be more applicable to use an offset similar to the 0.2% offset used to estimate the yield strength for standard tensile specimens. The ultimate stress, on the other hand, is determined from the maximum point on the load-displacement curve. Here the uncertainty in picking the point is much reduced, and there is little discrepancy between shear punch and tensile data.

In addition, shear punch tests were performed on a 0.5 mm thick slab taken from another dented (dynamic biaxial deformation by BRL) steel plate with the identification number of DH-25-04-83-22-160.[5] (This plate originally had a thickness of 1.645 cm with a surface size of 61 x 61 cm and was deformed by BRL using a hemispherical tup 7.94 cm in diameter.) This

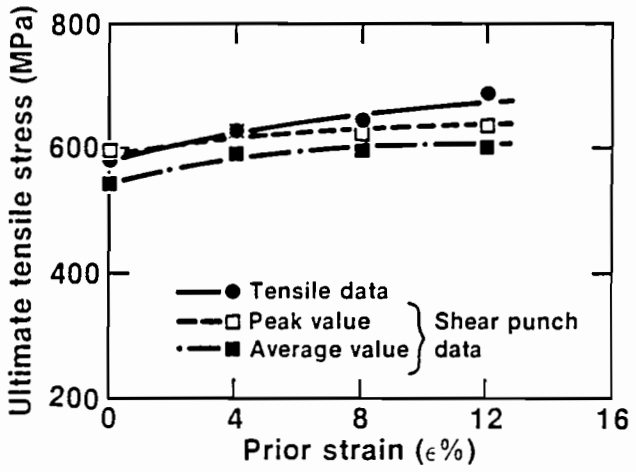


(a)

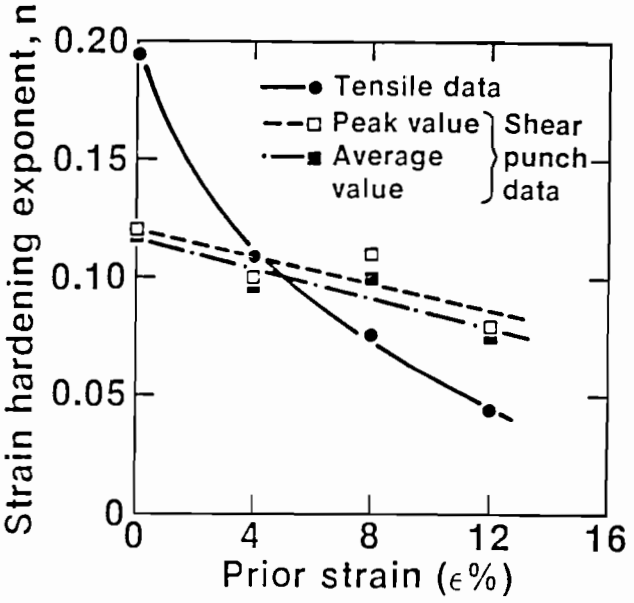


(c)

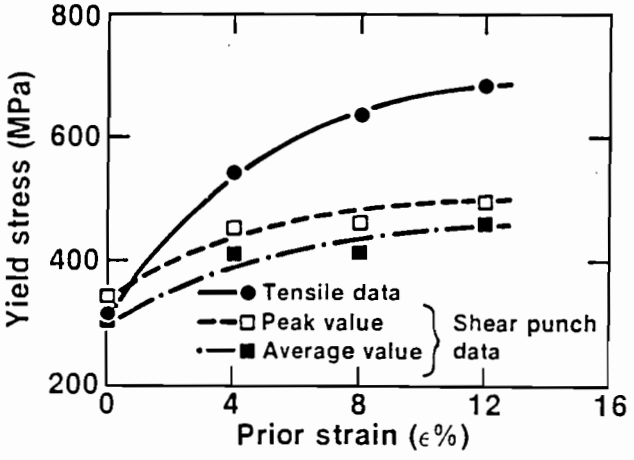


(b)

Figure 9. Comparison of uniaxial and shear punch data at various prior strain levels.

deformed plate contained a large crack on its convex side. In all cases, the shear punch data were analyzed to obtain estimates of uniaxial tensile yield stress, ultimate tensile stress, work hardening exponent, and the reduction in area. Figure 10 provides a summary of flow properties estimated from shear punch data from tests performed at the middle of the deformed slab. A summary of thickness measurements is also shown. The ultrasonic thickness measurements on this slab were within $\pm$1% of the corresponding mechanical measurements. These measurements were used to estimate an effective biaxial strain. As a first estimate, the stress state at the crack site can be taken as near-balanced biaxial tension, in which case the deformation and effective strain are equivalent to that for a uniaxial through-thickness compression test. Hence, the thickness change can be easily converted to effective strain, $\epsilon_{eff}$, and this is shown on the right axis at the top of Figure 10. The effective strain at the crack site is $\simeq$25%.

The BRL A515 plate (DH-25-04-83-22-160) was examined in regions away from the crack site using shear punch tests and the results were compared with those obtained from the undeformed and prestrained A515 plate. Far away from the crack the properties were similar to those measured on the other as-received (undeformed) plate, with three notable exceptions. First, the yield and ultimate strengths were slightly higher; second, there was less through-thickness variation in yield and ultimate stresses; and third, there was more variation in the reduction in area (RA). Near the crack site there was very little through-thickness variation in these properties. The data from the crack site suggest that the yield and ultimate stresses increase slightly and the RA decreases slightly in going from the concave to the convex surface. This variation is consistent with higher strains at the convex surface, and indeed the crack initiated on the convex surface.

As the crack site is approached, the thickness decreases, the strain increases, and the properties change accordingly. At the crack site itself, the yield strength increases to 490 MPa, the ultimate tensile strength (UTS) increases slightly to 593 MPa, the RA drops to ~33%, and the work hardening exponent (n) drops to ~0.06. The changes in yield strength, RA, and n are much more dramatic than the UTS. With the exception of the yield strength,

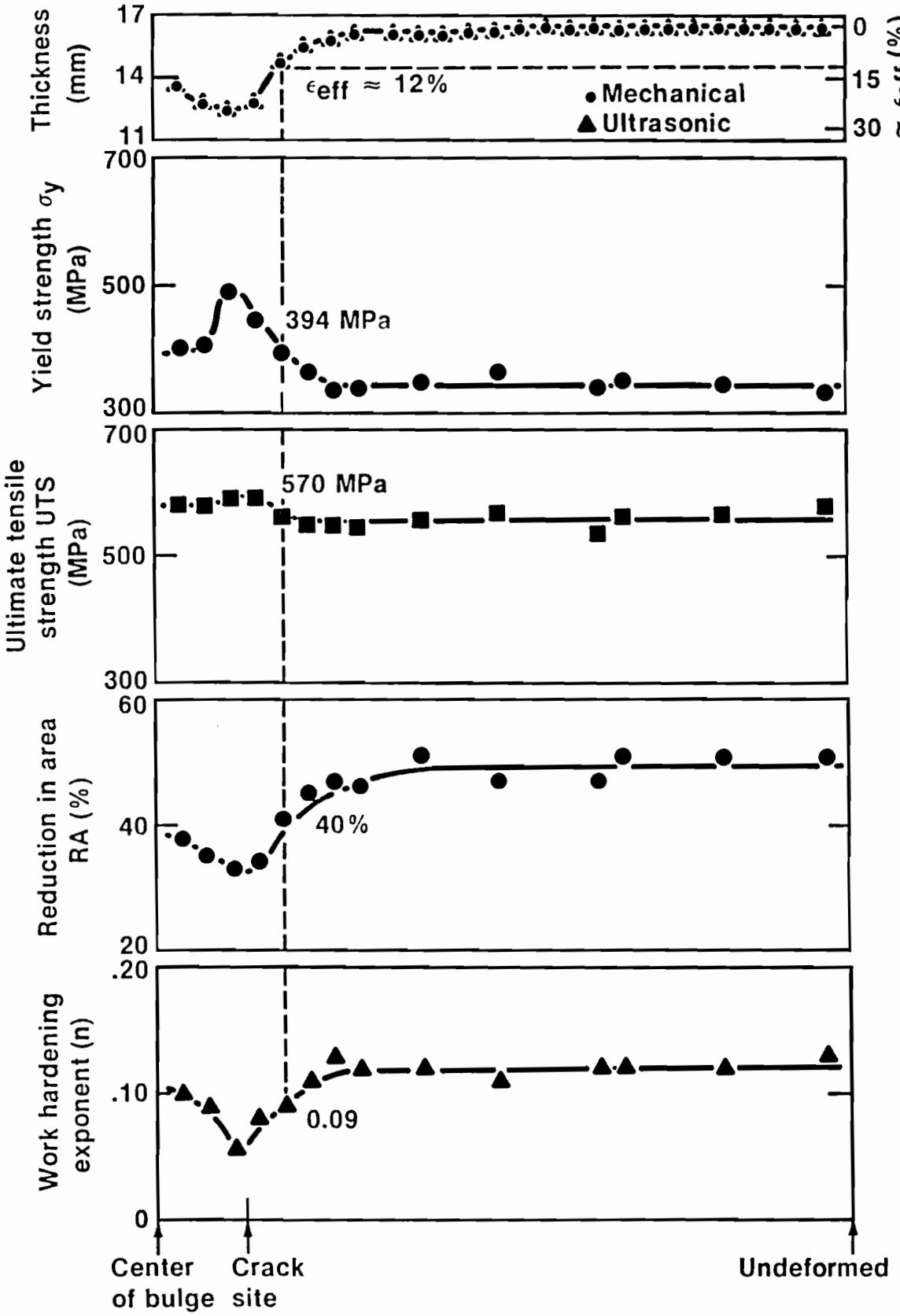


Figure 10. Variation of properties with position in bulged plated.

the changes in properties are consistent with those determined with shear punch tests on the prior-strained samples discussed earlier. As an example, the dashed line in Figure 10 shows property values at the 12% effective strain level. Referring back to Figure 9, it can be seen that these values are consistent (when comparing only shear punch data), except that the yield strength at the 12% effective strain level in the bulged plate is slightly lower than would be expected from the prior strain data. The discrepancy in yield strength is probably a result of some position uncertainty, the assumption of balanced biaxial tension in defining the effective strain (i.e., considering that the deformed plate thickness strain is equivalent to its biaxial strain), and comparing an effective work hardening due to a slow tensile test with that for a dynamic (hammer impact) test.

Fracture Toughness Instrumented Precracked Charpy. Twelve each T-L and T-S oriented precracked Charpy specimens, in the as-received condition, were tested over the temperature range of -45 to +75°C using a Sonntag Model SI-1 Charpy impact test machine. The dynamic stress intensity factor ($K_{Id}$) was determined over the test temperature range.

Static Fracture Toughness--Four sets of fracture toughness specimens having prior strains of 0, 4, 8, and 12% were tested over the temperature range of -45 to +75°C in accordance with ASTM Standard E-813-81. A total of 7 compact tension (0.5T) and 37 three-point bend (0.4T) specimens were tested on an MTS hydraulic testing machine using a computerized single-specimen unloading compliance technique. Data obtained from these tests were analyzed in accordance with procedures given in both ASTM Standard E-813-81 (for ductile fracture) and in Reference 6 (for cleavage fracture following appreciable elastic/plastic deformation).

The measured dynamic fracture toughness ($K_{Id}$) values for as-received material as a function of test temperature are shown in Figure 11 and the plane strain fracture toughness ($K_{Ic}$) data in Figure 12. In the dynamic fracture toughness tests at and below room temperature, brittle cleavage fracture was observed after no significant amount of crack extension. This is compared with the static fracture toughness results which show substantial dimple rupture at and below room temperature. It is expected

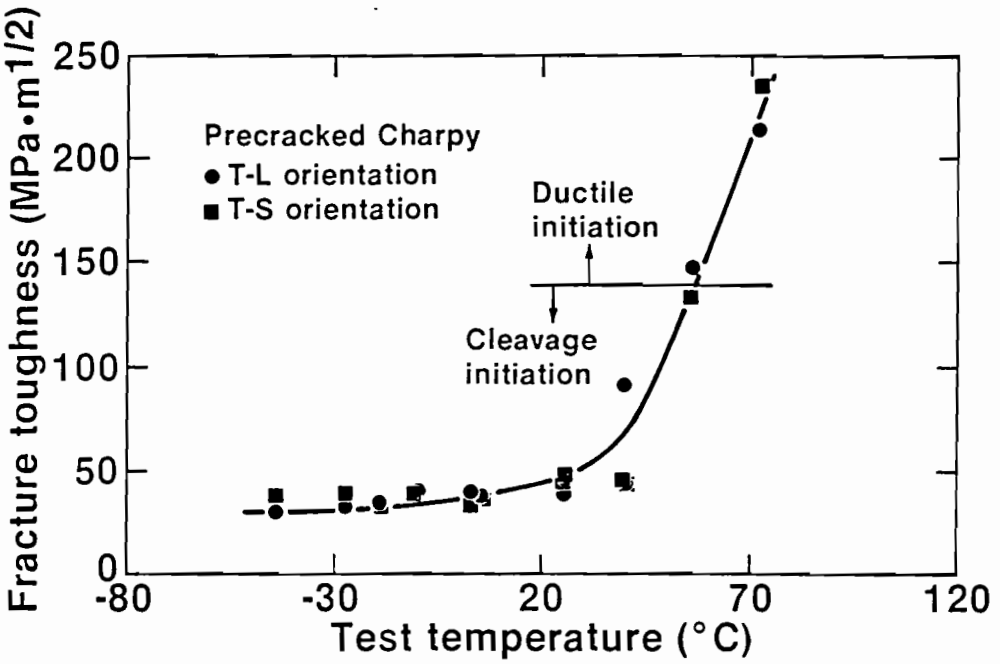


Figure 11. Dynamic fracture toughness ($K_{Id}$), vs. test temperature for A515 steel unstrained specimens.

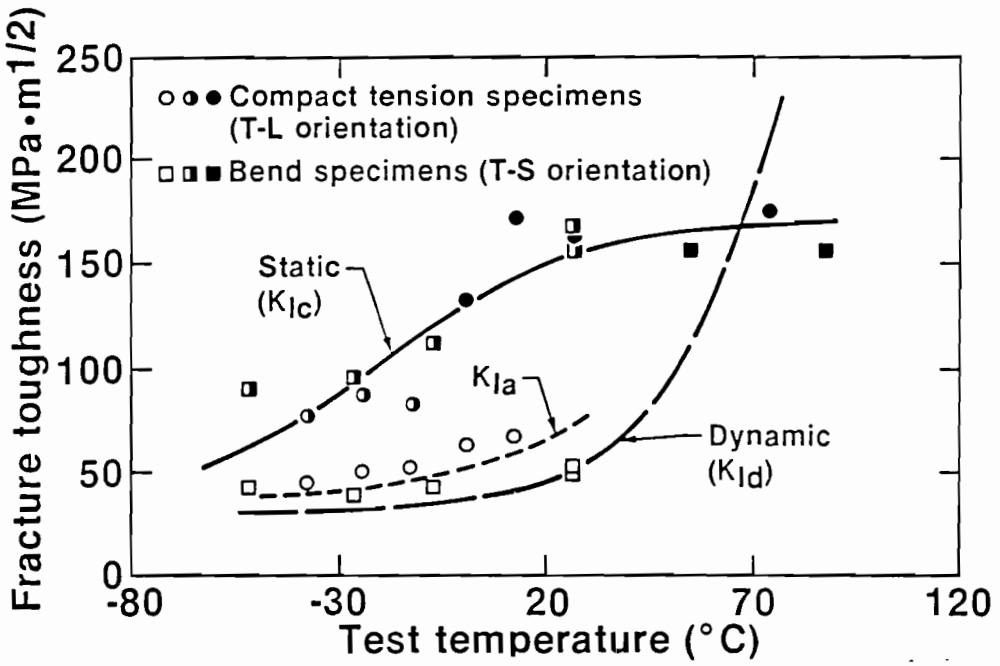


Figure 12. Fracture toughness values ($K_{Ic}$, $K_{Ia}$, $K_{Id}$) vs. test temperature for as-received A515 steel specimens.

that the accident condition will be represented by the dynamic results. The stress intensity factor for crack arrest, $K_{Ia}$, was calculated from the arrest load and measured crack size after cleavage arrest using the correlations given in Sections A3.5.3 and A4.5.3 of ASTM Standard E 399-83 for bend and compact specimens, respectively. In Figure 12, the solid symbols represent ductile initiation fracture, the half-filled symbols indicate cleavage initiation fracture, and the open symbols are for crack arrest data.

The effects of prior strain level on the $K_{Ic}$ and $K_{Ia}$ values are shown in Figure 13. Moreover, the effect of prior strain on the tearing modulus (T) at 75°C was determined, and this is shown in Table 2. The effect of prior strain was to decrease the upper shelf fracture toughness value ($K_{Jc}$) by about 25%, and it dropped the tearing modulus to about one third of its value for the as-received material. Hence, for this material, the tearing modulus is apparently a more sensitive parameter than $K_{Jc}$ in indicating changes in fracture behavior due to prior strain. It is also worth noting (Figure 13) that although prior strain did not affect $K_{Ia}$ at lower shelf temperatures, $K_{Ia}$ decreased with increasing prior strain in the transition temperature region.

Metallographic and fractographic examinations were conducted on the material in both the as-received and prior-strained conditions. The scanning electron microscope (SEM) examination of four fracture toughness specimens tested at 75°C showed that the fracture mechanism was the same for all conditions of the material, i.e., transgranular microvoid coalescence as evident from the ductile dimples. Moreover, the average spacing between major voids on the material fracture surface for all prior strains was roughly 250 $\mu$.

### 1.2.3 Discussion

NDE Observations and Correlations. Extensive surface cracking occurred in the dented areas of approximately half of the plates. In all cases where surface cracks, fractures, and tears occurred, they were observed to be located in the areas with the greatest degree of thinning. A significant percent reduction in thickness was observed in the plates.

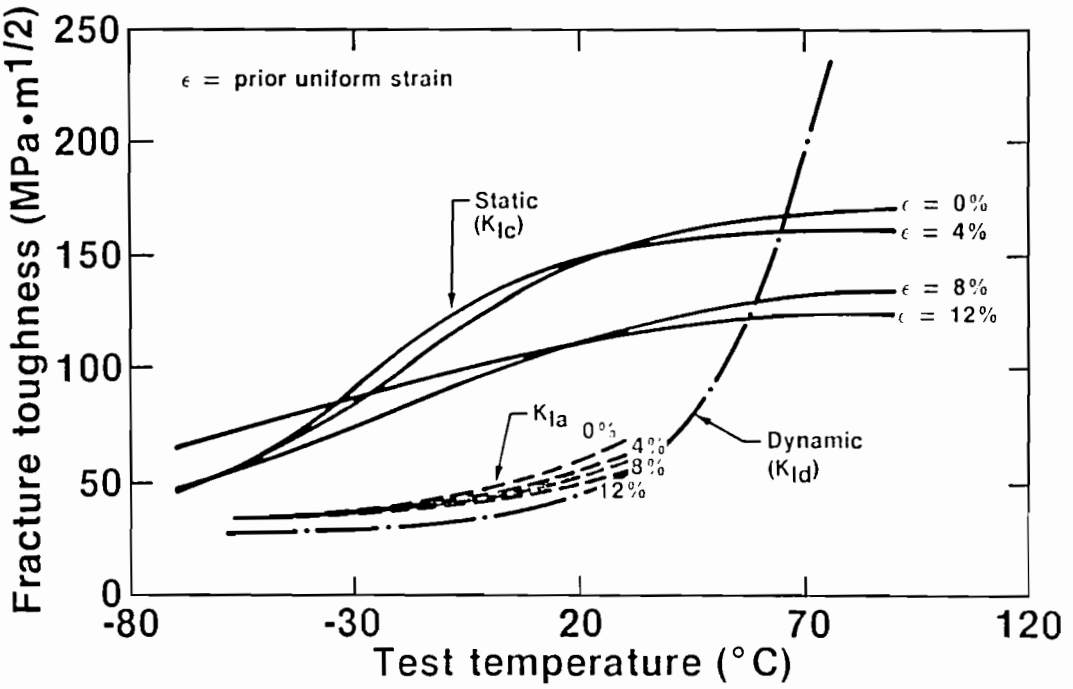


Figure 13. Effect of prior strain on fracture toughness.

TABLE 2. EFFECT OF PRIOR STRAIN ON THE FRACTURE TOUGHNESS AND TEARING MODULUS OF A515 STEEL AT 75°C

| Prior Strain (%) | Fracture Toughness, $K_{Jc}$ (MPa·m$^{1/2}$) | Percent of 0% Strain | Tearing Modulus | Percent of 0% Strain |
|---|---|---|---|---|
| 0 | 163 | 100 | 100 | 100 |
| 4 | 148 | 91 | 34 | 34 |
| 8 | 126 | 77 | 38 | 38 |
| 12 | 122 | 75 | 35 | 35 |

For this task, however, liquid penetrant examinations have served as a rapid and accurate method for locating and quantifying areas for comparison with investigations by other techniques. During the liquid penetrant examinations, the plate specimens showed no signs of cracking on the concave sides of the dents except for the tears when the thickness was completely penetrated. Approximately half of the plates, however, had some surface cracking on the convex sides. It was observed that the surface cracks occurred parallel to the rolling direction of the steel. The surface crack indications were measured (e.g. length of cracks, and number of surface cracks) and tabulated to see if there is a correlation between surface cracking and measurements of deformation such as depth of dent or percent reduction in thickness. Statistical analysis shows that a good correlation was not obtained between either the number or total length of surface cracks and reduction in thickness or depth of dent. This was demonstrated by the correlation coefficients, listed in Table 3 for linear regression, and the scatter plots (Figures 14 through 17). Forty-five plate specimens were included in this statistical analysis and none of these plates had through-thickness tears. In all cases, however, when surface cracks, fractures and tears occurred, they were observed to be located in the areas with the greatest degree of thinning. These areas of greatest thinning constitute the points where the residual strength is in question. As demonstrated earlier in this report, there was a correlation between the degree of thinning and mechanical properties.

The immersion ultrasonic tests showed that equipment can be developed to detect cracks open to the convex inside surfaces of the damaged areas on derailed tank cars in the field and estimate their sizes. All of the surface cracking was on the convex side of the dents which will not be accessible for direct liquid penetrant examinations in the field. The equipment used for the ultrasonic techniques described may be modified to be suitable for field application; presently, provisions must be made for removal of insulation and paint from the area of interest.

A contact ultrasonic thickness gauge was used to measure the thickness changes in the deformed areas of the plates. This ultrasonic testing unit was able to measure the thickness to within 0.13 mm (0.005 in.) on the

TABLE 3. LIST OF PLOTS OF DEGREES OF SURFACE CRACKING VERSUS VARIOUS MEASUREMENTS OF DEFORMATION AND THEIR RESPECTIVE CORRELATION COEFFICIENTS

| Plotted Values | Linear Correlation Coefficient (r) | Scatter Plot |
|---|---|---|
| Total Length of Cracks vs. % Reduction in Thickness | 0.312 | Figure 14 |
| Total Length of Cracks vs. Dent Depth | 0.415 | Figure 15 |
| Number of Cracks vs. % Reduction in Thickness | 0.105 | Figure 16 |
| Number of Cracks vs. Dent Depth | 0.473 | Figure 17 |

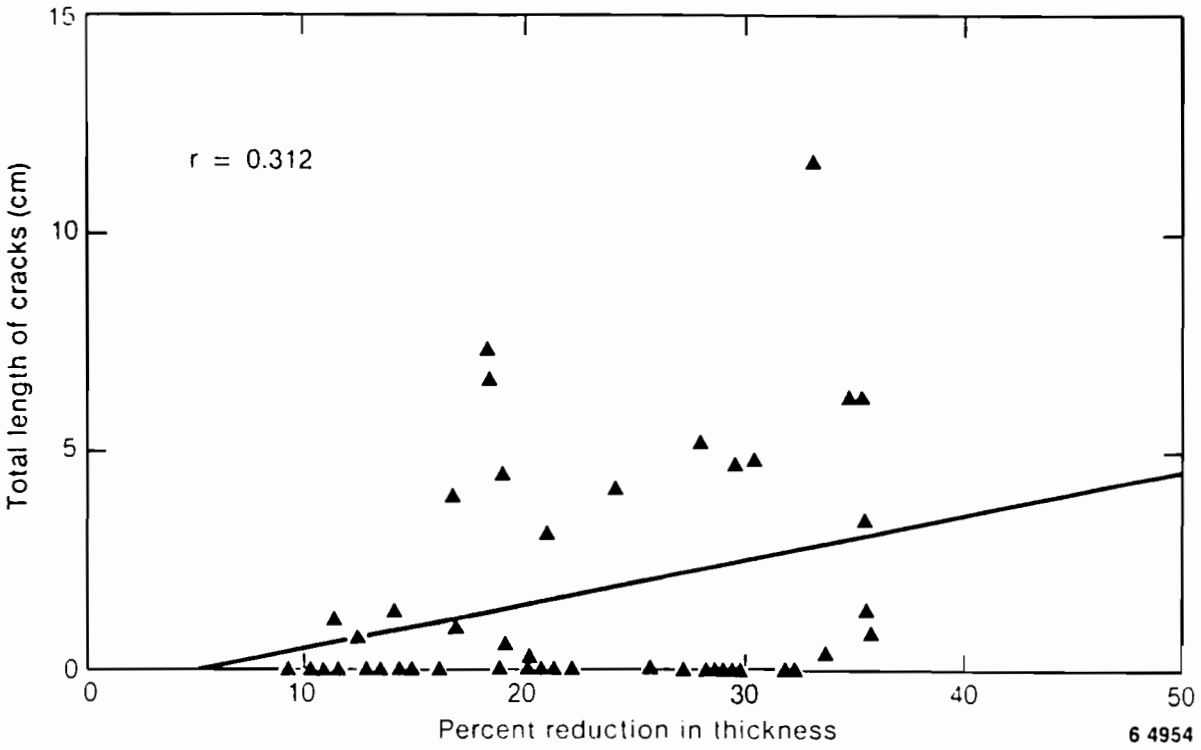


Figure 14. Scatter plot of total length of cracks vs. reduction in thickness.

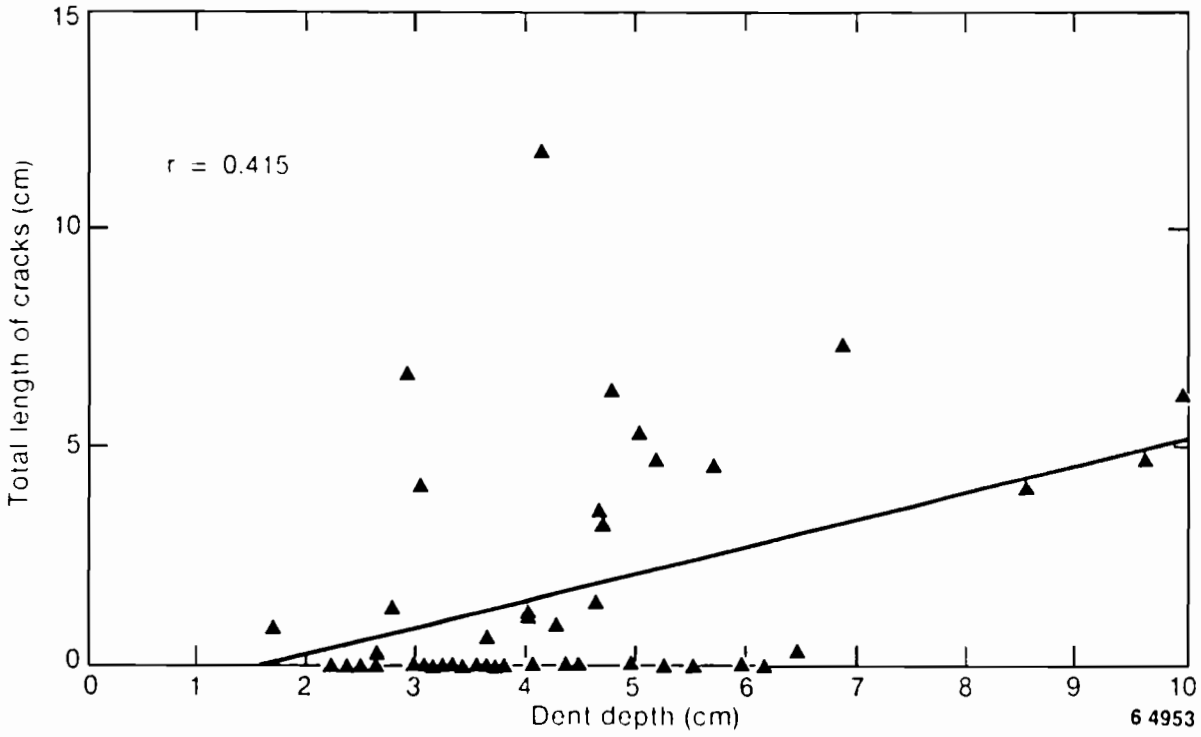


Figure 15. Scatter plot of total length of cracks vs. dent depth.

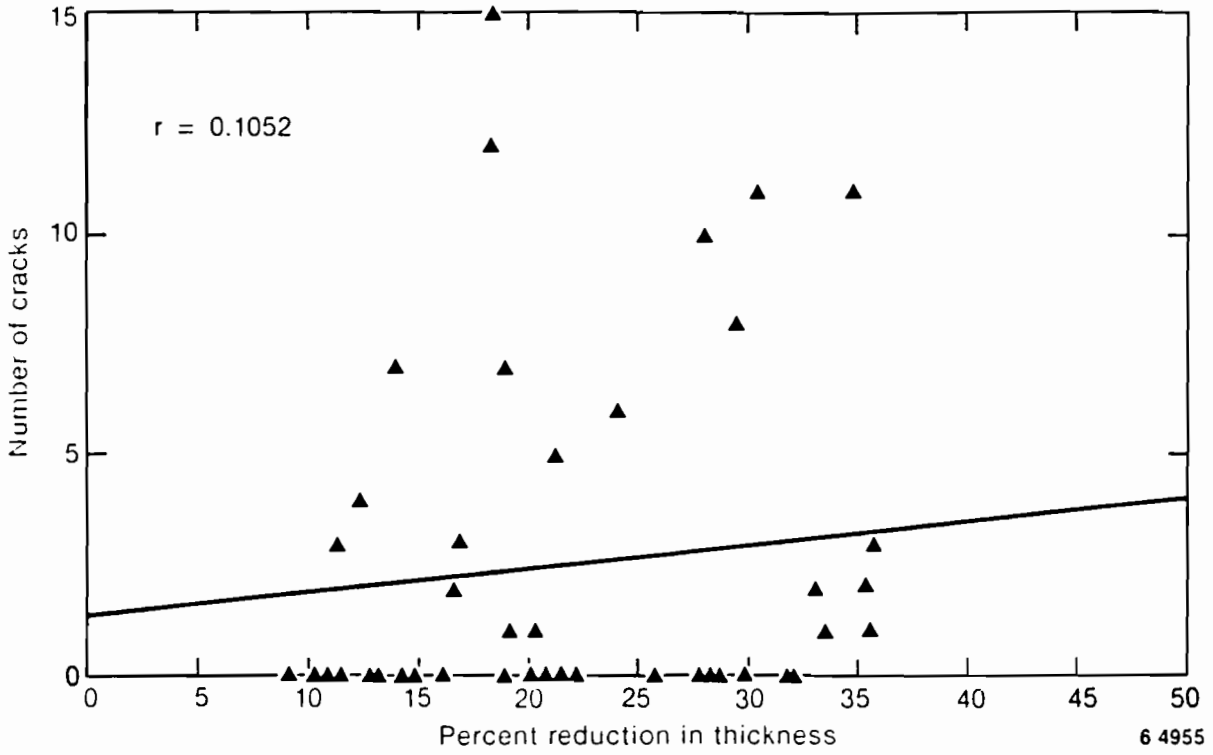


Figure 16. Scatter plot of number of cracks vs. reduction in thickness.

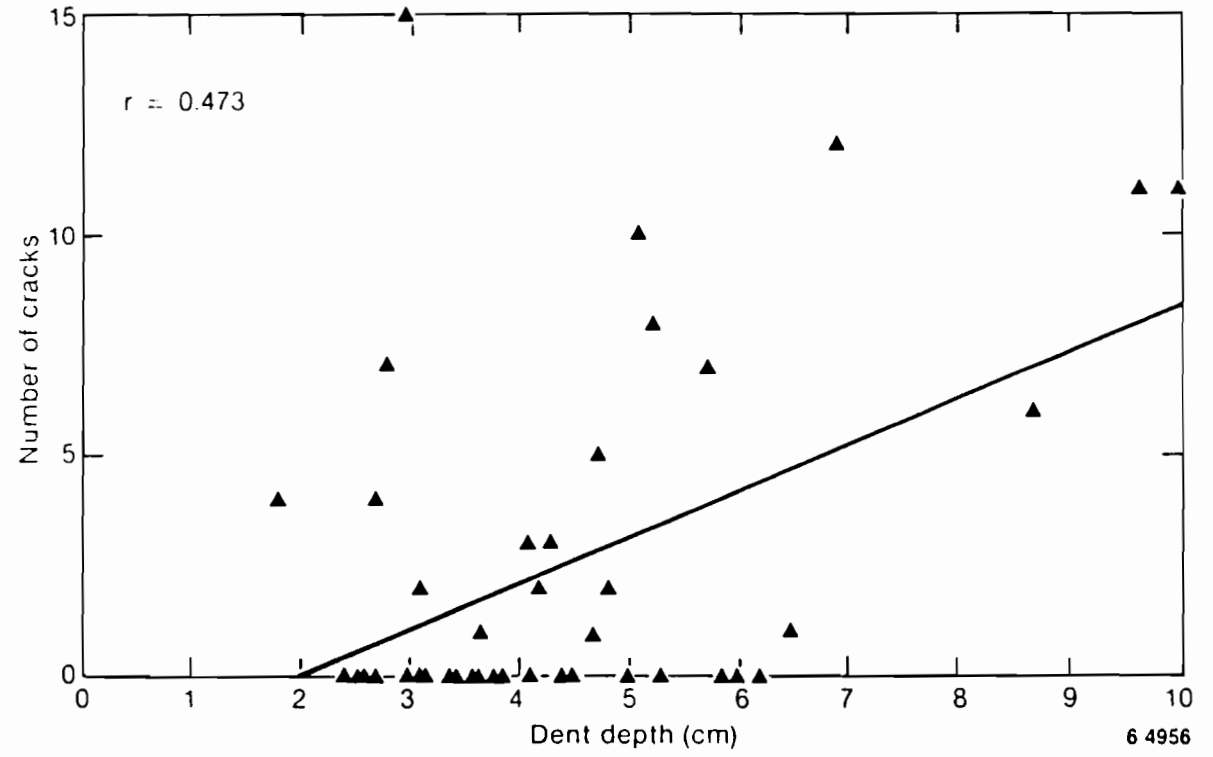


Figure 17. Scatter plot of number of cracks vs. dent depth.

cleaned surfaces for conditions with neither significant rust nor scale and no insulation. This was verified using mechanical techniques to measure thickness. From these measurements, a calculation of percent reduction in thickness was made for each plate. Reduction of plate thickness of as much as 37% was observed in some samples. These reductions were then compared to the data obtained by the other NDE examinations and fracture mechanics evaluations to determine if correlations do exist.

Tensile Results. Figure 7 showed nominal agreement between results obtained from tensile specimens and from shear punch tests. This consistency is also observed in Figure 9 for $\sigma_{max}$ and $\sigma_{ys}$ but not for n for undeformed specimens. The difference in n may be attributed to the simple relationship between $\sigma_{at}$ and $\sigma_{ys}$ and that engineering values are used as opposed to true tensile values. The difference between tensile and shear punch predictions increases with increased prior deformation and is significant for $\sigma_{ys}$ and n (expected since n is related to $\sigma_{ys}$). These results suggest that additional development is required before the shear punch test will provide accurate data. For any future tests, it is expected that tensile specimens will be used to measure the desired tensile properties.

A comparison between shear punch data in Figures 9 and 10 show the following:

| Figure Number | Tensile Test Results | | | | | |
|---|---|---|---|---|---|---|
| | at 0% Prior Strain | | | at 12% Prior Strain | | |
| | $\sigma_{ut}$ (MPa) | $\sigma_{ys}$ (MPa) | n | $\sigma_{ut}$ (MPa) | $\sigma_{ys}$ (MPa) | n |
| 9 | 540 | 310 | 0.12 | 600 | 456 | 0.075 |
| 10 | 560 | 340 | 0.12 | 570 | 394 | 0.09 |

Therefore, the material in Figure 9 with a 0% prior strain has a lower $\sigma_{ut}$ and $\sigma_{ys}$ than shown in Figure 10. But after 12% strain, the material in Figure 9 (prior strain by tensile specimen) showed a substantially higher $\sigma_{ys}$ than that in Figure 10 (prior strain by impact loading), whereas $\sigma_{ut}$ was only slightly greater in Figure 9

than in Figure 10, although the percent change is much higher for Figure 9. These data almost preclude differences due to strain rate effects for the prior strain since the material exposed to the lowest prior strain rate experienced the largest increase. It is not possible at this time to predict the effect of adiabatic heating (magnitude and time are not known) on the material exposed to the fast strain rate.

Test results in Figures 9 and 10 show the effect of prior strain (due to an accident condition) on tensile properties. The results in Figure 9 suggest that the changes in tensile properties are becoming saturated after about 12% prior strain. These data provide guidance for predicting the changes in tensile properties of material in a damaged railroad tank car.

Fracture Toughness. The results of fracture toughness tests based on dynamic (instrumented precracked Charpy specimens) and static (standard ASTM E 813 specimens and techniques) tests were provided earlier. Figure 12 shows that a static fracture toughness requirement, say 150 $MPa \cdot m^{1/2}$ at room temperature, may not be a relevant procurement specification since failure may be controlled by $K_{Id}$ = 50 $MPa \cdot m^{1/2}$ for an accident condition at the same temperature. These results are useful for evaluating requirements for design and fabrication of a new generation of tank cars. These results do not apply directly to the problem of estimating the safety of moving a damaged railroad tank car.

Figure 13 is applicable to the problem of estimating the safety of moving a damaged railroad tank car. These data are summarized in Table 2. It is apparent that any deformation greater than 8% has saturated the reduction in fracture toughness and any reduction greater than 4% has saturated the reductions in the tearing modulus. Figure 13 shows that the primary effect of prior strain is to reduce the fracture toughness and not to shift the curve to the right so cleavage fracture will be more likely to occur. The decrease in $K_{Ic}$ and the substantial reduction in the tearing modulus suggest that the chance of a brittle fracture is increased due to the damage caused by an accident.

The above results suggest that conservative and potentially useful predictions of the safety of moving a damaged railroad tank car may be made based on assuming that the material is operating on the lower shelf, where cleavage fracture occurs. In addition, these data also provide a means for developing material procurement specifications that could reduce the possibility of failures of moving damaged railroad tank cars. These same procurement specifications will increase the safety of tank cars during an accident.

## 1.3 FRA/NBS Deformed Tank Car Material

This section deals with a steel plate sample obtained from a railway tank car after it had been involved in an accident. The performance of the various steel plate grades in routine service is not in question here. The performance under accident conditions, which may involve severe impact loads at low temperatures and exposure to elevated temperatures while under pressure by flammable or toxic liquids, is of interest. These conditions can lead to vessel ruptures with catastrophic consequences. Improving the safety of tank cars under accident conditions is a complex problem involving design, materials, and fabrication processes. This section is concerned with materials, specifically the properties of steel plates relative to the specification of grades presently considered acceptable for tank car construction. It is necessary to develop data to establish a basis for changes, if warranted, in tank car design, specifications for procurement of materials, and the techniques used for construction.

The Federal Railroad Administration requested the National Bureau of Standards (NBS) to conduct metallurgical studies on steel plates samples removed from tank cars that have failed under a variety of accident conditions. A principal purpose of the metallurgical studies was to determine whether the plate conformed to the specification to which the tank cars were fabricated. Other purposes were to determine whether the specification, although adequate for normal service, was suitable under the conditions encountered in the accident, whether the plate exhibited properties not described by the specification, and whether a better specification would have prevented or at least reduced the severity of the failure.

Materials from the damaged railroad tank cars and the failure analysis reports developed by NBS were examined by the INEL to identify those pieces which represent the "typical" accident condition.

### 1.3.1 Evaluation of Accidents Described by 12 NBS Reports

The NBS evaluated a number of grades of plate from tank cars containing flammable or toxic liquids under pressure which were involved in a variety of railway accidents. The evaluations concentrated on the metallurgical properties of the plate to determine if the plates conformed to the respective specifications for chemical composition and mechanical properties. Tests were conducted to evaluate suitability of the steels for use as plate material for tank cars of the future. The results of these evaluations were contained in 12 reports,[7-18] which describe the chemistry, microstructure, mill practice, forming and welding techniques, weldments, strength levels, bending properties, and fracture toughness in some detail.

The plate specimens were obtained from samples cut from the damaged cars. Most samples were from undamaged or slightly damaged plate. Some samples contained the fracture but exhibited little other damage except for thinning adjacent to the fracture. Photographs taken at accident scenes show tank cars with severe dents containing through-thickness fractures (Ref. 16, Fig. 1), while other cars showed similar dents without apparent plate failure (Ref. 18, Photos C2-4, C2-12, 1-14). The NBS assignment did not include sampling such damaged areas to assess the residual properties in the damaged areas. Selecting plate samples with minimum distortion facilitated extraction of standard tensile, U-bend, and Charpy specimens used for the tests to produce the data in the cited NBS reports. While useful results were obtained from such specimens which will enable valid recommendations, it is hoped in the future that severely dented tank car plates will become available to enable correlations between NBS data, NDE testing, and mechanical property data in the damaged plate areas.

The results, from References 7-18, of Charpy V-notch impact tests, measurement of NDTT (nil-ductility transition temperatures), and examination of the fracture surfaces showed the following potential problem areas:

1. NDTT was in the nominal operating temperature range. This indicates that cleavage fracture may occur which may easily lead to catastrophic failure.

2. For those materials where NDTT was not measured, it was observed that the temperature corresponding to 15 ft-lb energy absorption for the Charpy V-notch impact test frequently fell within the normal operating temperature range. Early studies related 15 ft-lb to NDTT, but later research showed that the energy relation to NDTT was not constant but varied as a function of material thickness and yield strength. A number of the above references were reviewed and it was noted that the percent cleavage fracture ranged from 7 to 30% (with one of about 50%) for the temperatures corresponding to 15 ft-lb. This is an additional indication that a real possibility exists of cleavage fracture occurring during normal operating conditions.

3. Examinations showed that many failures were of a brittle nature. No attempts were made to distinguish between brittle-cleavage (lower shelf/transition temperature region) or brittle-dimple rupture (low fracture toughness associated with low upper shelf and/or low tearing modulus). The ability to identify which of the two brittle fracture mechanisms is the primary cause of the failures would be useful in identifying corrective action.

The overall safety record for railroad tank cars seems to be good; they perform their intended function and most only have problems when accidents occur. Even under accident conditions the percentage of failures is small, but because of the consequences of failure it is necessary to examine what could be done to reduce these failures. One way to answer this question requires knowledge of the accident conditions:

1. Strain rate

2. Temperature

3. Stress Conditions.

These data then provide the criteria used to procure materials and for establishing accept/reject criteria for fabrication in order to obtain a structure with greater resistance to failure during accident conditions.

### 1.3.2 Description of Chosen Sample and Basis for Selection

Since a major NBS objective was to establish whether the plates conformed to specifications, their samples were selected from relatively undamaged regions of the various damaged tank cars. Thus, only limited opportunities existed for the INEL comparison of plate dented under accident conditions to the unstrained and prestrained A515 Gr 70, or to the plate dented by the hemispherical tup of the BRL drop hammer.

A section of plate sample FRA-5 was shipped by NBS to the INEL for examination. Sample FRA-5 was removed from the shell plate of tank car No. SOEX 3037 that had contained liquefied petroleum gas and was involved in an accident near Crescent City, IL, June 21, 1970. This tank car had burst as a result of excess pressure that developed from overheating when the spilled contents from other ruptured cars burned.[9] It appears that this car had survived the accident and would have retained its contents had it not been overheated. The ambient temperature was about 12°C (53°F) when the accident occurred, but only an estimate could be offered for the temperature of the plate at the fracture site. The surface of sample FRA-5 contained no paint residue, and substantial thinning (in excess of 25%) before failure was noted. The lack of paint residue indicates the plate was exposed to at least 600°F (Ref. 11, p. 16). The fracture mode was in shear, which is to be expected at elevated temperatures. The NBS performed chemical analyses, made thickness measurements, and made macroscopic and microscope observations on sample FRA-5; however, they performed no mechanical property tests.

Sample FRA-5 was manufactured to ASTM A212-65, Grade 8, which does not require fine-grain practice for plates less than 5 cm (2 in.) thick, and which has since been replaced by ASTM A515-70 which does specify coarse grain practice. For the purposes of the intended material examinations, the specifications are considered to be equivalent. The FRA-5 sample was selected for NDE examination and miniature shear punch tests because of its similarity to BRL plate DH-25-04-83-22-160 (discussed in above). The FRA-5 plate exhibited in excess of 25% thinning (Ref. 11, Table 7) vs. 25% for the BRL plate, had the same nominal original thickness [15.87 mm, (.0625 in.), Ref. 8, Table 1] as the BRL plate, and both plates had the same grain size (ASTM 7-8).

### 1.3.3 NDE Results

The NBS plate was examined for surface cracks using the same liquid penetrant examination procedure used for the BRL plates. No surface cracking was observed on this plate. The same ultrasonic thickness gauge was also used for measuring the thickness change on the NBS plate. The ultrasonic scans were made approximately perpendicularly from the torch cut edge of the sample across the plate to the fracture surface. The original plate thickness was 19.0 mm (0.75 in.), rather than 15.8 mm (0.62 in.) as reported. The 19.0 mm (0.75 in.) plate thickness is consistent with the "high pressure service" requirement used for tank cars that carry LPG. The ultrasonic scans indicated a nearly uniform decrease in thickness from the original dimension to within about 64 mm (2-1/2 in.) of the fracture surface, and in some areas section thinning of as much as 80% near the fracture was observed in our sample of FRA-5.

### 1.3.4 Shear Punch Tests

Shear punch tests were used, even though there is limited ability to accurately quantify such tests, in order to (1) evaluate changes in tensile properties as a function of location in the thickness direction, and (2) compare with previous shear punch tests. Several 3 mm (1/8 in.) thick slices were cut from the plate so as to provide a representative cross-section oriented approximately perpendicular to the fracture surface.

The axis of the slices was assumed to be nearly parallel to the rolling direction of the plate, although this could not be confirmed by the NBS information. It was found that $\sigma_y$ = 360.9 and 356.0 MPa (52.3 and 51.6 ksi) at the surfaces and 301.5 MPa (43.7 ksi) in the center and $\sigma_{ut}$ = 507.8 and 512.0 MPa (73.6 and 74.2 ksi) at the surfaces and 471.3 MPa (68.3 ksi) at the center.

The test results are summarized in Figure 18 for the ultimate tensile strength, yield strength, and reduction in thickness as a function of distance from the failure. The most significant changes as a function of distance occur for the yield strength ($\sigma_{ys}$). The relative change in $\sigma_{ys}$ is very similar to that observed in Figure 9, although the NBS specimen experienced substantially more deformation (Figure 18), but at an elevated temperature. An examination of Figures 9 and 10 suggests that the change in yield strength reaches a maximum after about 12% strain. Figure 18 shows very little change in ultimate tensile strength as a function of distance from the fracture. This is somewhat inconsistent with the trends observed in Figure 9.

## 1.4 Comparison of BRL and NBS Results

### 1.4.1 Cleaned Surfaces

BRL Plates. Glass-bead blasting required to remove scale and rust; there was no insulation.

NBS Plate. Glass-bead blasting was not necessary, and there was no insulation.

### 1.4.2 Surface Inspection

BRL Plates. Liquid penetrant detected cracks on convex side of dent. No cracks detect on concave side.

NBS Plate. Liquid penetrant detected no cracks on convex side of dent.

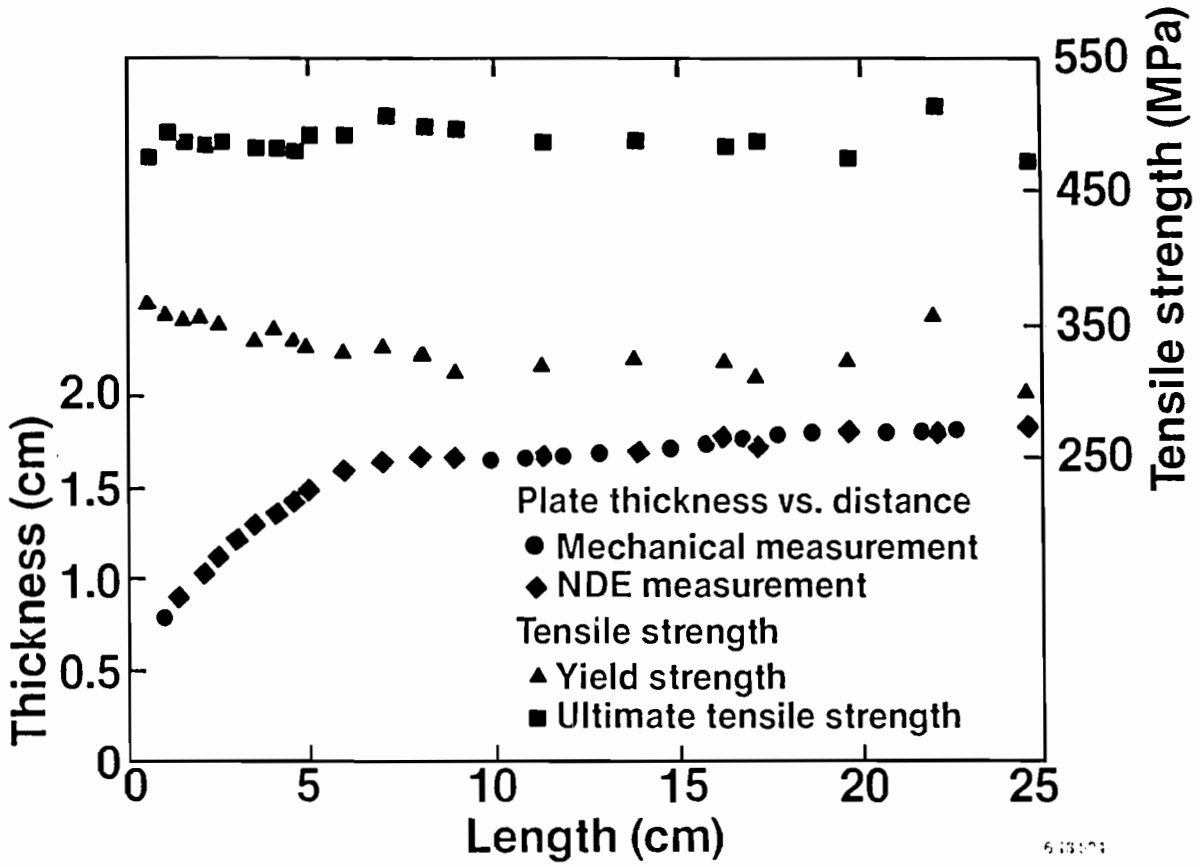


Figure 18. Relation between strength and reduction.

### 1.4.3 Ultrasonic Inspection

BRL Plates. UT was used to detect and characterize cracks; the capabilities were proven by comparison with results obtained by liquid penetrant.

NBS Plate. Was not used because no cracks were detected by liquid penetrant inspection.

### 1.4.4 Thickness Measurement

BRL Plates. A UT thickness gage was used to measure the thickness. Comparisons made with results obtained with a mechanical measurement technique showed that the UT results were within $\pm$ 0.13 mm (0.005 in.) of the mechanical measurements.

NBS Plate. A UT thickness gage was used to measure the thickness.

### 1.4.5 Tensile Test Results

BRL Plates. Standard specimens and miniaturized shear punch tests were conducted for comparison purposes. The latter are of interest because results may be obtained from locations as small as 1 mm diameter. Tests were conducted on a specimen that had experienced prestrain of 0, 4, 8, or 12%. The comparison showed that shear punch results were substantially lower for yield strength, nominally equal for ultimate tensile strength, and n ranged from being much lower at 0% strain to much higher at 12% prestrain than the standard test results. The results showed that yield strength increased and the strain hardening exponent decreased with prestrain increasing from 0 to 12%.

NBS Plate. Shear punch tests were conducted and results similar to those for the change in yield strength as a function of prestrain for the BRL plates were obtained. The NBS plate experienced much more deformation but at a higher temperature. Very little change was observed, as a function of percent reduced thickness for ultimate tensile strength and the strain hardening exponent.

### 1.4.6 Fracture Toughness

BRL Plates. Increasing prestrain had little effect on the nominal NDTT (transition from cleavage to a mixture of dimple rupture and cleavage) results, as identified by compact tension results, but had a substantial effect on reducing the upper shelf from 170 $MPa \cdot m^{1/2}$ at 0% prestrain to 125 $MPa \cdot m^{1/2}$ at 12% prestrain. In addition, the tearing modulus was significantly reduced from 100 at 0% prestrain to 34 at 4 - 12% prestrain.

NBS Plate. No measurements were made.

### 1.4.7 Observed Difference

BRL Plates. The greatest reduction in thickness did not occur at maximum depth but along the side where the tup and die interacted to create a significant shear stress as opposed to a nominal bending stress.

NBS Plate. Substantial deformation at a much higher temperature.

### 1.4.8 Comments Based on NBS Metallurgical Analysis of Failed Railroad Tank Cars

NBS Plate. Many failures were of a brittle nature since temperatures corresponding to NDTT and 15 ft-lb were within the normal operating range.

## 1.5 Summary

The BRL plates provided a unique opportunity to use a single material that had experienced different degrees of deformation to evaluate NDE techniques and changes in mechanical properties. These tests showed the adequacy of UT techniques for measuring wall thickness and detecting and characterizing defects in the damaged regions for material that had been glass-bead blasted for removal of scale and rust from the surfaces. Tests of deformed material showed that the yield strength increased and both fracture toughness and the tearing modulus decreased with increasing deformation. These data provided the baseline needed to understand the

problem, but the results cannot be used at this time to adequately predict the behavior of other materials damaged in accidents because the material-to-material differences are too great.

The NBS plate was selected from a number of plates of materials removed from failed railroad tank cars which had been stored at NBS after their metallurgical analyses. NDE evaluation techniques used to examine this piece were found to be as successful as when used for the BRL plates. Shear punch tests conducted to provide estimates of tensile properties showed changes due to deformation very similar to that experienced by the BRL plate. This may be fortuitous because the NBS plate experienced more deformation but at a substantially higher temperature.

An evaluation of the NBS reports led to the observation that a number of failures were of a brittle nature since temperature corresponding to NDTT and 15 ft-lb were within the normal operating range. No distinctions were made as to whether brittle fracture was due to cleavage or low fracture toughness.

# 2. STRESS ANALYSIS METHODOLOGY

## 2.1 Introduction

Railroad tank cars may become severely damaged during accidents. The purpose of this task was to determine the feasibility of developing a catalog of solutions for different deformed tank car shapes that could be taken to the accident site to aid personnel in deciding the method to be used to move damaged tank cars which may contain hazardous chemicals. The damage to the tank car may occur at any location on the tank. Stresses caused by lifting or moving the car after an accident may cause a rupture of the car. For this reason it is important to examine different lifting methods before actually attempting to lift the car. A part of this task is the development and evaluation of techniques for performing a stress analysis associated with handling a damaged tank car.

A special purpose, large displacement, large strain computer code will be required to perform the inelastic stress analysis for this task since a large amount of permanent deformation of the tank may occur during an accident. There are several inelastic stress analysis computer codes available but most of them are limited to small displacements and small strains (about 2 percent). Much larger strains are expected in this analysis. A survey of computer codes was made during this investigation and six large displacement inelastic codes were identified. A 1978 version of one of these codes, ADINA, is presently available on the INEL computer system. Since the cost of each of these codes is quite substantial (at least $1,000 per month to lease or at least $26,000 to purchase) the decision was made to solve two verification problems using the 1978 version of ADINA to assess its ability to perform the solution. The 1978 version of ADINA may be unacceptable for the analysis of the tank cars due to a poor comparison of results for a cylindrical geometry verification problem to results from other codes. A third verification problem was solved by an outside vendor using the ABAQUS code and the results are included in this report.

This section begins with a discussion of the survey perfomed to identify computer codes having the capabilities required to solve this large displacement problem. The results of two verification problems found using the 1978 ADINA code and a third verification problem using ABAQUS are then presented. Next, the solution methodology is presented. Details of the finite element model are discussed including element type to be used, type of analysis to be performed, and the material properties to be used. These details are based on the use of the 1984 version of ADINA.

## 2.2 Computer Code Survey

A survey of computer codes was made to identify codes capable of performing a large displacement inelastic analysis of a 3-dimensional problem. A catalog of approximately 800 structural mechanics computer code abstracts is contained in Reference 19. The abstracts include descriptions of the code, the range of application of the code, and the computer type on which the code operates. Six computer codes having a high probability of performing the tank car analysis were identified in the survey. The costs of five of the codes are shown in Table 4. The sixth code, WECAN, is a large, general purpose code written by Westinghouse Electric Co. that is only available for use through their computer service bureau. Three of the other codes (ABAQUS, ANSYS, and MARC) are available for use on the CYBERNET computer service bureau. (The remaining two codes, ADINA and NISA, are not available from a service bureau.) The use of a service bureau may be a viable alternative to the purchase of one of these codes. However, personnel at Hibbit, Karlsson and Sorenson (authors of ABAQUS) said that they have found that the lease cost on ABAQUS ($1,950 per month) can be used up rather quickly when running on a service bureau. That would depend, of course, on the size and number of runs being made.

Abstracts of the six identified codes, as given in Reference 19, are shown below. These abstracts include a summary of capabilities of the codes. It is not implied that all capabilities shown in the abstracts are required to perform the tank car analysis.

TABLE 4. SUMMARY OF COSTS OF NONLINEAR COMPUTER CODES

| Code Name | Lease Cost | One[a] Time Binary Cost | Maintenance Cost[b] | Source Code Cost[c] |
|---|---|---|---|---|
| MARC | $2000/mo. for minimum of 12 mo. | $50,000 | $12,000/yr | $60,000 Additional |
| ANSYS | $1000/mo. minimum for minimum of 12 mo. | -- | -- | Source code not available |
| NISA with DISPLAY plotting program | $2000/mo. | $60,000 | $4,000/yr | $100,000 $5,000 for personal computer version available in early 1986 |
| ADINA | -- | -- | -- | $26,000 (additional $10,000 for input pre-processor and plotting program) |
| ABAQUS | $1950/mo. for minimum of 12 mo. (includes maintenance and support) | $70,200[d] | -- | $20,000 additional over the one time binary cost for one year lease on source |

a. The one time binary cost is for a machine language (compiled) program. No source code is included and, therefore, no updates are possible unless a new binary code is obtained. This cost may not include installation of the code on the computer. The installation cost may be up to $5,000 maximum.

b. The maintenance cost includes periodic updates to the code (error correction and/or improvements to the code) that are supplied by the code vendor.

c. The source code is a listing of the actual statements comprising the code. No updates by the user are possible unless the source code is purchased.

d. The one time binary cost is equal to three years lease cost prepaid. This cost includes one year of maintenance and support. After the first year, one year maintenance contracts can be purchased (if desired) at 2/3 of the current lease cost.

### 2.2.1 ABAQUS

ABAQUS is a general purpose program for linear and nonlinear static and dynamic analysis. A heat transfer capability is included in the program. Visco-elastic response and creep and swelling are provided as well as modal extraction for frequency determination. Two approaches are available to solve nonlinear problems: direct user control of increment size and automatic control. Contact/impact problems may be handled and a gap/friction contact option is available.

### 2.2.2 ADINA

ADINA is a program for linear and nonlinear static and dynamic analysis. The nonlinearities may be due to large displacements, large strains and nonlinear behavior. Vibration and dynamic analysis includes computation of eigenvalues and eigenmodes, and dynamic response. The stability analysis can handle nonlinear collapse, dynamic instability, and postbuckling. Four different analysis procedures are available: linear elastic analysis, material nonlinear only, total Lagrangian formulation, and updated Lagrangian formulation.

### 2.2.3 ANSYS

Structural analyses and heat transfer analyses are possible in linear or nonlinear range. The heat transfer capabilities are: steady state and transient analysis; conduction, convection, and radiation. Also available are coupled thermal-fluid capability, coupled thermal-electric capability, and wave motion analysis. Inelastic materials may be included. Elastic material properties may be up to a fourth order polynomial function of temperature. Plastic stress-strain curves may be input for up to five temperatures.

### 2.2.4 MARC

MARC is a general purpose program for the linear and nonlinear static and dynamic analyses for 2D and 3D structures. The program consists of

three different libraries: element, material, and structural library. The element library contains over 60 elements. The material library has 35 different models. The structural library contains 15 structural procedures. The user may combine any components from any of the three libraries. Some program features are tying DOF, joining shell and solid elements, and user supplied constraints. Modal and proportional damping and lumped masses can be used in dynamic analysis.

### 2.2.5 NISA

NISA is a general purpose program for the linear and nonlinear analysis of 2D and 3D structures. The heat transfer capabilities include both steady-state and transient heat conduction analyses. Dynamic analysis features include natural frequency and mode shape, and linear transient analysis. Modal damping is included. Other capabilities are earthquake analysis, shock spectrum analysis, and harmonic analysis. The material models included are: linear elastic, orthotropic, nonlinear elastic-plastic, and nonlinear elastic incompressible. Lumped or consistent masses may be used in the dynamic analysis.

### 2.2.6 WECAN

WECAN is a general purpose program for the linear and nonlinear static and dynamic analyses of 2D and 3D structures. Heat transfer capability is included in the program. Some dynamic capabilities are natural frequencies, response spectra analysis, and seismic analysis. Lumped and consistent mass matrices may be used. Fluid-structure interaction problems may be handled and piping system analysis is possible.

## 2.3 Code Verification Sample Problems

### 2.3.1 Flat Plate and Cylindrical Roof Sample Problems

In the previous section of this report six codes were presented. The 1978 version of ADINA[20] is installed on the computer at INEL and is available for use. The decision was made to solve some large deflection

sample problems to demonstrate the solution capability of the 1978 ADINA code. If this version was found to be acceptable then substantial cost savings would be available since the acquisition of another code, as identified in Table 4, would not be necessary.

Large deflection sample problems are difficult to find. Two simple problems were run on the 1978 ADINA. The first problem was a simply supported square plate under a uniformly distributed pressure loading. (This problem is verification problem No. E4.2 of the MARC computer code originally presented in a paper by Levy.[21]) The displacement results from 1978 ADINA compared to within 2 percent of the results from MARC and also the theoretical solution by Levy. The solution by Levy is considered to be exact since it is a solution to the actual governing differential equation rather than an approximate method, i.e., variational methods or finite element techniques. The accuracy of the solution is supported by the fact that finite element solutions using two independent codes, ADINA and MARC, yielded the same results. The maximum center deflection from ADINA for a 0.345 MPa (50 psi) uniform pressure was 10.3 mm (0.406 in.) compared to 10.5 mm (0.413 in.) as reported by Levy. The plate thickness is 6.35 mm (0.25 in.) so the deflection was considered large. Therefore, the large displacement capability of 1978 ADINA was demonstrated for this problem.

The second problem was the Scordelis-Lo cylindrical roof with dead weight loading. This problem has been used as a benchmark for several computer codes. A schematic of the problem and the convergence performance of several commercial plate and shell elements are shown in Figures 19 and 20 (see Reference 22). The author of Reference 22 did not include ADINA in his study. In this work the roof was modeled using 8-node and 16-node thin shell elements of the 1978 ADINA. The predicted deflection at the midside of the free edge was only about 2/3 of the theoretical solution value. The theoretical value was also verified by the use of several other codes. After an independent in-house review and consultation with the authors of ADINA, no reason for the difference in results could be determined.

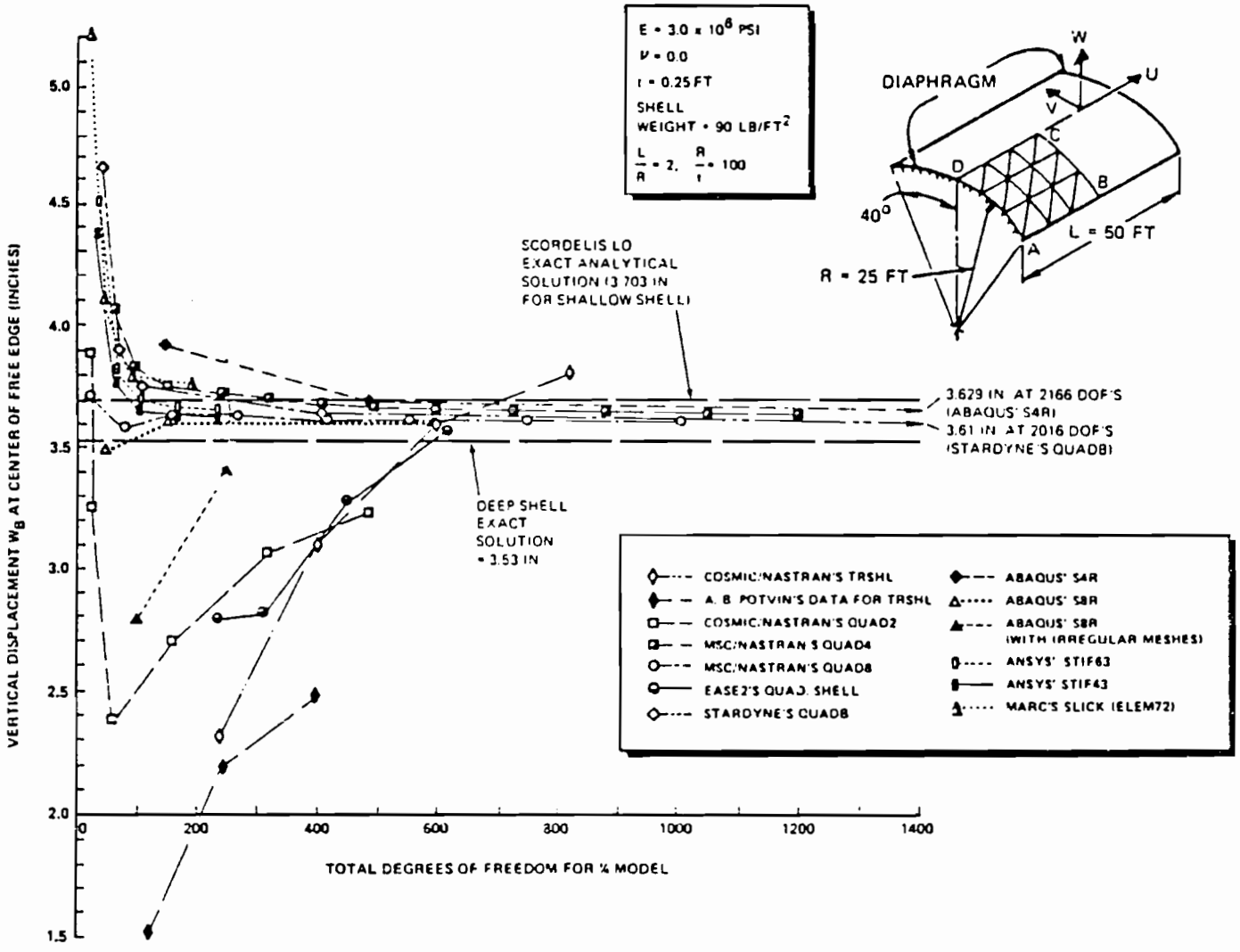


Figure 19. Convergence performance of codes evaluated in this study.

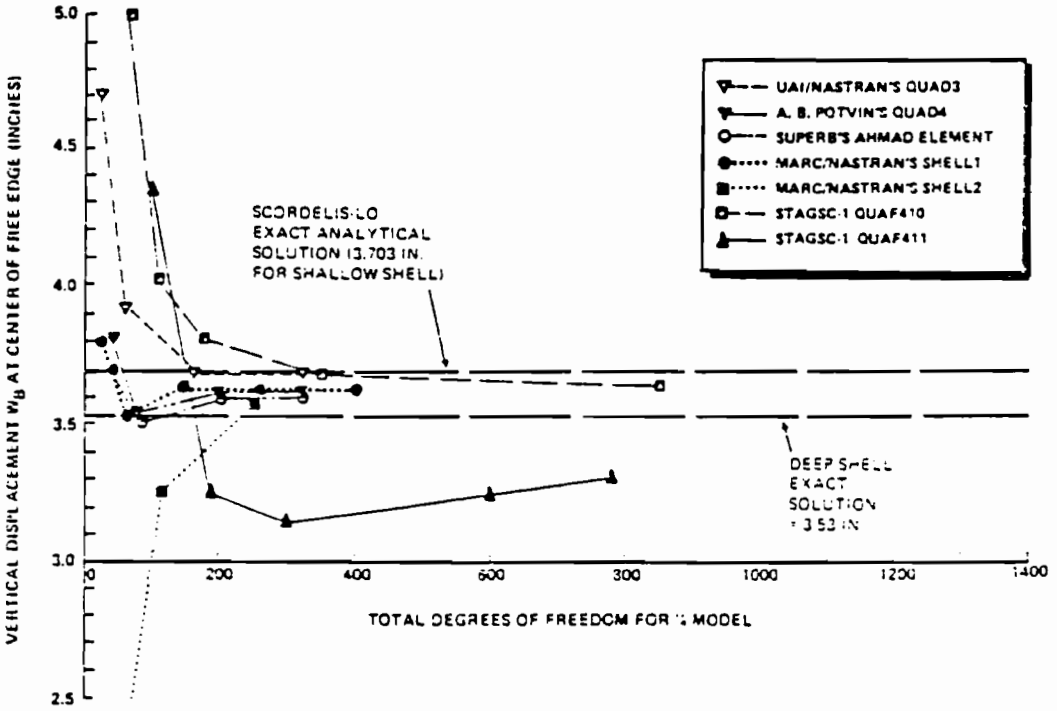


Figure 20. Convergence performance of other codes.

These two sample problems are applicable to the tank car analysis. The flat plate problem simulates the end of the tank car. The cylindrical roof problem simulates the cylindrical portion of the car. If the candidate computer code is able to solve these two types of geometry then there is a high probability that the code can perform the tank car analysis.

Consideration is now being made at the INEL to purchase the latest version (1984) of ADINA through other sources of funding. Discussions with ADINA Engineering personnel indicated that the current version should provide an accurate solution to the cylindrical roof sample problem. If the current ADINA is purchased these sample problems will be run again.

Another problem, a cylinder with opposing concentrated loads (see Figure 21), has been solved by an outside vendor using ABAQUS. This problem simulates a point load on a cylindrical tank so it is directly applicable to the tank car analysis. These results are included in the next section of the report and can be used as a final check for the code chosen for the tank car analysis.

### 2.3.2 Pinched Cylinder Sample Problem

An inelastic analysis using the ABAQUS computer code of a pinched cylinder, as shown in Figure 21, was subcontracted to Control Data Corporation. ABAQUS was chosen for this solution since it is considered by people in the structural computer code business to have the most modern solution techniques incorporated into the code. Also, ABAQUS is considered to have the most capability to solve large deflection-large strain problems (reportedly up to about 10 percent strain). The dimensions of the cylinder and boundary conditions are shown in Figure 21. The material in this problem was assumed to be elastic-perfectly plastic with a Young's modulus of 207,000 MPa (30 million psi) and a yield strength of 207 MPa (30,000 psi). (The ABAQUS code also permits the use of a material with strain hardening.) The finite element model is shown in Figure 22. The model was constructed using the S8R rectangular general shell element. This element has eight

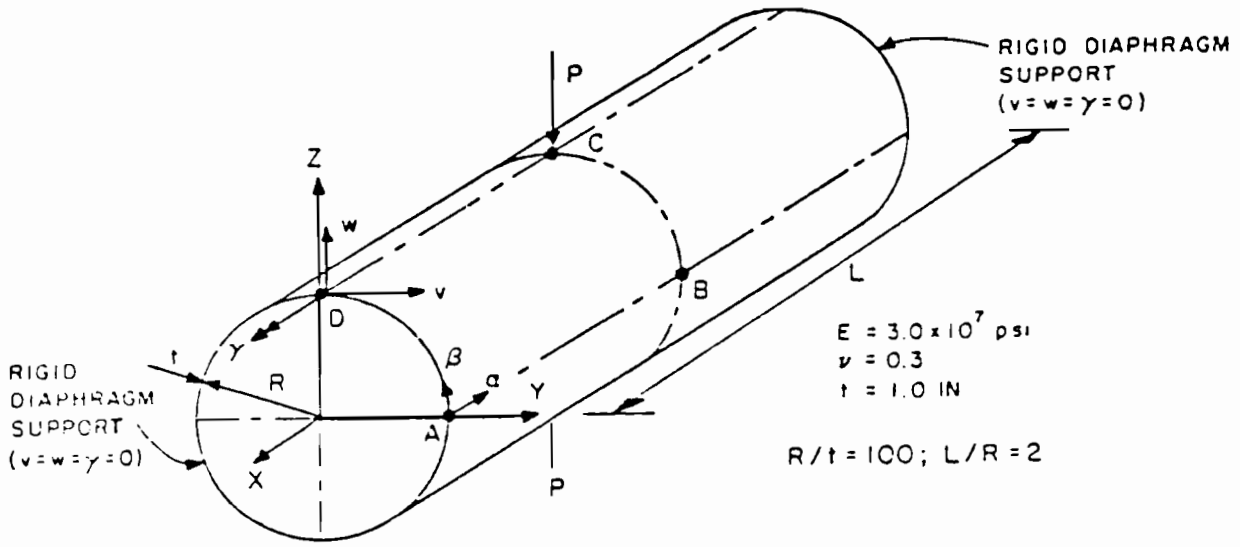


Figure 21. A pinched cylindrical shell.

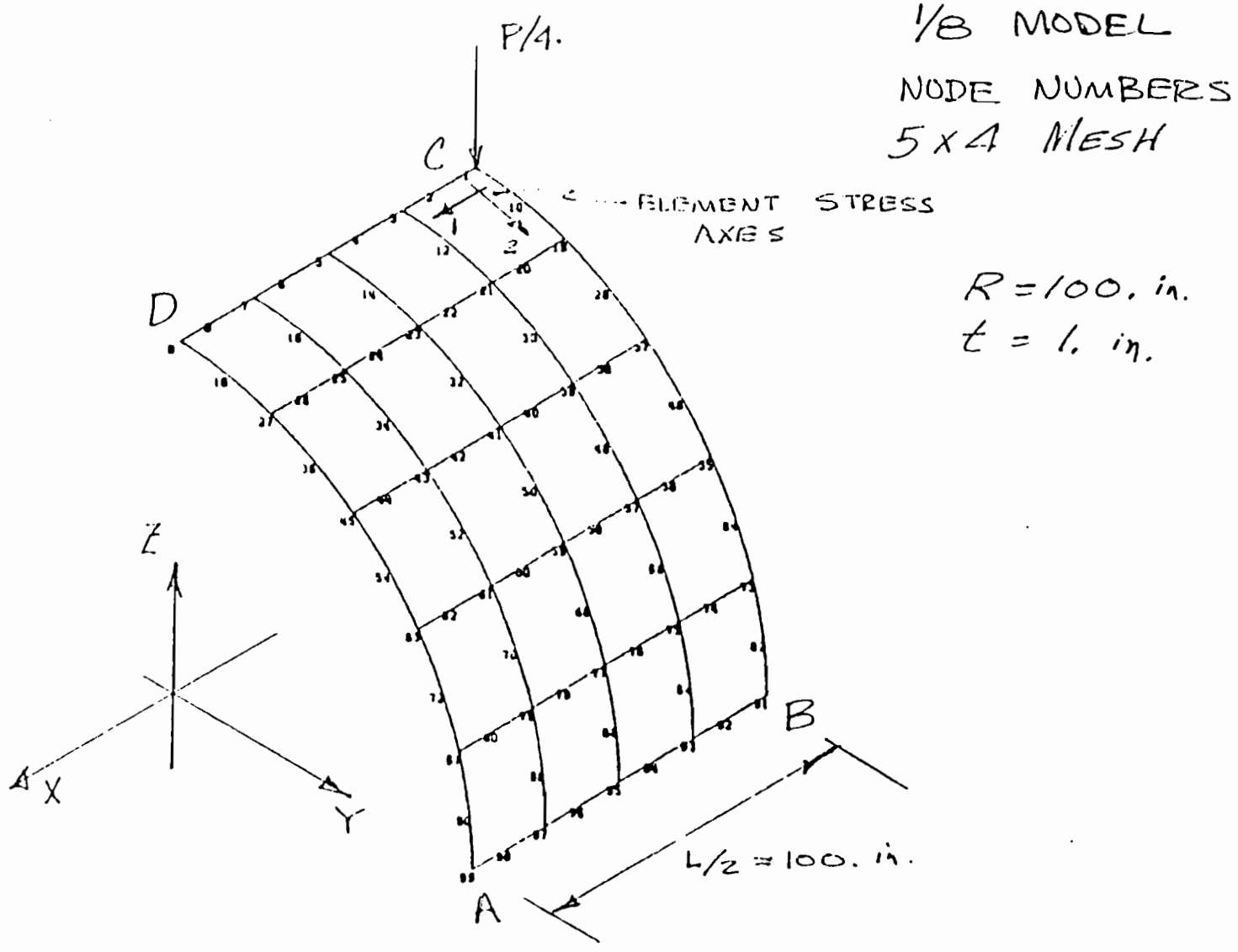


Figure 22. Finite element model of a pinched cylindrical shell.

node points, all of which are at the shell mid-plane. Stresses and strains are calculated at four integration points inside the element. In this analysis nine output locations were specified through the shell thickness. Only the stress at the outer surface of the shell was printed in the output in order to reduce the amount of computer output. Sufficient information was obtained, however, to assess the capability of ABAQUS to solve this problem. Displacements were calculated at the mid-plane integration points and then extrapolated to the node points by the ABAQUS code.

Three cases were run. They were (1) an elastic analysis, (2) an inelastic analysis using small displacement theory, and (3) an inelastic analysis using large displacement theory. The displacement results for these three cases are shown in Figure 23. The results using the large displacement theory are the most realistic results since the geometry is continually updated during the solution. It is interesting to note the large difference in displacements given by large and small displacement theories.

Initial yielding of the shell near the load occurred at a load of just over 31,818 kg (70,000 lb). The displacement at this load was 9.14 mm (0.36 in.). As the load was increased the area of the shell reaching yield increased. At the end of the solution convergence problems occurred because the load versus deflection curve had become nearly flat. The additional displacement for a small increase in load was more than the amount that the ABAQUS code allowed. When convergence problems occur the code decreases the load and attempts to perform a solution using the smaller load. If the solution does not converge the process is repeated a few more times. If convergence still does not occur the program stops. The load and deflection at the end of the solution were 55,618 kg (122,360 lb) and 52.43 mm (2.064 in.), respectively.

Although much larger displacements are expected in the tank car analysis, it is felt that ABAQUS can perform the solution to the inelastic analysis. No strain hardening of the material was considered in this

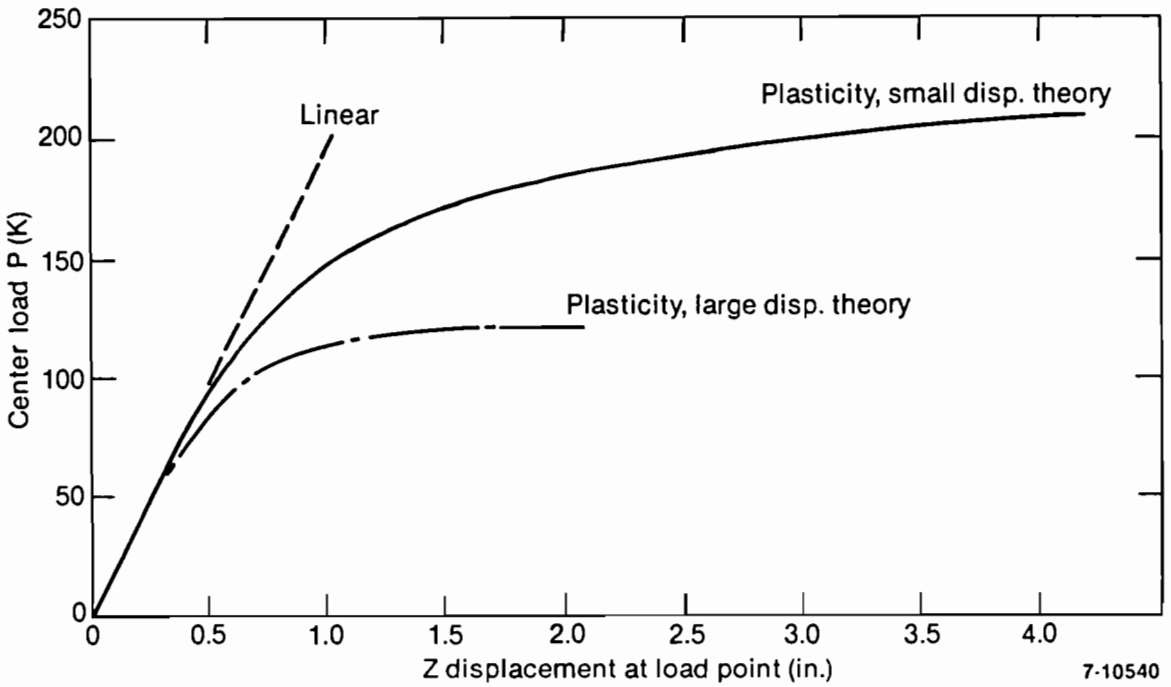


Figure 23. Displacements of a pinched cylindrical shell.

sample problem. The addition of strain hardening would cause the load versus deflection curve to have more slope and, therefore, convergence problems would be less likely.

It was originally intended to perform this solution on ANSYS in addition to the ABAQUS solution presented above. Due to funding difficulties the ANSYS solution was not obtained. It is recommended that this solution be obtained in order to provide a better basis for selecting the appropriate large deflection computer code.

There is no known solution to this problem. The only ways to verify that this ABAQUS solution is correct is by one of the following methods:

1. Conduct analyses using other codes. (If other codes are used but different solutions are obtained there is no way to identify which solution is correct.)

2. Perform experiments to verify that the solution is correct.

3. Continue the search for another verified solution.

## 2.4 Solution Methodology

The details of the finite element model to be used in the analysis will be discussed, along with the analysis type, element type, and material properties. Material property data required for the analysis will be identified. The solution catalog will also be discussed. Since there is no verified computer code currently available at the INEL to perform this solution and since we are considering the purchase of the 1984 version of ADINA, the analysis details will be written assuming that the 1984 version of ADINA will be used in the analysis. The capabilities of the code are contained in the user's manual.[23] The user's manual also contains some recommendations for using various features of the code, i.e., the type of shell element which gives the best results. These recommendations will be mentioned where applicable. If another code is used for the analysis, the capabilities of other codes are probably

sufficiently similar to ADINA that changing to another code would not cause any serious difficulty.

### 2.4.1 Analysis Type

The time in which the damage occurs to the tank car and the time in which the lifting operation is performed will probably be much longer than the lowest natural period of the tank car. Therefore, a step-by-step nonlinear static analysis will be adequate and no dynamic effects will be considered.

### 2.4.2 Element Type

The shell element will be used to perform the analysis. ADINA contains two different shell elements including a 3-node triangular shell element and a variable (4 to 32) node rectangular shell element. The authors of ADINA recommend the use of either the 4 or 16 node element having all of the nodes located on the shell mid-plane. A model constructed using the 4-node elements would require more elements to define the tank than a model constructed using 16-node elements. The 16-node elements use a higher order integration scheme which is more expensive. It is recommended that the 4-node element be used in order to keep the model as simple as practicable and to keep computer costs down.

It may be desirable to be able to determine the amount of thinning of the material in the damaged region. The 4-node shell element will not calculate the strain in the thickness direction because the normal stress in that direction was assumed to be zero in the element formulation. This assumption is also made for the higher order shell element which have nodes on both the top and bottom surfaces of the element. Regardless of the computer code used, the only way to find the strain in the thickness direction is to construct the finite element model from 3-D continuum elements. More than one element through the thickness direction would probably be required, therefore, increasing the number of elements in the model and also the computer time required. It is possible to model most of the tank car with shell elements and local regions with 3-0 continuum

elements using 1984 ADINA. Transition elements are used to connect the two different element types together. This method would allow finding the amount of thinning without increasing the model size and computer cost greatly.

### 2.4.3 Material Properties

Permanent deformation of the tank car occurs during an accident. The metal is stressed above its yield stress. Elastic strain rebound occurs after all of the energy from the accident is absorbed by the deformed region of the tank car. The elastic rebound is a small portion of the total strain caused by the accident since the yield strain of typical varieties of steel is only about 0.2%. Residual stresses are now present in the permanently deformed region. These residual stresses depend on the amount of permanent deformation, i.e., the maximum stress (or strain) in the material during deformation.

Stress versus strain curves (including strain hardening) for the original and deformed portions of the tank car are required to perform the stress analysis. Some of the data to be used to construct this curve for the deformed material is contained in Reference 24. The stress versus strain curve for the original material can be found from appropriate tests. Different material properties will be assigned to the damaged and undamaged portions of the tank car model.

The ADINA computer code does not permit the change of material properties of shell elements during the solution of a problem. Therefore, it is proposed to use the actual stress-strain curve for the deformed material with a yield stress corresponding to the maximum strain expected for the particular case being considered. (The variation of yield stress versus permanent strain is reported in Reference 24.) This technique should give the best estimate of the residual stresses.

### 2.4.4 Solution Catalog

Inelastic analyses of several different accident conditions will be required to create a catalog of solutions. Some of the major variables to be considered in the analysis are tank car design, tank car material, damage location, lifting method, and permanent deformation amount. Each one of these variables should be varied separately.

## 2.5 Summary

Railroad tank cars may become severely damaged during accidents. Moving a car containing hazardous materials safely is mandatory. Residual stresses and enhanced collapse modes due to deformation are present in the damaged area of the car. Additional stresses caused by lifting or moving can combine with these residual stresses and rupture or collapse the tank.

A methodology for the inelastic stress analysis of these tank cars is presented in this report. A special purpose, large displacement, large strain computer code is required to perform the stress analysis since a large amount of permanent deformation may occur to the tank. Many computer codes are capable of performing a small strain (less than about 2 percent) inelastic analysis but much larger strains are expected for the tank. A survey of computer codes identified only six codes having the capabilities required. They are ABAQUS, ANSYS, ADINA, MARC, NISA, and WECAN. The costs of purchasing or leasing these codes are substantial. The least expensive code to purchase is ADINA ($26,000). The least expensive code to lease is ANSYS ($1000 per month for a minimum 12 month lease). (A personal computer version of NISA has just become available at a cost of $5,000 but it is felt that a model with sufficient detail would not fit on a personal computer.)

An earlier (1978) version of ADINA is available on the INEL computer system. Two verification problems were run on this code to assess its adequacy for use in the tank car analysis. A good comparison of results for a large deflection analysis of a square plate was observed between the results obtained using the 1978 ADINA and MARC. However results for a

large deflection analysis of a cylindrical roof obtained from the 1978 ADINA did not compare well with results from several other codes. The 1978 ADINA, therefore, may not be acceptable for use in the tank car analysis. Another problem, a cylinder with a concentrated load, has been solved by an outside vendor using ABAQUS. The results from this vendor solution are included in the report and can be used as a final check for the code chosen for the tank car analysis. The purchase or lease of one of the six codes is recommended for this solution. The chosen code must be verified before its use.

A discussion of details of the stress analysis finite element model are presented. Several different inelastic analyses will be required because of different tank car designs, tank car materials, damage locations, and lifting methods. A catalog of these solutions will then be used by personnel at the accident site to determine the safest method to be used in moving or lifting the damaged car.

There are six codes available which offer a high probability of solving the tank car problem. They are ABAQUS, ANSYS, ADINA, MARC, NISA, and WECAN. The 1978 version of ADINA did not accurately solve a problem with cylindrical geometry and a uniform loading. A pinched cylinder problem was solved using ABAQUS, but the results were not compared to results from any other type of solution. The ABAQUS solution does show that the code can perform this type of analysis. One of the six codes listed above (including the current version of ADINA) should be considered for the analysis. Once a code is chosen it is necessary to verify that it is producing correct results. The verification may be done by comparing results against those obtained from other codes, experiments, or analytical solutions. ABAQUS is probably the best code to perform the tank car analysis because it has the most modern solution techniques and also has a high strain (10 percent) capability. Further, the methodology presented in this report can result in a catalog of solutions which, in turn, can allow the safe transport of damaged tank cars.

# 3. EVALUATION OF DAMAGED TANK CAR STRUCTURAL INTEGRITY--HYDROSTATIC BURST TESTS OF DAMAGED 1/5 SCALE RAILROAD TANK CARS

## 3.1 Introduction

The purpose of this study is to determine if a correlation exists between the derailed tank car damage, caused by a coupler striking the tank head, and the hydrostatic burst pressure of the tank. Twelve 1/5-scale-model tank cars were impacted by the Ballistic Research Laboratory (BRL) several years ago for the purpose of simulating damage done to an actual full size tank car during a derailment. These tanks were provided to EG&G Idaho, Inc., under contract to the Federal Railroad Administration, for performance of hydrostatic burst tests on selected tanks.

The cylindrical tanks, with domed heads, were approximately 366 cm long, 55.9 cm in diameter, and made of 0.318 cm thick carbon steel. A sketch in Figure 24 identifies the dimensions, configuration, and materials. Some tanks were covered with a 0.953 cm coating of insulation and all had at least one indented or punctured end.

The purpose of these burst tests was to correlate the type of mechanical damage with the burst test data. The damage done to the tanks was assessed using NDE techniques; visual, liquid penetrant, and ultrasonic examinations were performed to measure the deformation, surface cracks and penetrations, and thickness, respectively. The tanks required rebuilding because all had at least one punctured end. The rebuilding of the tanks resulted in four usable tanks, two of which were instrumented and burst tested. The dented end of each of the tanks was instrumented using strain gauges and acoustic emission sensors, in addition to the tank's pressure transducer. The tanks were filled with water and hydrostatically burst tested to failure using a positive displacement pump.

## 3.2 Assessment of the Tank Damage

Some of the tanks had an outer skin of insulation. The insulation was examined and found to contain no asbestos and, therefore, posed no safety

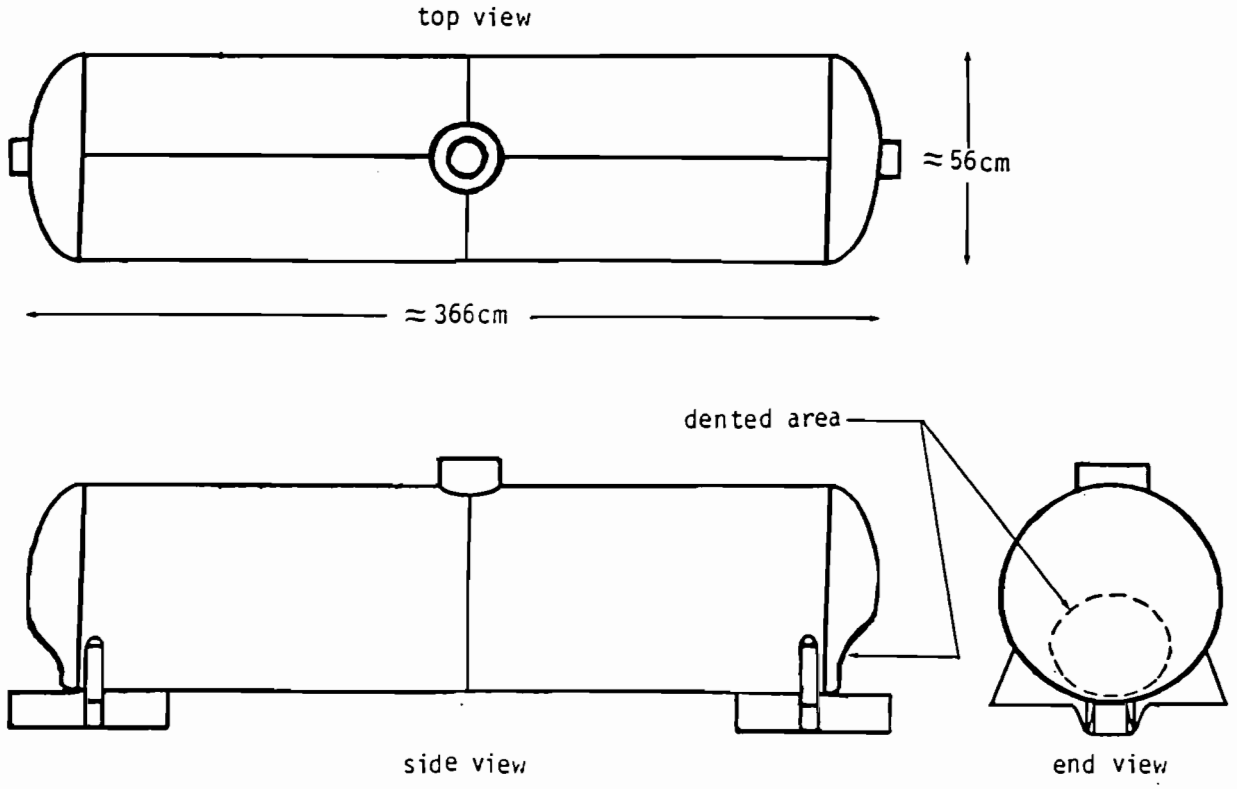


Figure 24. Dimensions and configuration of the tanks.

hazard. Some insulation and paint were removed in order for the damage on the tanks to be assessed with NDE techniques. The insulation was chipped off and the paint removed by lightly glass-bead blasting the necessary areas. It was found by earlier experiments with the 68 BRL plates that lightly glass-bead blasting the dented areas did not mask the surface cracks; therefore, the results of liquid penetrant examinations of the damaged area were valid.

Visual, liquid penetrant, and ultrasonic examinations were conducted on both surfaces of the head to determine the extent of damage. A Magnaflux Dual-Purpose Penetrant Test System was used for the liquid penetrant examinations. This is a specialty penetrant system which combines the flaw detection capabilities of both the color contrast and fluorescent penetrant systems. This system gave the best resolution out of several penetrant systems tested. The liquid penetrant examination procedure used is described in Appendix A. Wall thickness measurements were made using a longitudinal wave (compressional wave in which the particle motion or vibration is in the same direction as the propagated wave) ultrasonic thickness gauge. The maximum amount of wall thinning was approximately 12.5 percent.

The damage on these tanks was confined to the ends, with varying severity of dents, and in some cases, the damaged end had been penetrated. On those dented areas that were not penetrated and on those that were penetrated, no surface cracks were found. In all of the tanks, however, at least one end had been penetrated and in some cases both ends. Therefore, the tanks had to be rebuilt in order to perform the burst tests.

## 3.3 Reworking of the Tanks

On those tanks with one head penetrated, the penetrated ends were cut off. There were enough unpenetrated ends to fabricate four tanks for the burst tests. All of the girth and longitudinal welds of the remaining pieces of tanks were examined using liquid penetrant and radiography to determine the integrity of the welds. The less critical welds at flanges and leg supports were examined visually. No surface cracks were found by

the liquid penetrant examinations. Radiography revealed areas of small porosity, melt-through, tungsten inclusions, and undercut, all of which are acceptable under Section VIII, Division 1, Paragraph UW-51, "Radiographic Examination of Welded Joints", of the ASME Boiler and Pressure Vessel Code. These acceptable end pieces of the 1/5 scale model tank cars were matched and welded together so as to provide four tanks for the hydrostatic burst tests. One new girth weld was required per tank in constructing the four tanks. This weld was of acceptable quality, as evaluated by radiography, and considered to be as good as or better than the original welds on each tank. These new welds did not fail during the burst tests.

## 3.4 Instrumentation of Tanks

Since the behavior of the dented area of each tank was being studied, only the damaged end of each of the tanks was instrumented. A pressure transducer was used, as shown in Figure 25, to indicate the pressure applied during the burst tests. In addition to measuring the pressure during the burst tests, the damaged end of each tank was instrumented with strain gauges and acoustic emission sensors. The strain gauges consisted of a normal elongation, three channel rosette strain gauge located on an undamaged area of the dented end and three high-elongation (20%), three channel, rosette strain gauges located in the area of the dent as shown in Figure 26. Figure 27 shows the locations of the strain gauges. Four acoustic emission sensors were positioned in a rectangular pattern so as to use a planar scheme to locate cracking within that rectangular pattern on the damaged end of each tank (see Figure 28). Figure 29 is a schematic of the acoustic emission testing setup. Also, a video tape was used to document each burst test.

## 3.5 Hydrostatic Burst Tests

After each tank was instrumented, it was hydrostatically tested to failure using a positive displacement pump. The dented areas of the tank ends nearly returned to their original shape and the radius of the undamaged cylindrical section of Tank #410A increased in radius from 27.9 cm to approximately 35.6 cm (see Figure 30).

Figure 25. Pressure transducer used for the burst tests.

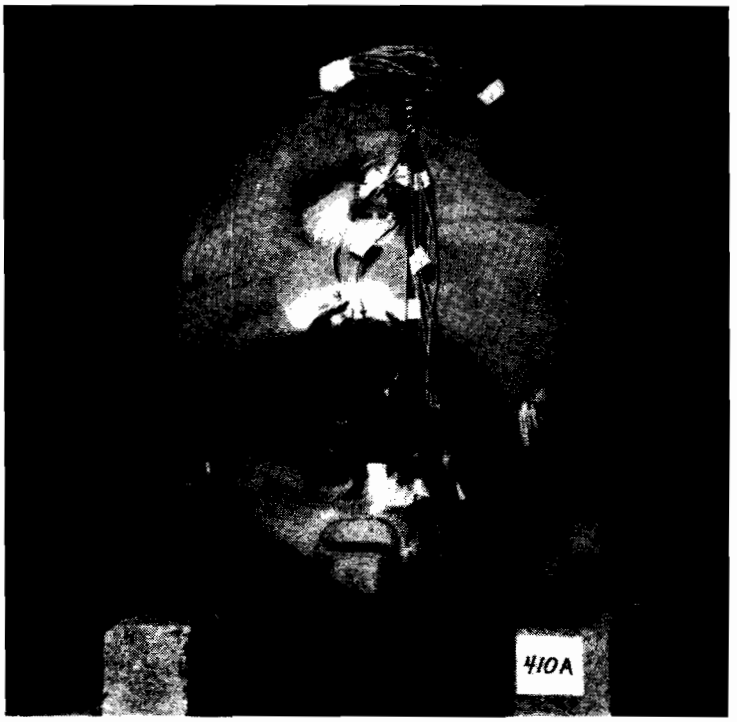


Figure 26. Locations of strain gauges used on Tank #410A.

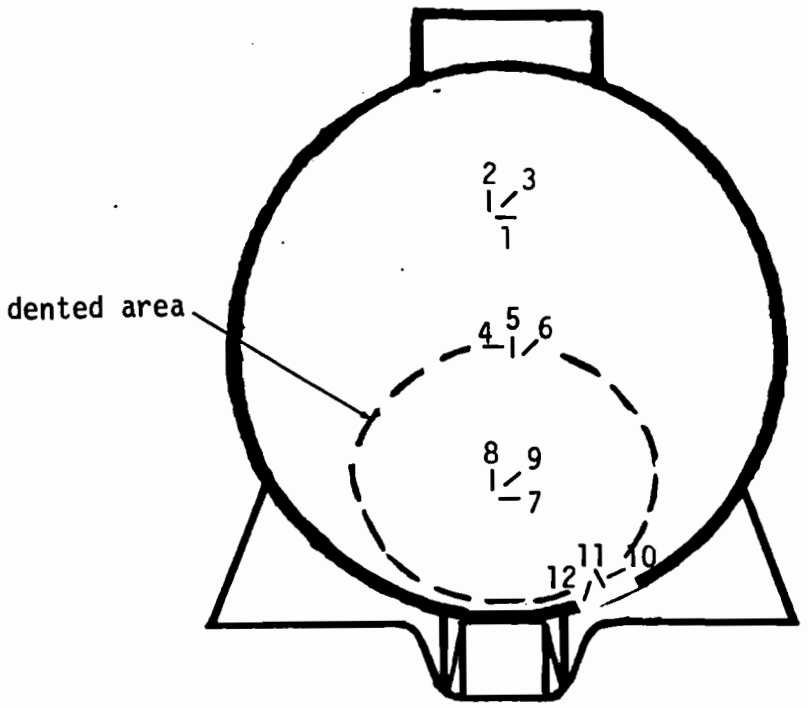


end view

Figure 27. Locations of the strain gauges.

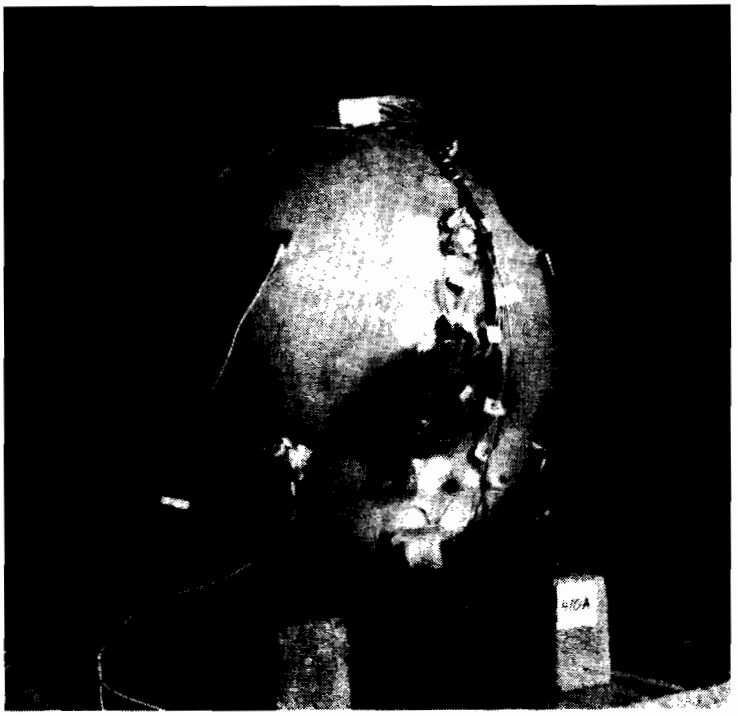

Figure 28. Locations of acoustic emission sensors on Tank #410A.

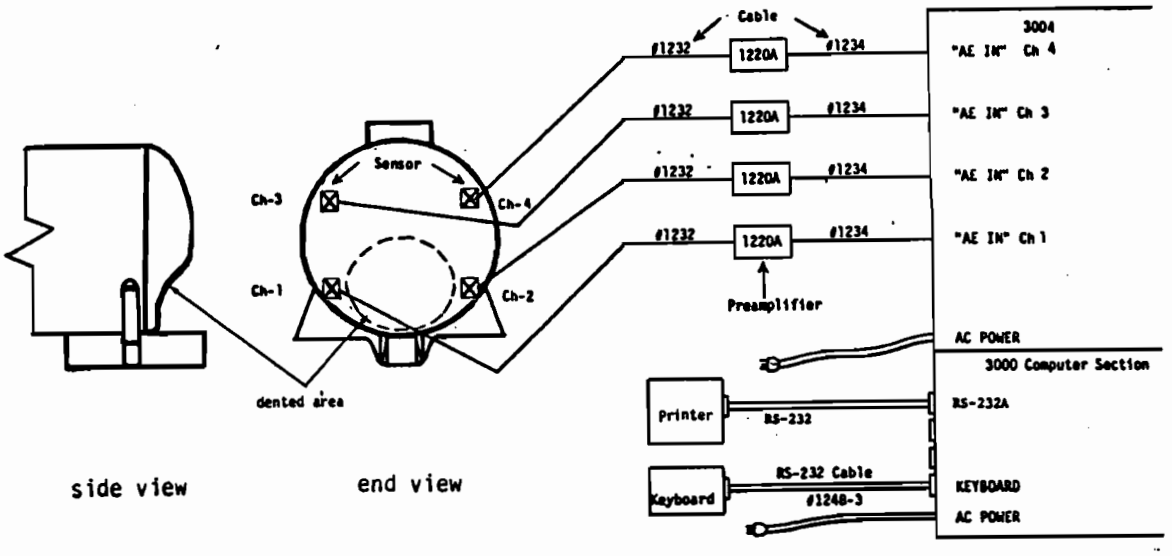


Figure 29. Acoustic emission setup.

Figure 30. Increase in radius of undamaged cylindrical section.

The tanks did not fail in either the area of the damaged ends or new welds made during rebuilding. Failure occurred at original welds on the undamaged cylindrical sections of the tanks. Tank #410A failed at the weld that attaches the leg support to the tank (see Figure 31) and tank #401A failed in the weld joining the flange and cylinder (see Figure 32). Because both tanks failed in locations other than damaged heads, the other two of the four available tanks were not tested since it was assumed that they would behave in the same manner.

## 3.6 Analysis of Hydrostatic Burst Test Results

Failures occurred at the welds of the leg support on Tank #410A and the flange on Tank #401A. These welds were not radiographed because of the geometry and large difference in thickness between the flange and tank material. Failure at these locations could be due to: excessive porosity, cracks, incomplete fusion, incomplete penetration, slag inclusions, etc. Using a simplified approach of the applied stress (J) equals Pr/t where r ranged from 27.9 to 35.1 cm for Tank #410A, the nominal hoop stress ranged from 166 to 248 MPa. This stress is assumed to be less than the ultimate tensile strength for the weld and the base metal. But a simplified estimate may be made from the increase in radius from 27.9 to 35.6 cm that the nominal strain at failure was 27%. The elongation suggests that the fracture did not result from a fracture mechanics mechanism, but was probably due to plastic overload. The same is very likely true for Tank #401A, but a failure analyses was not performed because the substantial deformation suggested that the tank did not behave similarly to a full scale tank car.

The wall thickness (0.318 cm on the 1/5 scale models reduced from 1.59 cm on an actual tank car) of the tanks contributed to the tests not simulating the behavior of a damaged tank car. The type of damage on the thin wall tanks did not simulate the type of damage that would be observed on the thicker walls of an actual damaged tank car. The extent of surface cracks and wall thinning on the thinner material was much less than that of

(a)

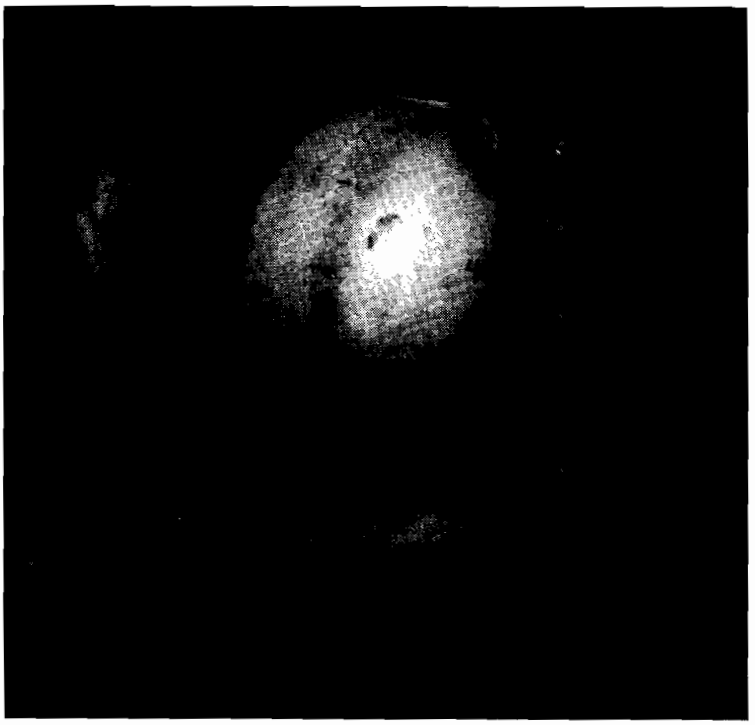

(b)

Figures 31. Location of rupture on Tank #410A.

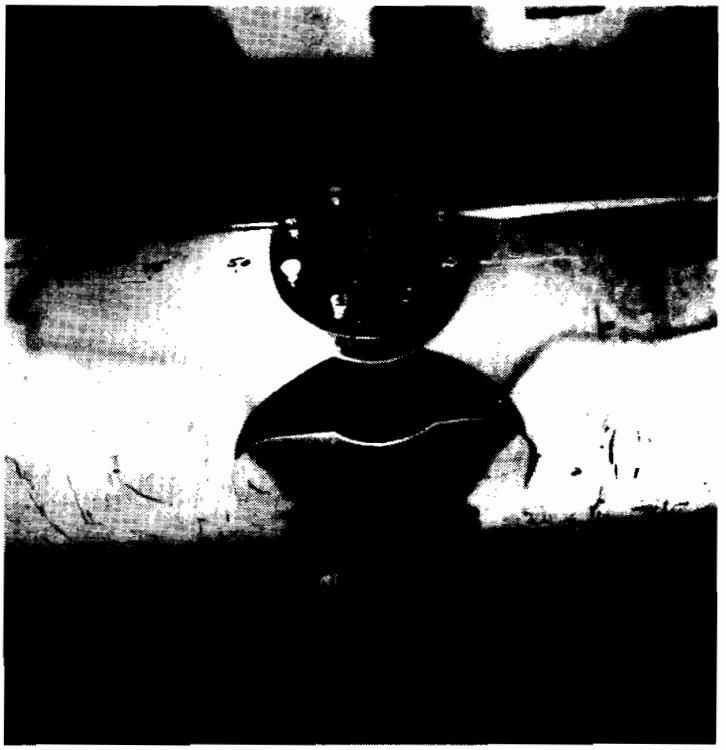

(a)

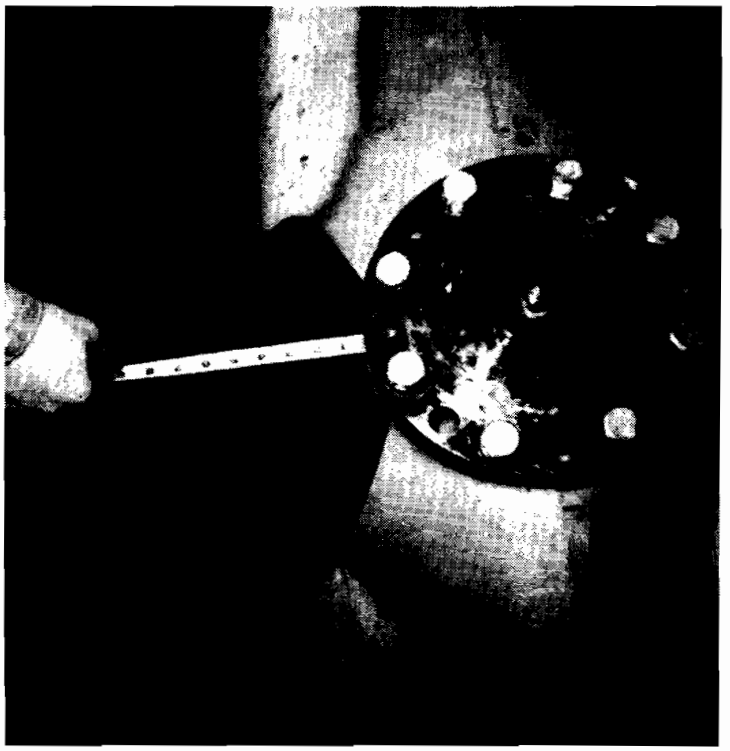

(b)

Figure 32. Location of rupture on Tank #401A.

the thicker material of an actual damaged tank car. Also, the smaller wall thickness (0.318 cm) behaves differently ("oil-canning") when put under a stress than the larger wall thickness (1.59 cm) of an actual tank car.

Useful information was obtained during the burst tests. The pressure transducer data shows the types of stresses involved. The strain gauge data shows the "oil-canning" effect that the burst test had on the damaged zone of the tanks. The acoustic emission system collected data during the oil-canning of the tanks, but did not pinpoint the location of rupture because the point of rupture did not occur within the instrumented area.

### 3.6.1 Pressure Transducer Data

Using the pressures recorded during the hydrostatic burst test, a stress versus elapsed time plot was generated for each tank. The axial stresses were calculated using the equation:

$$\text{Stress (MPa)} = (P \cdot R)/(2 \cdot t)$$

where P is the pressure measured by the pressure transducer (MPa), R is the cylindrical radius of the tank (cm), and t is the wall thickness of the tank (cm).

Figure 33 shows stress versus elapsed time for Tanks #401A and #410A. The figure shows that Tank #401A ruptured at a stress of approximately 200 MPa and Tank #410A ruptured at a stress of approximately 197 MPa. The figure does not show the failure portion of the test because the time required to conduct each test was approximately two hours. Once the peak pressures, shown were obtained they remained constant even though pressurization continued throughout the test. Therefore, the stress increased only due to the change in radius, but the failure strain was substantial for each test. The average failure strain for Tank #410A was 27.6% and lower for the other tank.

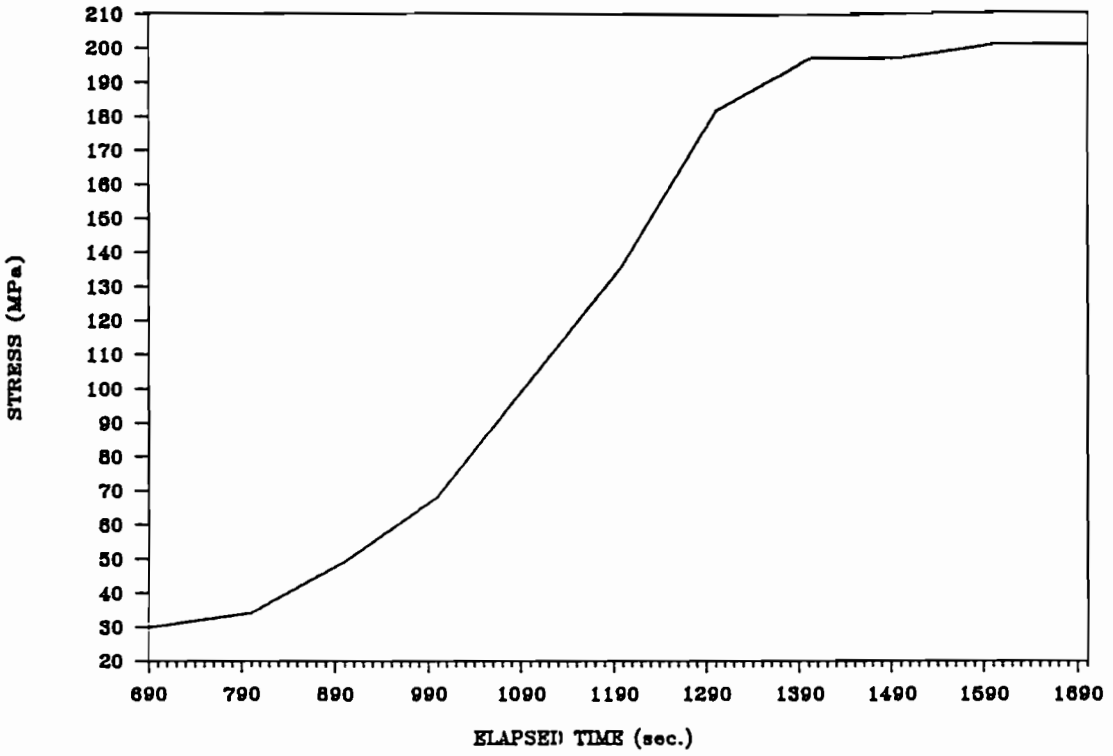


(a)

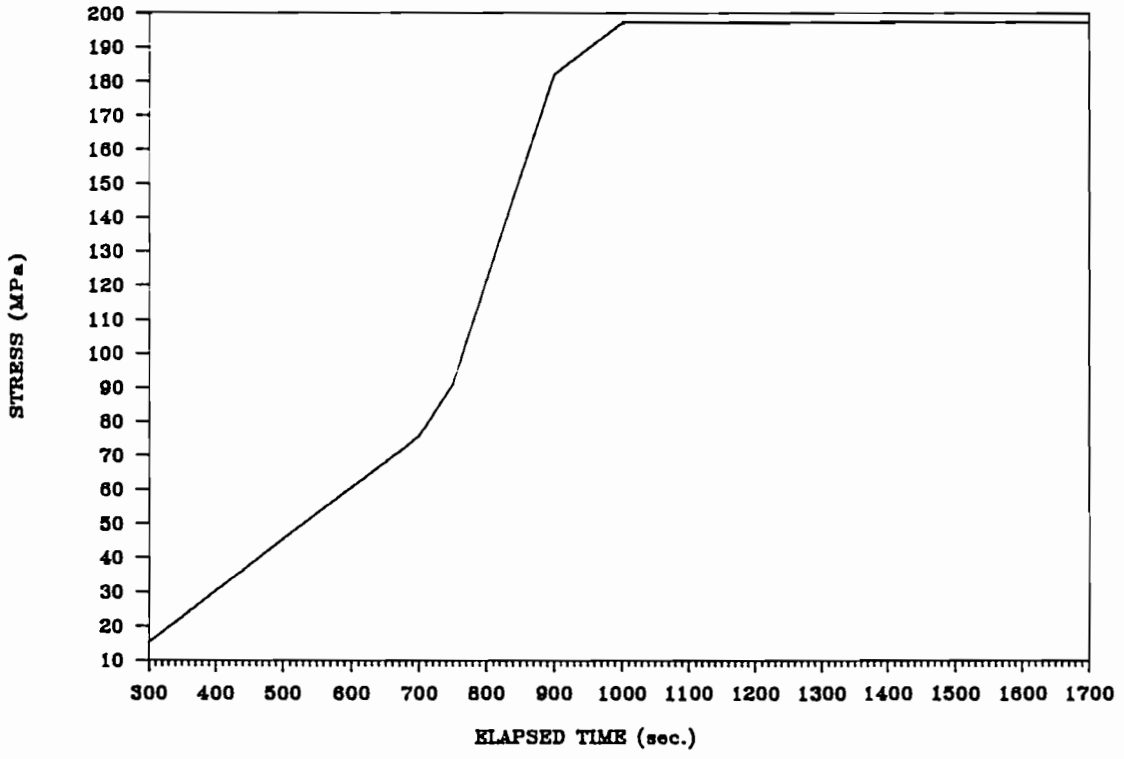


(b)

Figure 33. Axial stress vs. elapsed time for Tanks #401A and #410A.

### 3.6.2 Strain Gauge Data

The recorded strain gauge data indicated the displacement of the material in different locations in the area of the dent during the burst test. The figures in Appendix B show the displacement of the material at the locations of the strain gauges on Tanks #401A and #410A, respectively, while the dents returned to their original shapes. These figures are plots of strain versus pressure and show the "oil-canning" effect that the burst test had on the damaged areas of the tanks.

The strain gauges were located in or adjacent to the damaged region in the dome, see Figure 27, since this is where failure was expected if the 1/5 scale tanks represented the conditions of an actual tank car. Since the failures occurred in the cylindrical portion of the tank at a substantial distance from the damaged areas, the strain gauge data are of limited use. The results for Tank #401A are summarized as follows:

- Gauges 1-3, the strain ranged from 3% to 5%.
- Gauges 5-7, the strain was initially compressive due to the damaged area being forced back to its original position at which time some tensile strain (reduction in compressive strain) occurred.
- Gauges 8-10, substantial peak strains on the order of 40%-50% occurred followed by decreasing tensile strain.
- Gauges 11-12, substantial compressive strains of nominally 65% were observed.

The peak strain of 40%-50% observed for Gauges 8-10 is considerably greater than the average value associated with failure in the cylindrical section. At this time it is not possible to explain why Gauges 8-10 showed the substantial decrease in tensile strain.

### 3.6.3 Acoustic Emission Data

The acoustic emission technique used was a rectangular planar location scheme that locates flaws, during the burst test, within the rectangular area formed by the four sensors. The location technique is based on triangulation using the difference in the time of arrival of the acoustic emission signal at the four sensors. Because the location of the rupture was outside of this rectangular area, this scheme did not pinpoint the location of rupture. The technique is capable of locating the source even under these conditions, but the specific equipment used had a boundary for accepting/rejecting signals. Some data were collected, however, during the "oil-canning" of the damaged areas of the tanks. Other schemes and/or more than one acoustic emission system are recommended in future burst tests to better locate the point of rupture.

## 3.7 Summary

The tanks did not fail at the damaged areas. Instead, failure occurred at original welds on the undamaged cylindrical sections of the tanks. Since the first two tanks failed in locations other than the instrumented areas, only two of the four available tanks were tested.

The type of damage on the thin wall tanks did not simulate the type of damage that would be observed on the thicker walls of an actual damaged tank car. Useful information about the 1/5-scale tanks was collected during the burst tests. The pressure data shows the types of stresses involved: one tank ruptured at a stress of 200 MPa and another ruptured at a stress of 197 MPa. The strain gauge data shows the "oil-canning" effect that the burst test had on the tanks. The acoustic emission system collected data during the oil-canning of the tanks but did not pinpoint the location of rupture because the point of rupture did not occur within the instrumented area.

# 4. APPLICATION OF MOIRE INTERFEROMETRY

## 4.1 Introduction

Moire interferometry was utilized, in a joint preliminary, effort by the Idaho National Engineering Laboratory (INEL) and the Association of American Railroads (AAR), as a novel alternative for determining residual stresses of railroad components such as wheels and rails subject to time elapsed wear. Unlike traditional strain gages, which are by nature discrete and average over their gage length, moire interferometry yields full-field in-plane displacement on the free surface of the specimen.

## 4.2 Test Results and Discussion

The sensitivity to in-plane displacement utilized for this study was approximately 33 mm; in-plane displacement sensitivity can be as great as 0.2 mm if desired. The 33 mm sensitivity was chosen because of the large amount of residual displacement expected from sectioning the rail components (roughly 0.2 in. closure after a saw blade cut on a 33 in. diameter wheel). Moire interferometry (diffraction) gratings were applied to a test wheel at the FRA Transportation Test Center in Pueblo, Colorado. The grating was protected and the wheel was sectioned. The sectioned pieces were then sent back to the INEL where the moire grating could be interpreted. The results to be presented are considered extremely preliminary as much of the technique for this application was worked out during this small-scale effort.

Figure 34 shows a sketch of the cross section of the wheel geometry that was sectioned. The moire gratings (300 l/mm) were put on the 0 degree and 90 degree portions of the ring corresponding to section 2 of the wheel. Figures 35, 36, and 37 show the moire patterns after the cutting occurred on the wheel. Figure 35 shows the hoop and radial patterns for the 0 degree cut. Figure 36 shows the hoop and radial displacement patterns for the 90 degree cut. Figure 37 shows the shear displacement fields for both the 0 and 90 degree cuts. In all figures each fringe is a line of constant in-plane displacement; the displacement increment between fringes is

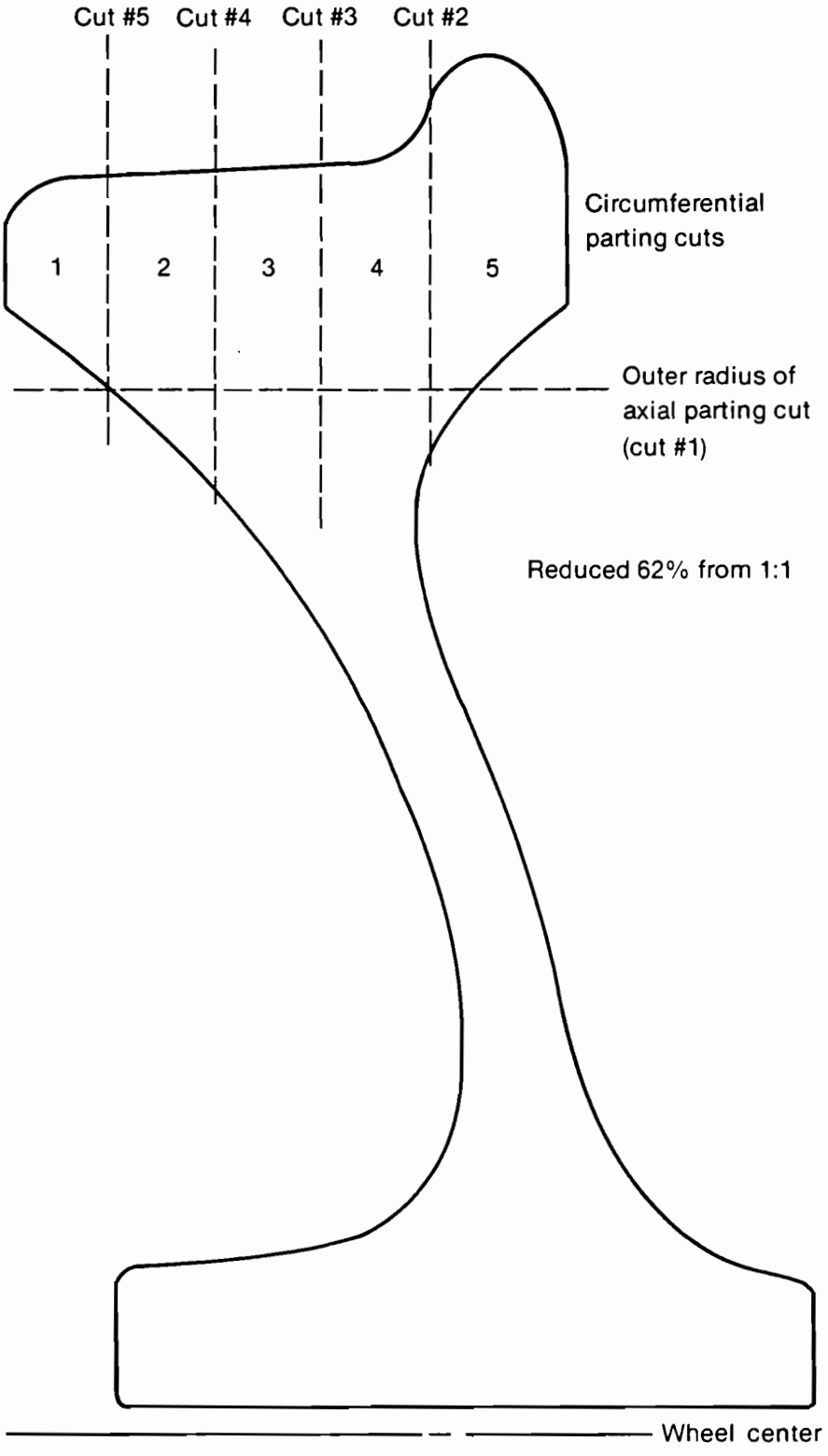


Figure 34. Railroad wheel slicing plan.

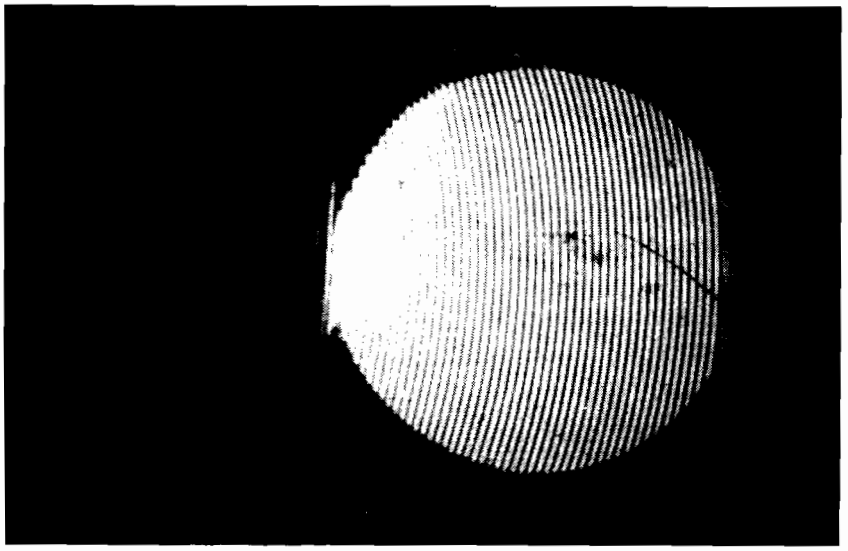

Hoop in-plane displacement field field (f = 300 ℓ/mm) Mag = 10.4/7.0

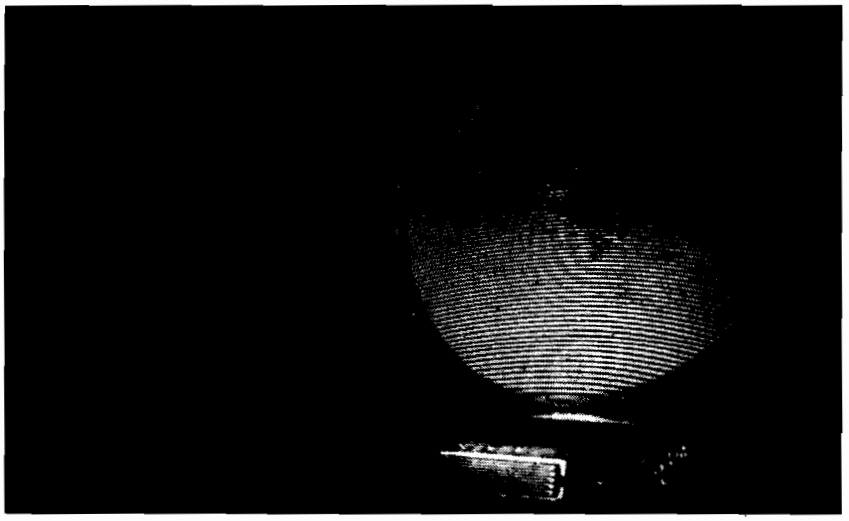

Radial in-plane residual displacement field (f = 300 ℓ/mm)
M = 4.5/3.5

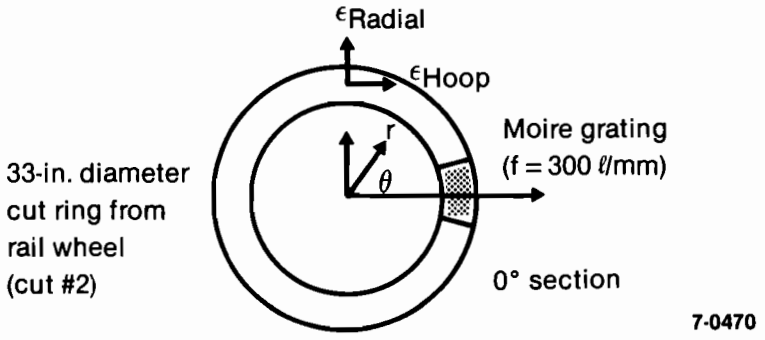


Figure 35. Elastic residual displacement field, 0° section.

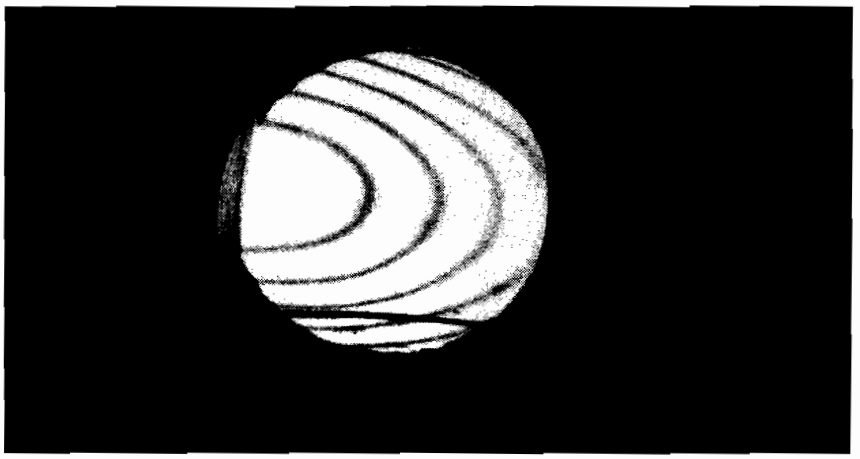

Hoop in-plane residual displacement field (f = 300 ℓ/mm) Mag = 7/6.3

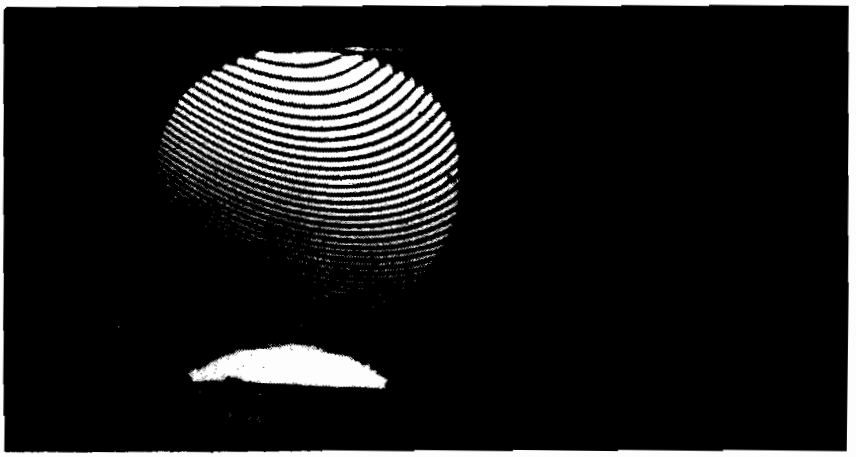

Radial in-plane residual displacement field (f = 300 ℓ/mm)
Mag = 7.5/6.3

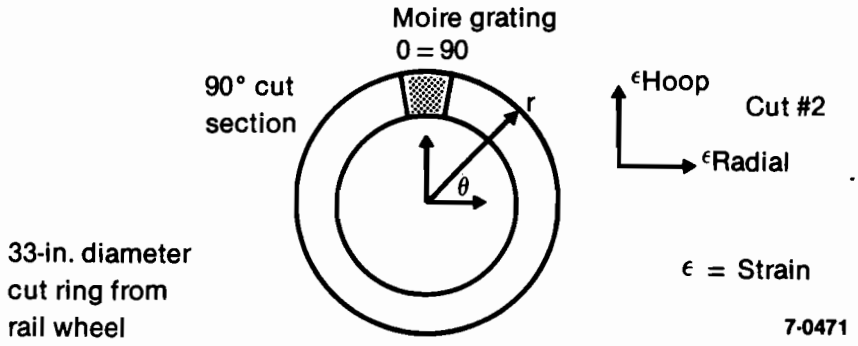


Figure 36. Elastic residual displacement field, 90° section.

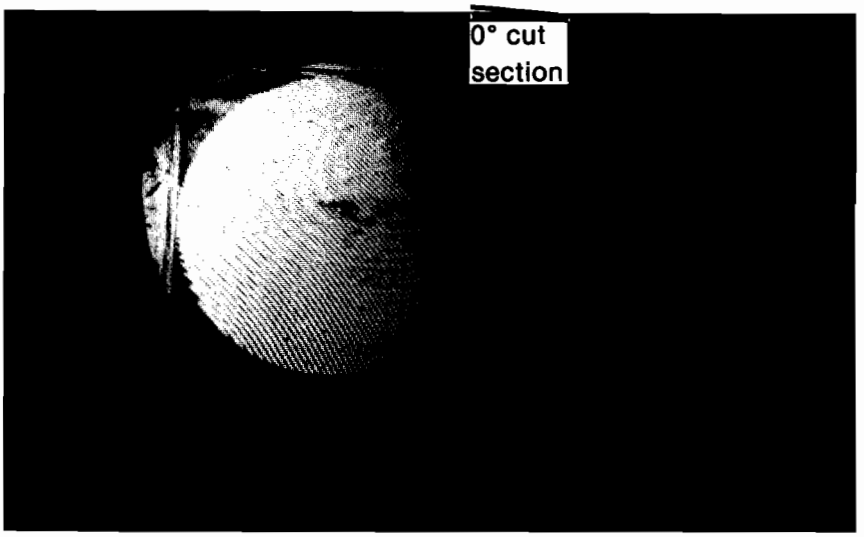


Shear (r-$\theta$) in-plane displacement field (f = 300 $\ell$/mm) Mag = 7.4//7.0

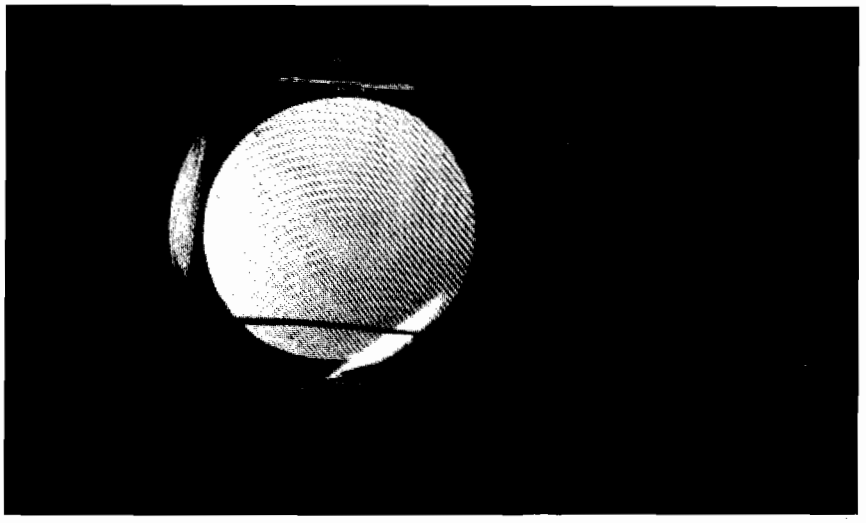

90° cut section in-plane shear (r-$\theta$) displacement field (f = 300 $\ell$/mm) Mag = 6.5/6.3

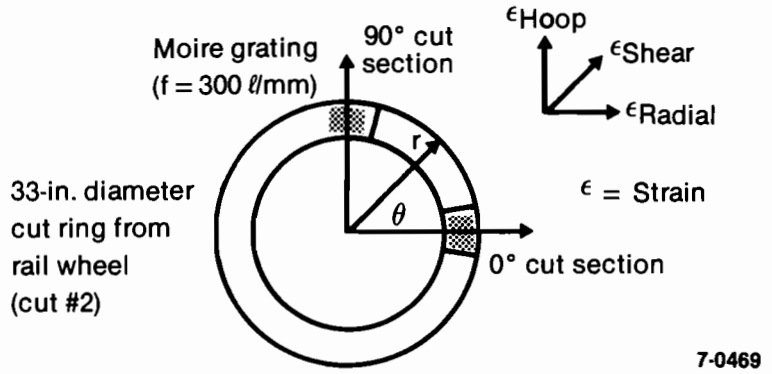


Figure 37. Elastic residual displacement field, shear displacement.

33 mm. Strain is determined by differencing each fringe over its relative gage length. A zero or null pattern exists before the actual wheel residual displacement occurs due to imperfection in the moire diffraction gratings and moire interferometry system optics. Typically this pattern is subtracted out from the final deformed pattern. For the 0 and 90 degree sections, subtracting the null pattern from the deformed hoop displacement patterns produced averaged preliminary strain results of 1700 and 2200 microstrain respectively. The average strain results from measuring the closure of the ring after sawing was 1900 to 2000 microstrain.

Current speculation regarding the 0 and 90 degree radial deformation patterns is that there is less that 50 microstrain in these directions since first-cut measurements of the radial null patterns for these cases are approximately the same as the deformed patterns. More accurate measurements of the radial strain were not obtained as it was not possible to subtract out the radial null pattern from the deformed radial displacement patterns. (The same problem was encountered for the shear strain.) This is accomplished routinely under conditions of laboratory experiments but requires more control for field conditions.

Of the three displacement components for the 0 and 90 degree sectioned pieces, only the hoop strain may be determined accurately at this time. The average hoop strain for the 0 and 90 degree pieces appears to be close to the value obtained from the closure of the ring after the saw cut which initially separated the ring. Further work must be performed in accurately identifying the null displacement patterns for the radial and shear strains in the 0 and 90 degree rings.

# 5. CONCLUSIONS

The conclusions are presented according to the major tasks.

## 5.1 NDE/Fracture Correlation Study

This study was conducted using sixty-eight flat plate specimens fabricated from ASTM A515 Grade 70 and using a steel plate sample obtained from a railroad tank car after it has been involved in an accident. The conclusions are provided for each of these two studies.

### 5.1.1 FRA/BRL Plates

NDE. UT techniques were successfully used to measure the wall thickness [to an accuracy of 0.13 mm (0.005 in.)] and to detect and characterize cracks. These measurements were made on materials that had been cleaned by glass-bead blasting to remove scale and rust. In addition, there was no insulation on these materials.

Mechanical Properties. Tensile test results showed the changes in $s_{ys}$ and $s_{ut}$ as a function of prior deformation. Changes in tensile properties become saturated after 12% prestrain. These data may be used for predicting changes in tensile properties of a material in a damaged railroad tank car. These data were augmented by using shear punch tests which provided verification of data trends but were also shown to be of questionable use for quantitative comparisons.

An analysis of the safety of moving a damaged railroad tank car should assume the material is operating on the lower shelf of the ductile-to-brittle transition curve. A method exists for developing procurement specifications that could reduce the possibility of tank cars failing during an accident or while moving a damaged tank car.

### 5.1.2 FRA/NBS Deformed Tank Car Material

NDE. The ultrasonic thickness gauge was successful in measuring the thickness of the NBS plate. It was not necessary to clean the surface of the NBS plate since it had experienced very little corrosion.

Mechanical Properties. The shear punch tests showed an increase in yield strength but little change in the ultimate tensile strength as a function of the percent reduction in thickness.

A review of the failure analyses[6-17] for actual tank cars identified one feature of significance: a majority of the failures occurred by brittle fracture. This suggests the following significant conclusions:

1. Estimates of structural integrity should be based on the fracture toughness associated with the lower shelf.

2. The use of a specification based on appropriate fracture mechanics criteria should have a significantly reduce catastrophic failures of damaged railroad tank cars.

3. Knowledge of strain rate, temperature, and applied stresses associated with accident conditions should be used to identify the criteria for procurement of materials and fabrication to ensure a structure with greater resistance to impact loading.

## 5.2 Stress Analysis Methodology

The following conclusions with respect to computer capabilities were made from this study.

1. There are six codes available which offer a high probability of solving the tank car problem. They are ABAQUS, ANSYS, ADINA, MARC, NISA, and WECAN.

2. The 1978 version of ADINA did not accurately solve a problem with cylindrical geometry and a uniform loading. One of the six codes listed above (including the current version of ADINA) should be considered for the analysis.

3. A pinched cylinder problem was solved using ABAQUS but the results were not compared to results from any other type of solution. The ABAQUS solution shows that the code can perform this type of analysis.

4. Further testing of the codes is required in order to select the best code. It is also necessary to verify that the code is producing correct results.

Further, it was concluded that the methodology presented in this report can result in a catalog of solutions which, in turn, can allow the safe transport of the damaged tank cars.

### 5.3 Hydrostatic Burst Tests of Damaged 1/5 Scale Railroad Tank Cars

The type of damage on the thin wall tanks did not simulate the type of damage that would be expected on the thicker walls of an actual damaged tank car as identified below:

1. The extent of surface cracks and wall thinning on the cars was much less than that expected of the thicker material of an actual car.

2. When pressurized, the thinner walls behaved differently than an actual thicker wall would. The scale model walls acted like a membrane, there was no appreciable bending stress because of the thin wall, which is not representative of an actual railroad tank car.

3. The test illustrated the effectiveness of using acoustic emission techniques to detect and locate the origin of cracking before catastrophic failure occurs.

## 5.4 Application of Moire Interferometry

Preliminary tests showed that moire interferometry could be used successfully to determine the residual stresses of railcar components such as wheels. This technique provides full-field, in-plane displacement measurements at the free surface which provide considerable advantage over more traditional techniques such as strain gages.

# 6. RECOMMENDATIONS

It was previously noted that the ability to predict the safety of moving a damaged railroad car required input from the following:

1. NDE to detect and size cracks, quantify damage (measure wall thickness and magnitude of dent), and provide information as to if and where subcritical crack growth is occurring in the structure.

2. Applied stresses.

3. Fracture mechanics based technology to predict failure conditions.

Each of these inputs is complicated and they are interdependent. Therefore a program plan, see Table 1, has been developed showing a chronological sequence of events that enhances the interaction between these three areas and should provide useful models in the shortest time period. Explicit recommendations are provided as follows for each of the four tasks presented in this report.

## 6.1 NDE/Fracture Correlation Study

### 6.1.1 Nondestructive Examination

Conduct preliminary evaluations of abilities of existing UT techniques to measure thickness and detect and characterize defects in actual damaged tank cars that do not have insulation attached and in plates with insulation attached. These tests would include the development of an approach for estimating the depth of cracks.

### 6.1.2 Mechanical Properties

A two-phase approach is recommended. The first phase is to identify the involvement of cleavage and/or low tearing modulus in developing brittle fracture. Test results from damaged BRL plates showed that the fracture toughness and the tearing modulus were reduced as the amount of deformation

increased. This suggests that predictions of the consequences of moving a damaged railroad tank car may be performed using the fracture toughness associated with the lower shelf.

The second phase will then identify criteria that may be used to formulate specifications for procurement of materials with increased resistance to failure. Because of consequences of railroad tank car failures, both during an accident and during the cleanup operation, it is recommended that estimates of the strain rate, temperatures, and stress levels associated with "typical" accidents and with moving a damaged car be determined. These data could provide the basis for establishing accept/reject criteria for material procurement and tank car fabrication. These criteria could reduce failures that occur during an accident as well as failures that occur when damaged railroad tank cars are moved.

## 6.2 Stress Analysis Methodology

One of the six codes identified in the report is recommended for stress analysis. Further testing of the codes is required in order to select the best code. Once a code is chosen it is necessary to verify that it is producing correct results. The verification may be done by comparing results against those obtained from other codes, experiments, or analytical solutions. ABAQUS is probably the best code to perform the tank car analysis because it has the most modern solution techniques and also has a high strain (10 percent) capability.

## 6.3 Hydrostatic Burst Tests of Damaged Railroad Tank Cars

For future tests, if scaled versions of tank cars are used, it is recommended that the wall thickness not be reduced. This change in thickness relative to tank geometry can be treated by analytical methods. Also, more areas of the tanks should be instrumented, including the use of additional strain gauges and acoustic emission detectors. Additional information that would be useful in performing future burst tests includes a complete design description, fabrication history, and deformation procedures along with the supporting test results.

## 6.4 Application of Moire Interferometry

It is recommended that:

1. More tests be conducted in a controlled environment. The previous tests were conducted in an uncontrolled shop/industry environment. As a result, much of the limited time was spent developing technique for the industry environment rather than understanding the type of data produced.

2. Controlled specimens be developed with known strain and deformations to exactly calibrate the moire interferometry results. Not only was time expended on developing a technique never taken to a industry environment, but the data were on a complicated residual stress state rather than a simple stress state that would help identify any problems encountered in interpreting the moire interferometry data.

If the moire interferometry is developed to the stage necessary for accurate residual stress state determination, a substantial advance could be made in understanding the problem of residual stresses. Instead of discrete point-by-point strain gage measurements that average spatially over a region where high stress gradients can occur, moire interferometry, with its full field nature, provides continuous, quantitative maps of deformation over the entire region of interest.

## 7. REFERENCES


1. L. S. Beller, J. D. Mudlin, W. G. Reuter, and M. A. Tupper, "Survey of Nondestructive Methods for Evaluating Tank Cars," INEL, September, 1983.

2. United States Government Printing Office, Hazardous Materials Regulations of the Department of Transportation, Tariff No. BOF-6000-B, Subpart C, December 22, 1981, pp. 512-514.

3. 1981 Annual Book of ASTM Standards, Part 4.

4. G. E. Lucas, J. W. Sheckherd, G. R. Odette, and S. Panchanadeesaran, J. Nuc. Mat. 122 & 123, 49-34 (1984).

5. W. P. Wright, Report FRA/ORD-84-04, May 1984.

6. J. R. Hawthorne, B. H. Menke, F. J. Loss, H. E. Watson, A. L. Hiser, and R. A. Gray, EPRI NP-2782, 1982.

7. G. E. Hicho and C. H. Brady, "Hazardous Materials Tank Cars - Evaluation of Tank Car Shell Construction Material, (Report No. 1), NBS Report 312.01/14, September 28, 1970.

8. C. G. Interrante and G. E. Hicho, "Metallurgical Analysis of a Steel Shell Plate Taken From a Tank Car Accident Near South Byron, New York, (Report No. 2), NBS Report 312.01/35, October 22, 1971.

9. C. G. Interrante, G. E. Hicho, and D. E. Harne, "A Metallurgical Analysis of Five Steel Plates Taken from a Tank Car Accident Near Crescent City, Illinois," (Report No. 3), NBS Report 312.01/39, March 10, 1972.

10. C. G. Interrante, G. E. Hicho and D. E. Harne, "A Metallurgical Analysis of Eleven Steel Plates Taken from a Tank Car Accident Near Callao, Missouri," (Report No. 4), NBS Report 312.01/51, September 19, 1972.

11. C. G. Interrante, J. G. Early, and G. E. Hicho, "Analysis of Findings of Four Tank-Car Accident Reports," (Report No. 5) Nat. Bur. of Stand. NBSIR 75-655, NTIS PB 251097/AS, FRA OR&D 75-50, January 1975.

12. C. G. Interrante, "Impact Properties of Steels Taken from Four Failed Tank Cars," (Report No. 6), Nat. Bur. Stand. NBSIR 75-656, NTIS BP 255854, FRA OR&D 75-51, January 1975.

13. J. G. Early and C. G. Interrante, "A Metallurgical Investigation of a Full-Scale Insulated Rail Tank Filled with LPG Subjected to a Fire Environment, (Report No. 7), Nat. Bur. of Stand, NBSIR 75-657, January 1975.

14. J. G. Early, "Ambient and Elevated Temperature Mechanical Properties of AAR MI28-69-B Steel Plate Samples Taken from Fire Tested Insulated Tank Car RAX 202, (Report No. 8), Nat. Bur. of Stand, NBSIR-75-725, May 1975.

15. J. G. Early, "A Metallurgical Analysis of an ASTM A212-B Steel Tank-Car Head Plate, (Report No. 9), Nat. Bur. Stand., NBSIR 78-1582, NTIS PB 81/20598, FRA OR&D 81/32, Sept. 1978.

16. J. G. Early and C. G. Interrante, "A Metallurgical Evaluation of Two AAR M128 Steel Tank Car Head Plates Used in Switchyard Impact Tests, (Report No. 10), Nat. Bur. of Stand, NBSIR 80-2039, May 1980.

17. C. G. Interrante, S. R. Low, and J. G. Early, "Observations of the April 8, 1979 Railroad Accident at Crestview, Florida," (Report No. 11), Nat. Bur. of Stand, NBSIR-84-2858, April 1984.

18. C. G. Interrante, S. R. Low, C. H. Brady, and G. E. Hicho, "Metallurgical Observations of 21 Plate Steel Samples Taken from Seven Tank Cars Involved in the April 18, 1979 Railroad Accident at Crestview, Florida," (Report No. 12), Nat. Bur. of Stand., NBSIR 84-2981, November 1984.

19. Billy Fredrikson and Jaroslav Mackerle, Structural Mechanics Finite Element Computer Programs, 1970-1983, 4th Edition, AEC, Advanced Engineering Corporation, Linkoping, Sweden, July 1983.

20. K. J. Bathe, ADINA-A Finite Element Program for Automatic Dynamic Incremental Nonlinear Analysis, Acoustics and Vibration Laboratory, Massachusetts Institute of Technology, Report 82448-1, September 1975, revised 1978, Cambridge, Massachusetts.

21. S. Levy, Bending of Rectangular Plates with Large Deflection, NACA Report 737, Washington, D.C., 1942.

22. Henry Fong, "An Evaluation of Eight U.S. General Purpose Finite Element Computer Programs," Paper No. 82-0699-CP presented at the 23rd AIAA/ASME/ASCE/AHS Structures, Structural Dynamics and Materials Conference, May 10-12, 1982, New Orleans.

23. ADINA--A Finite Element Program for Automatic Dynamic Incremental Nonlinear Analysis, User's Manual, Report No. AE 84-1, ADINA Engineering Inc., Watertown, MA, December 1984.

24. F. M. Haggag, et al., The Use of Miniaturized Tests to Predict Flow Properties and Estimate Fracture Toughness in Deformed Steel Plates, EG&G Report to be published.

# APPENDIX A
# LIQUID PENETRANT EXAMINATION PROCEDURE

## General Description

The Magnaflux Dual Purpose Penetrant Test System was used. This is a specialty penetrant system which combines the flaw detection capabilities of both the color contrast and fluorescent penetrant systems. This system gave the best resolution out of several penetrant systems tested.

## Materials

A. SKC-NF/ZC-7B Cleaner/Remover - Intended for use with all Magnaflux test methods and materials.

B. DP-P1 Dual Purpose Penetrant

C. DP-D1 Dual Purpose Developer

## Pre-examination

A. Plates were lightly glass-bead blasted to remove the corrosion layer from the areas of examination.

B. Area of examination was thoroughly cleaned with SKC-NF/ZC-7B Cleaner/Remover.

C. Excess cleaner was removed with clean, dry cloth and plate surfaces were allowed to dry for five minutes before applying penetrant.

## Penetrant Application

A. DP-P1 penetrant was applied by brushing over the examination surface, including 1/2 inch outside of the area of interest.

B. Penetrant was allowed to dwell and was kept completely wetted for 10 minutes.

Penetrant Removal

A. Excess penetrant was removed with clean dry cloths.

B. Adhering penetrant was then removed with a cloth dampened with water, then wiped with dry cloths. Remaining penetrant was then removed with a cloth dampened with SKC-NF/ZC-7B.

C. Drying time was 10 minutes.

Developer Application

After agitating, DP-D1 developer was sprayed on in a thin uniform coat.

Interpretation

A. White light was used.

B. Interpretation was made 20 minutes after the developer was applied.

Post Examination Cleaning

A. Penetrant materials were removed with cloths soaked with water.

B. Examination area was then flushed with SKC-NF/ZC-7B and wiped with dry cloths.

# APPENDIX B

## STRAIN VS. PRESSURE PLOTS FOR TANKS #401A AND #410A

The damaged end of each tank was instrumented with strain gauges. The strain gauges consisted of one three channel rosette strain gauge located on the undamaged area of the dented end and three high-elongation (20%), three channel rosette strain gauges located in the area of the dent. See Figure 27 for a sketch showing the locations of the strain gauges. The strain gauge data show the "oil-canning" effect that occurred during pressurization on the damaged zone of the tanks. The data indicated the displacement of the material in different locations in the area of the dent during the burst test. The figures in this Appendix show the displacement of the material at the locations of the strain gauges (Figure 27) on tanks #401A and #410A.

The strain gauges were located in or adjacent to the damaged region in the dome, (see Figure 27) since this is where failure was expected if the 1/5 scale tanks represented the conditions of an actual tank car. Since the failures occurred in the cylindrical portion of the tank at a substantial distance from the damaged areas, it is expected that the strain gauge data will be of limited use. The results for tank #401A are summarized as follows:

- Gauges 1-3, the strain ranged from 3% to 5%.
- Gauges 5-7, the strain was initially compressive due to the damaged area being forced back to its original position at which time some tensile strain (reduction in compressive strain) occurred.
- Gauges 8-10, substantial peak strains on the order of 40%-50% occurred followed by decreasing tensile strain.
- Gauges 11-12, substantial compressive strains of nominally 65% were observed.

The peak strain of 40%-50% observed for Gauges 8-10 is considerably greater than the average value associated with failure in the cylindrical section. At this time it is not possible to explain why Gauges 8-10 showed the substantial decrease in tensile strain.

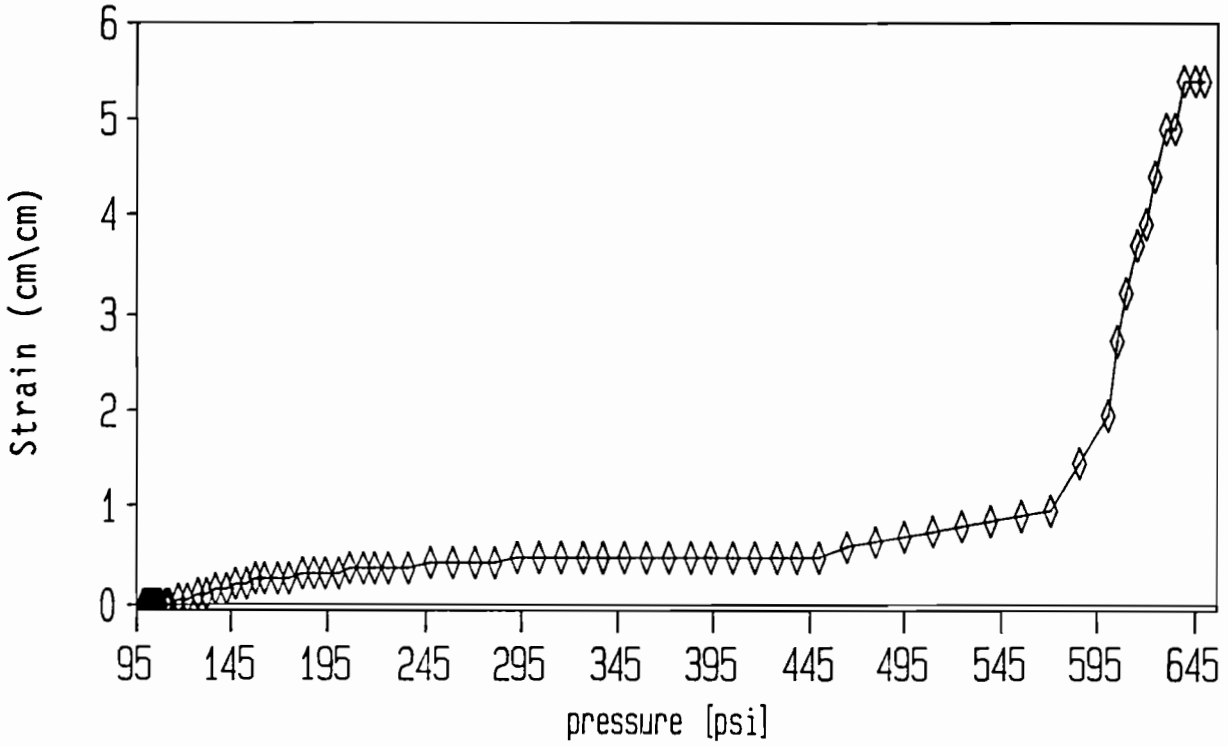


Figure B-1. Tank #401A, Strain Gauge #1.

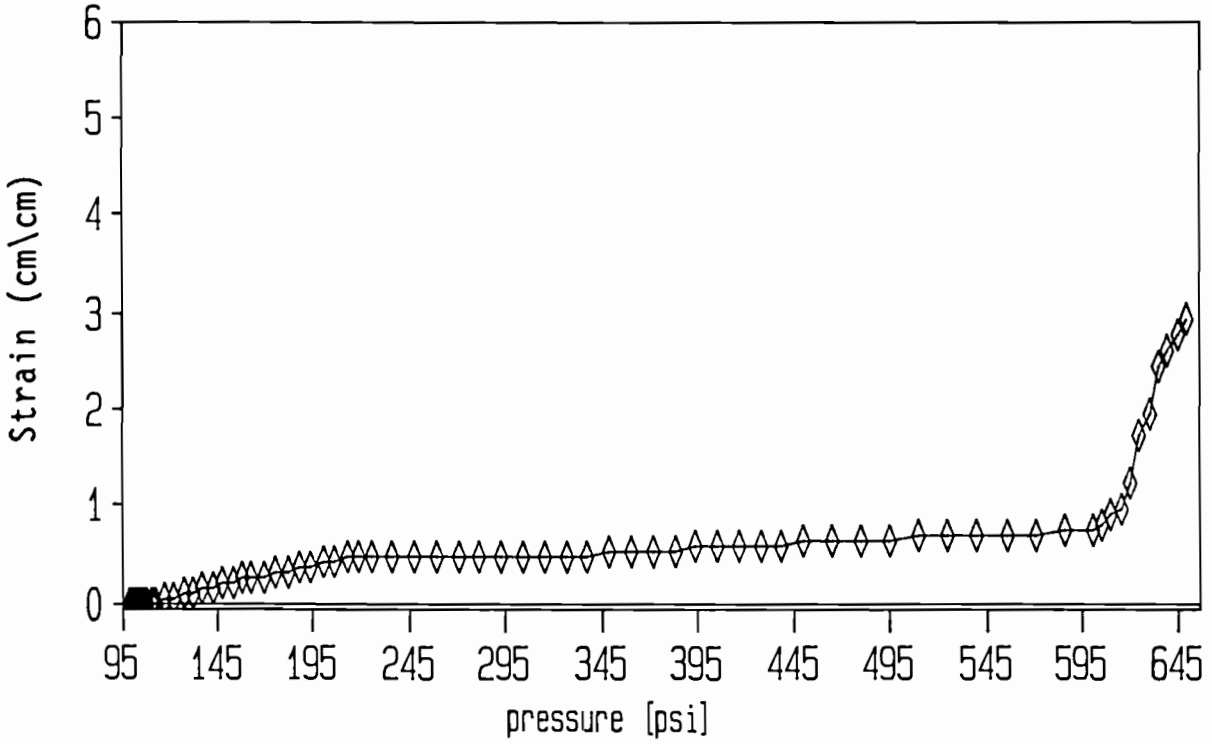


Figure B-2. Tank #401A Strain Gauge #2.

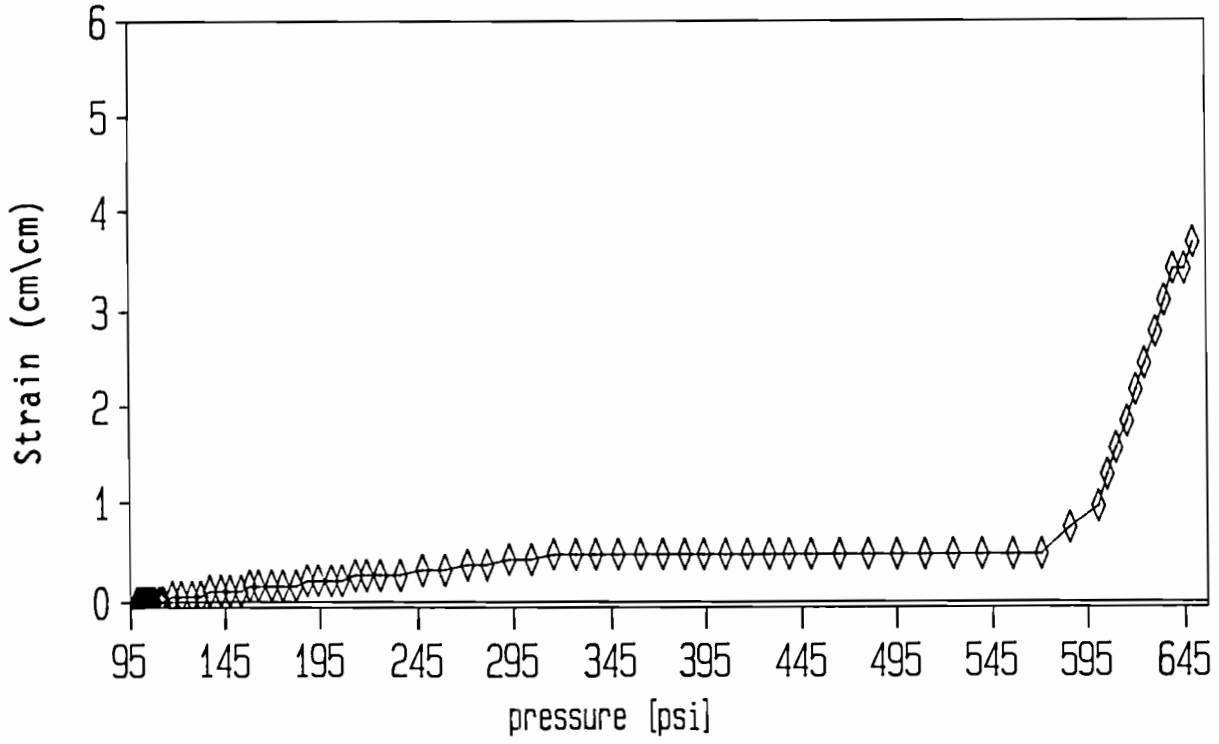


Figure B-3. Tank #401A Strain Gauge #3.

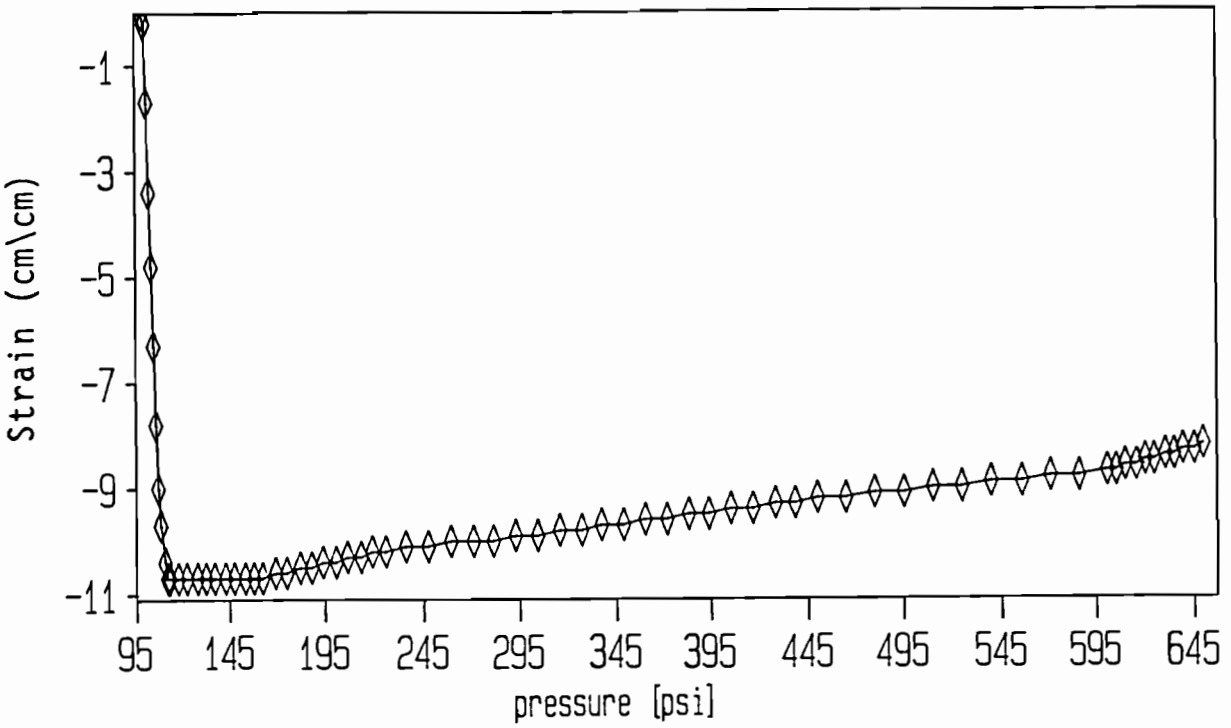


Figure B-4. Tank #401A Strain Gauge #5.

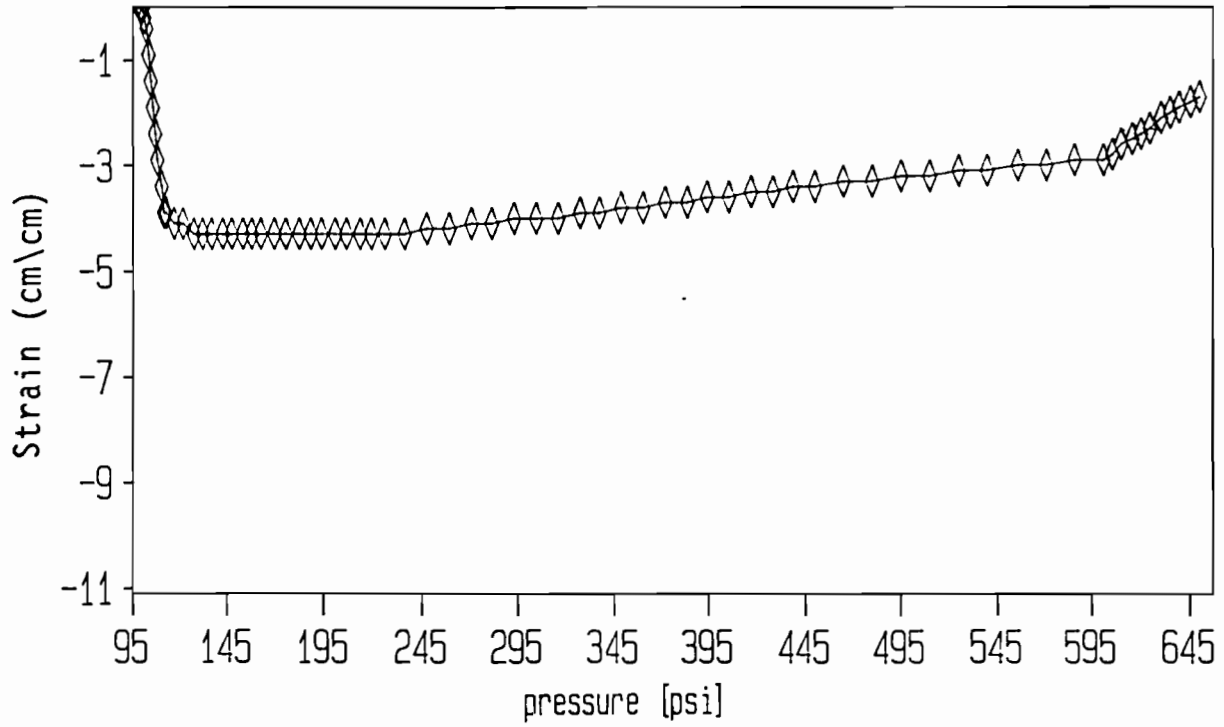


Figure B-5. Tank #401A Strain Gauge #6.

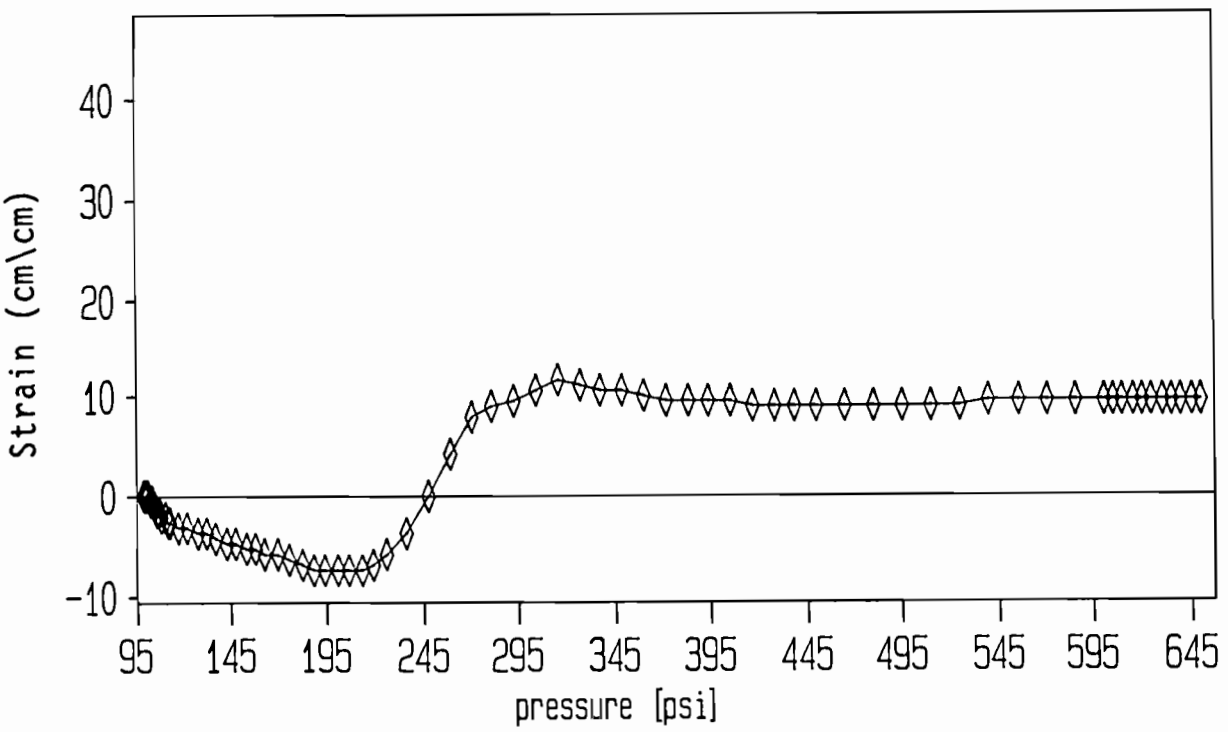


Figure B-6. Tank #401A Strain Gauge #7.

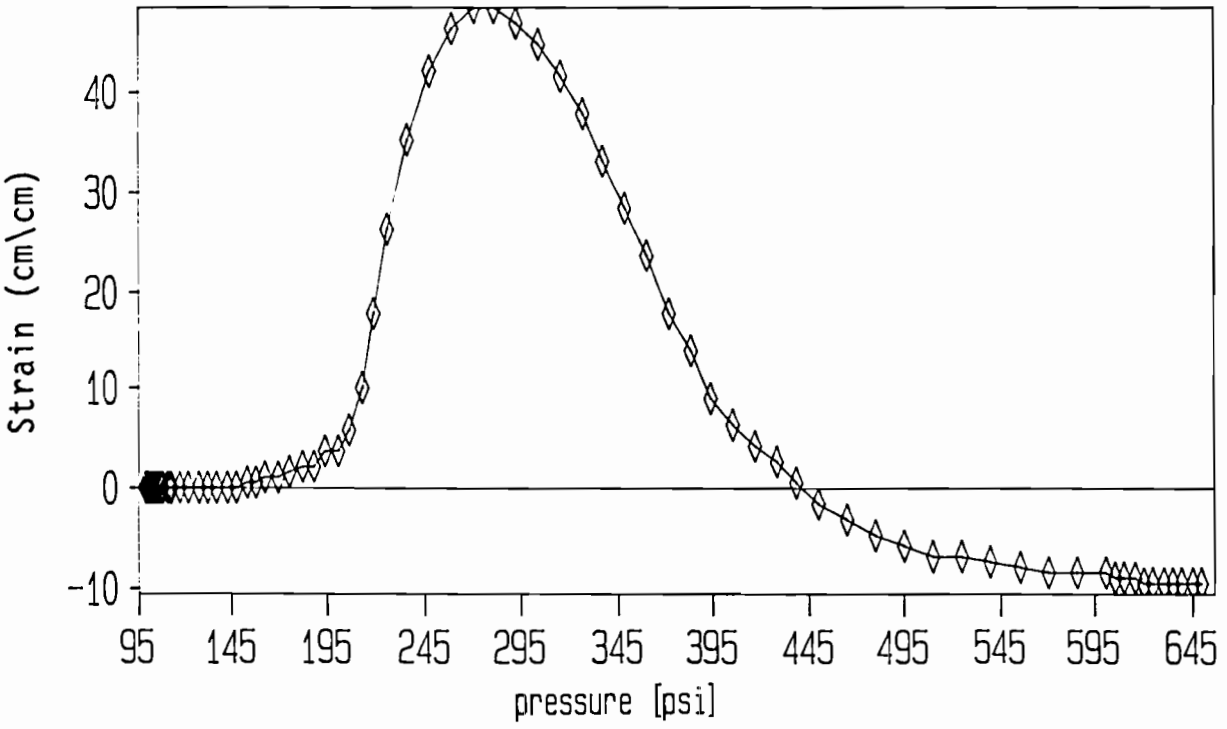


Figure B-7. Tank #401A Strain Gauge #8.

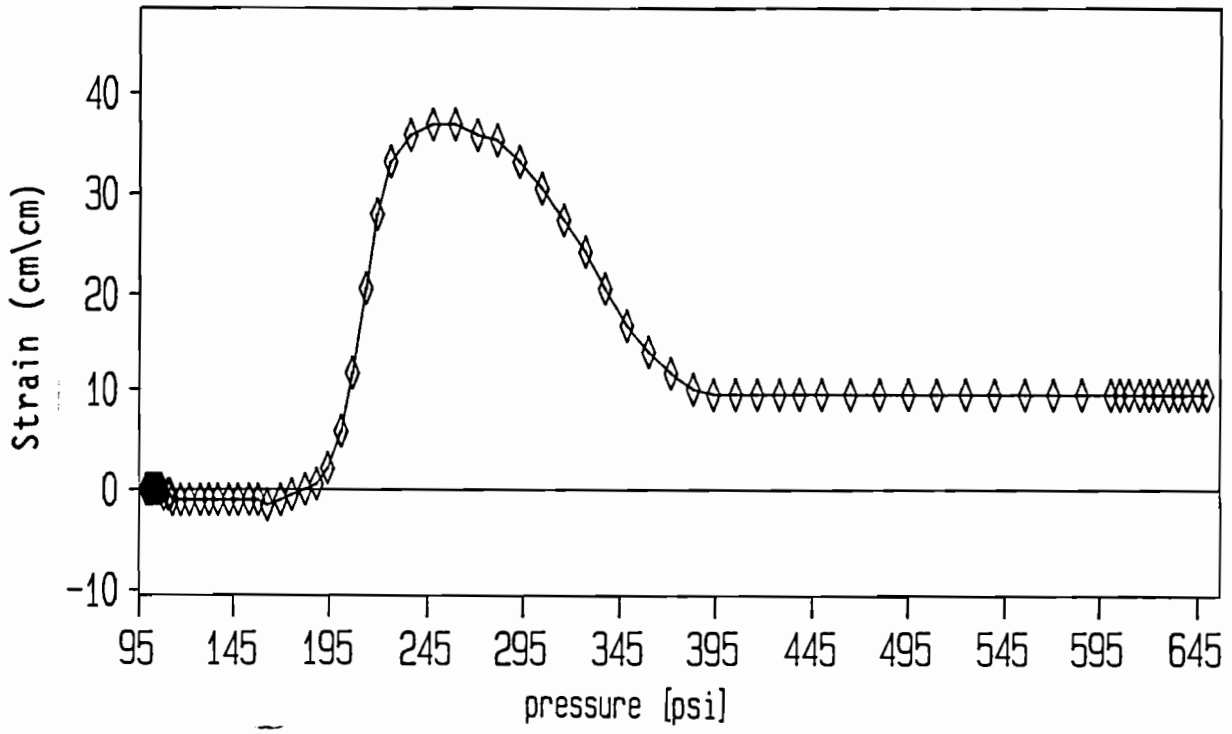


Figure B-8. Tank #401A Strain Gauge #9.

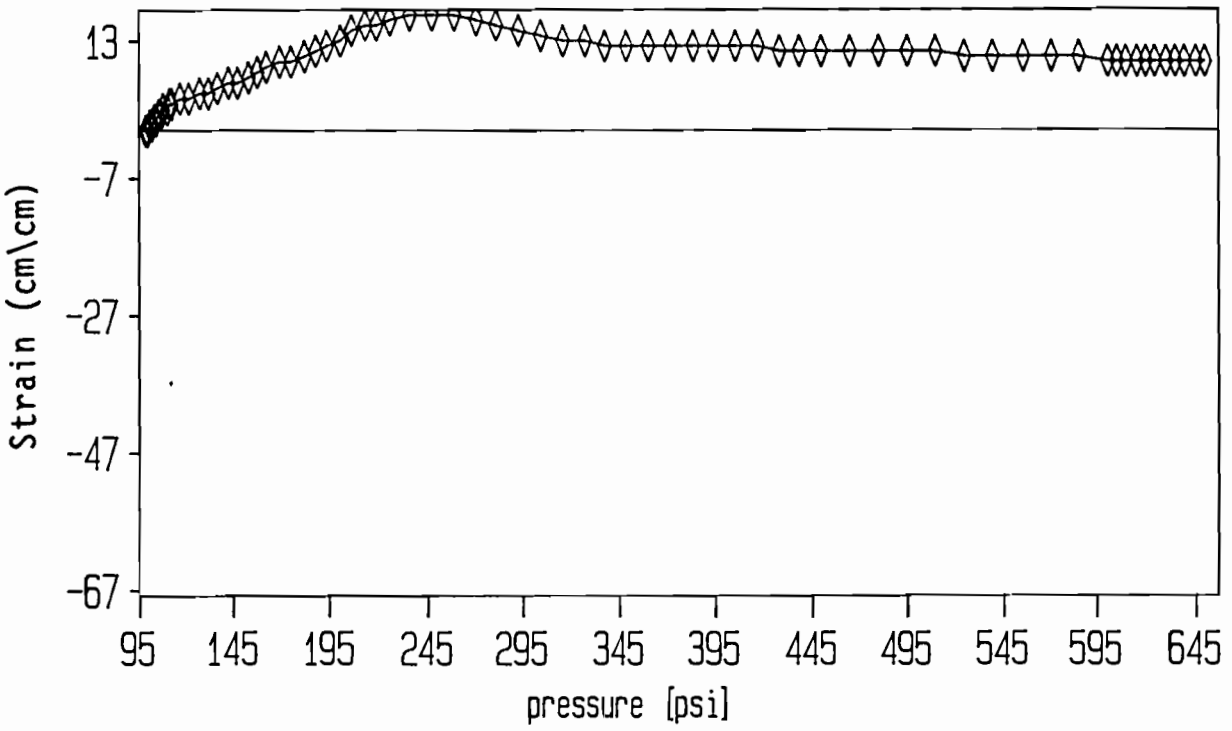


Figure B-9. Tank #401A Strain Gauge #10.

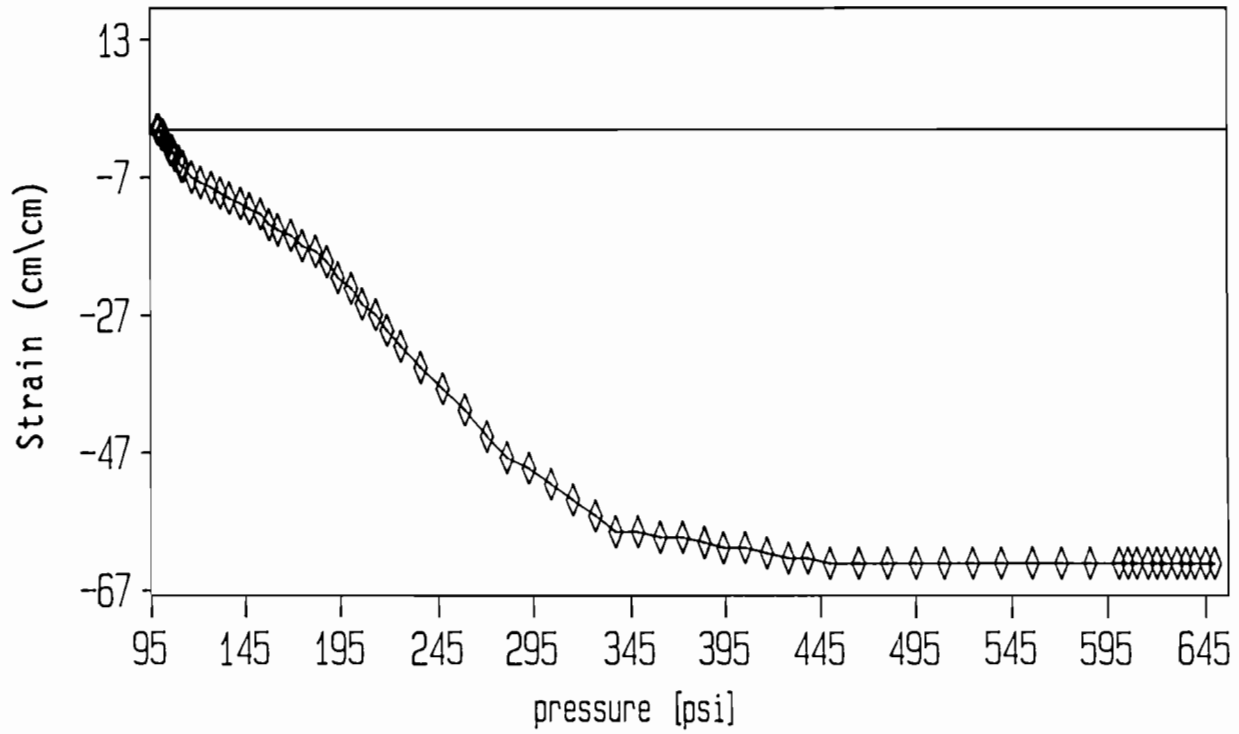


Figure B-10. Tank #401A Strain Gauge #11.

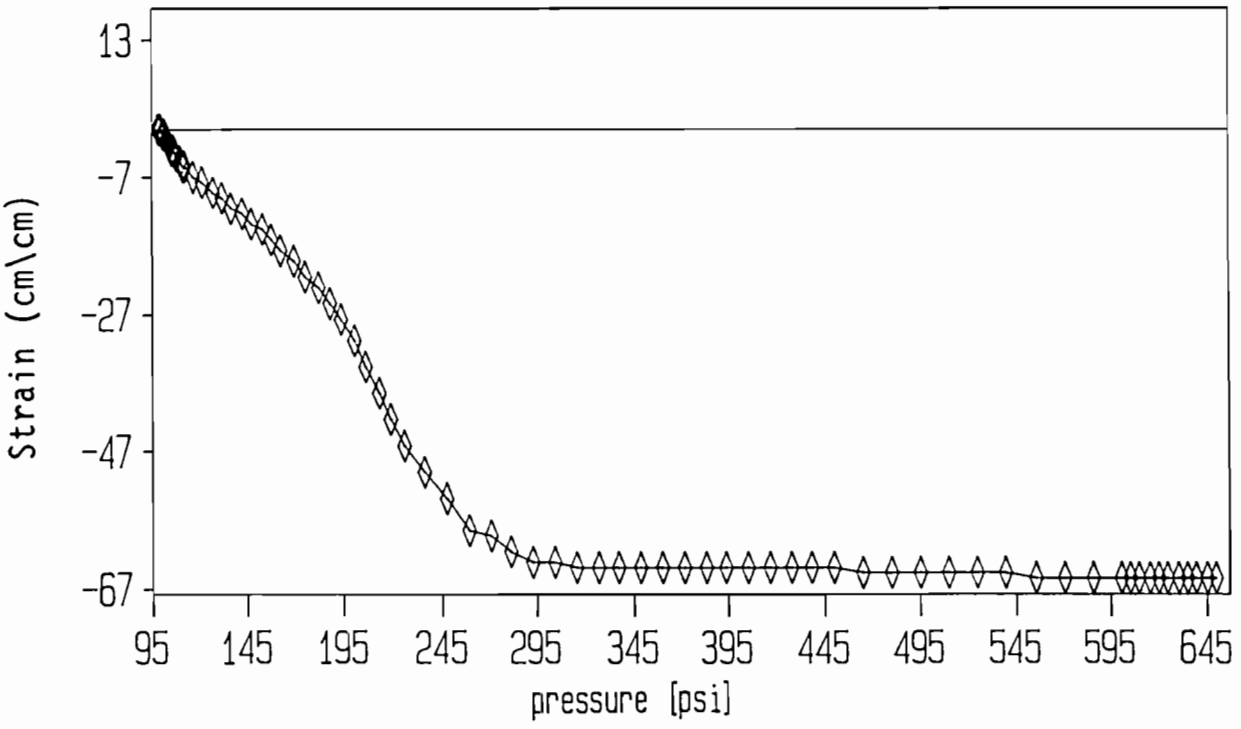


Figure B-11. Tank #401A Strain Gauge #12.

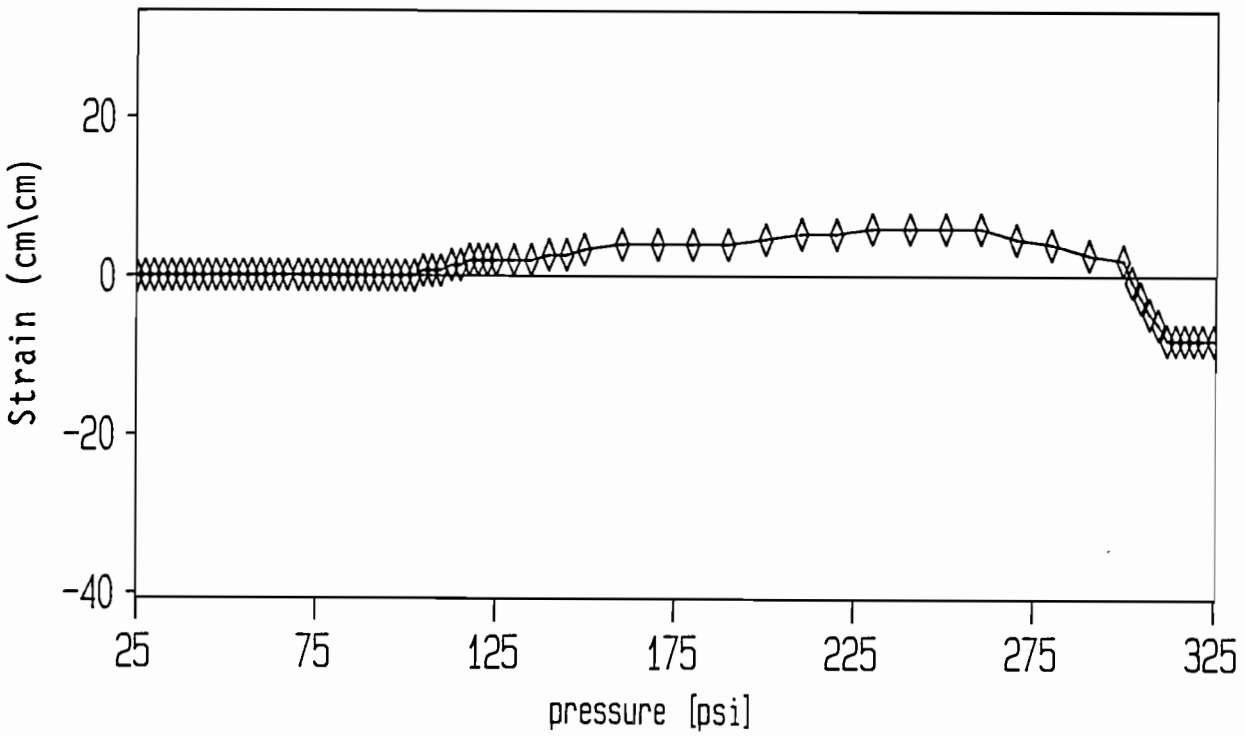


Figure B-12. Tank #410A Strain Gauge #7.

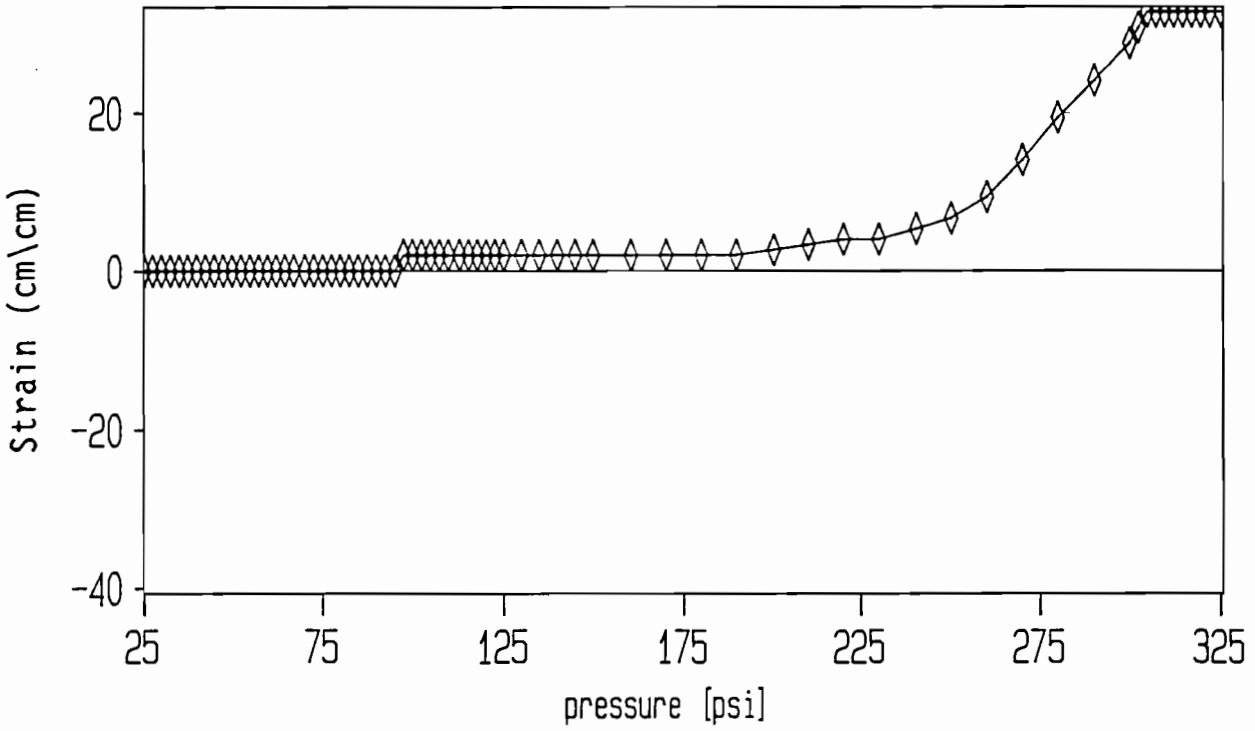


Figure B-13. Tank #410A Strain Gauge #8.

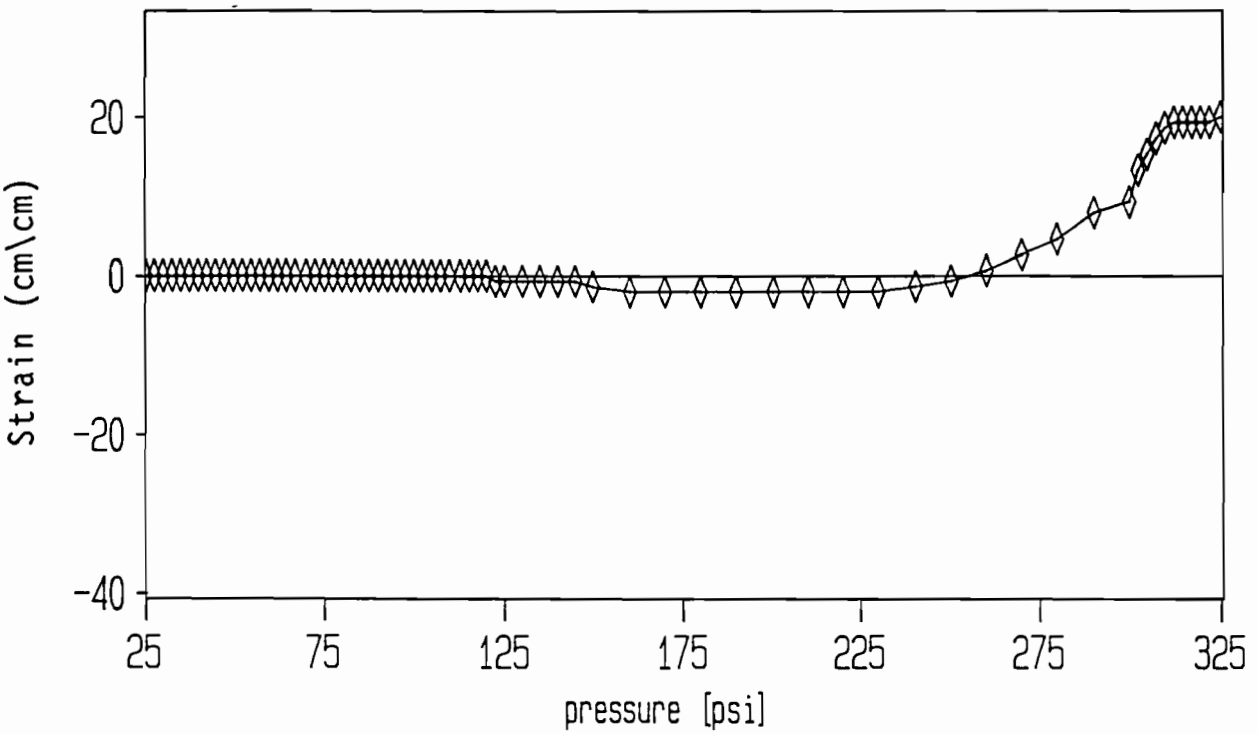


Figure B-14. Tank #410A Strain Gauge #9.

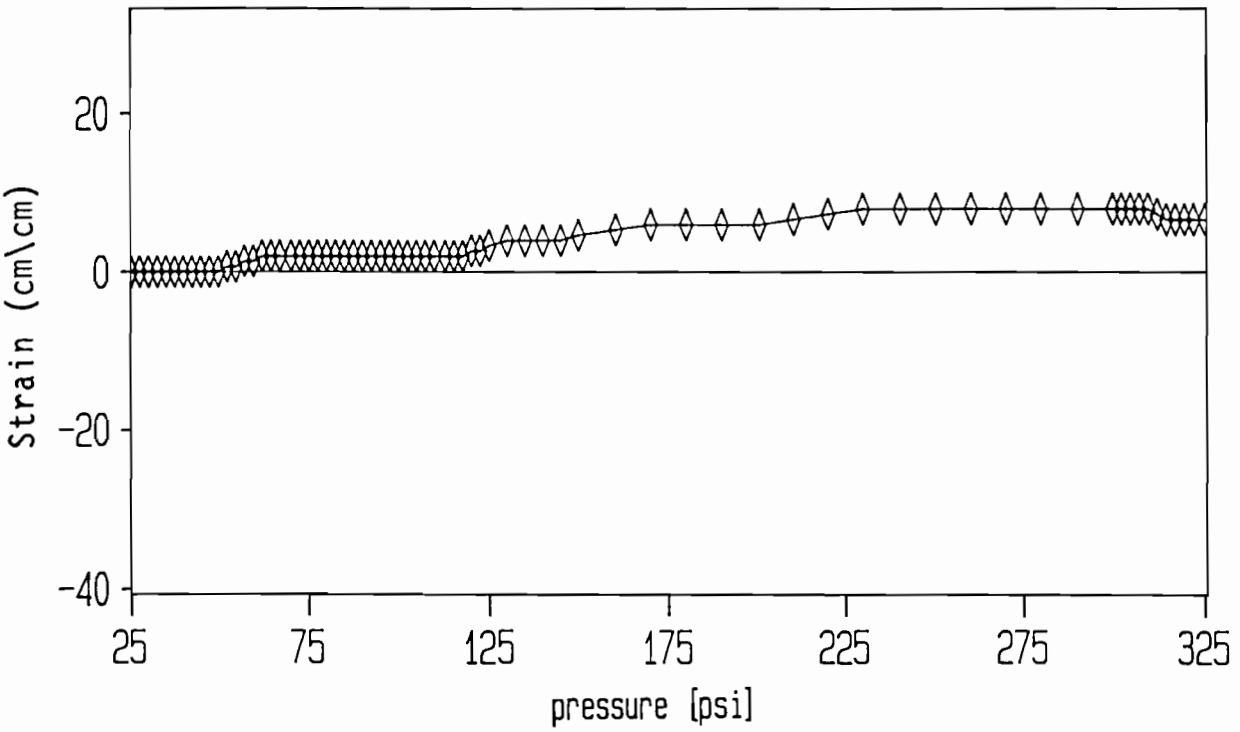


Figure B-15. Tank #410A Strain Gauge #10.

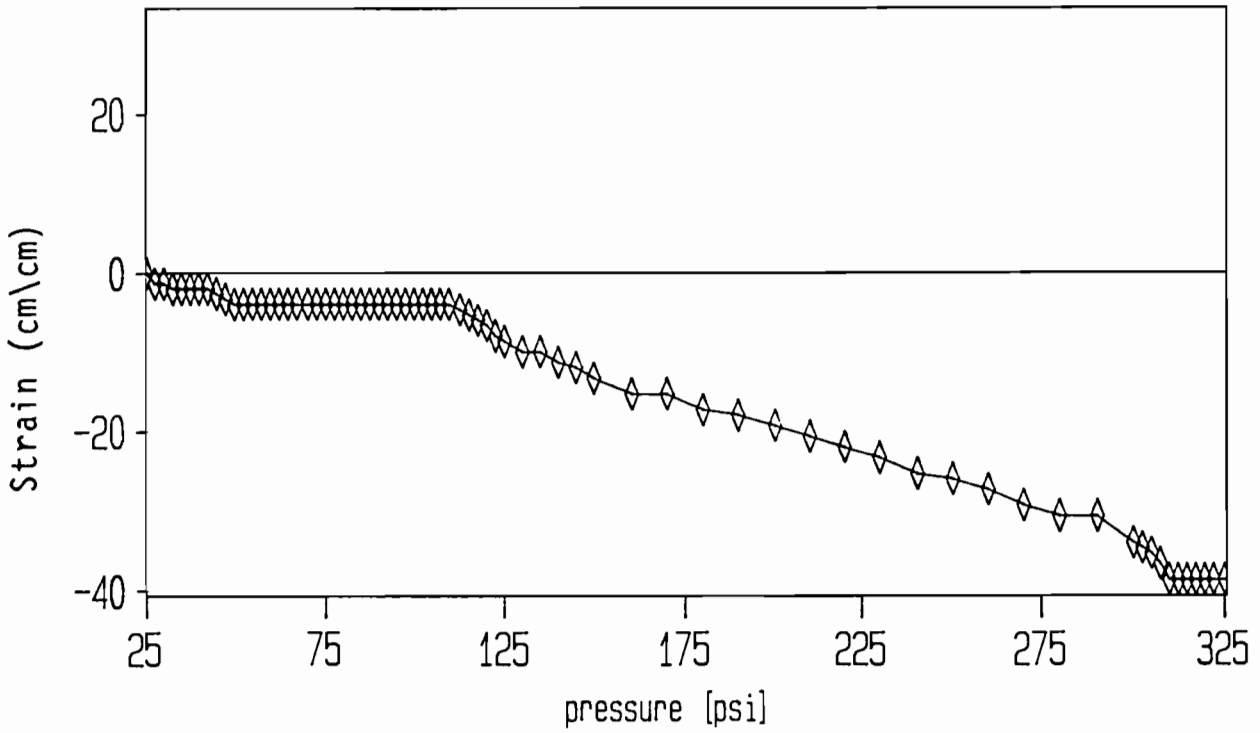


Figure B-16. Tank #410A Strain Gauge #11.

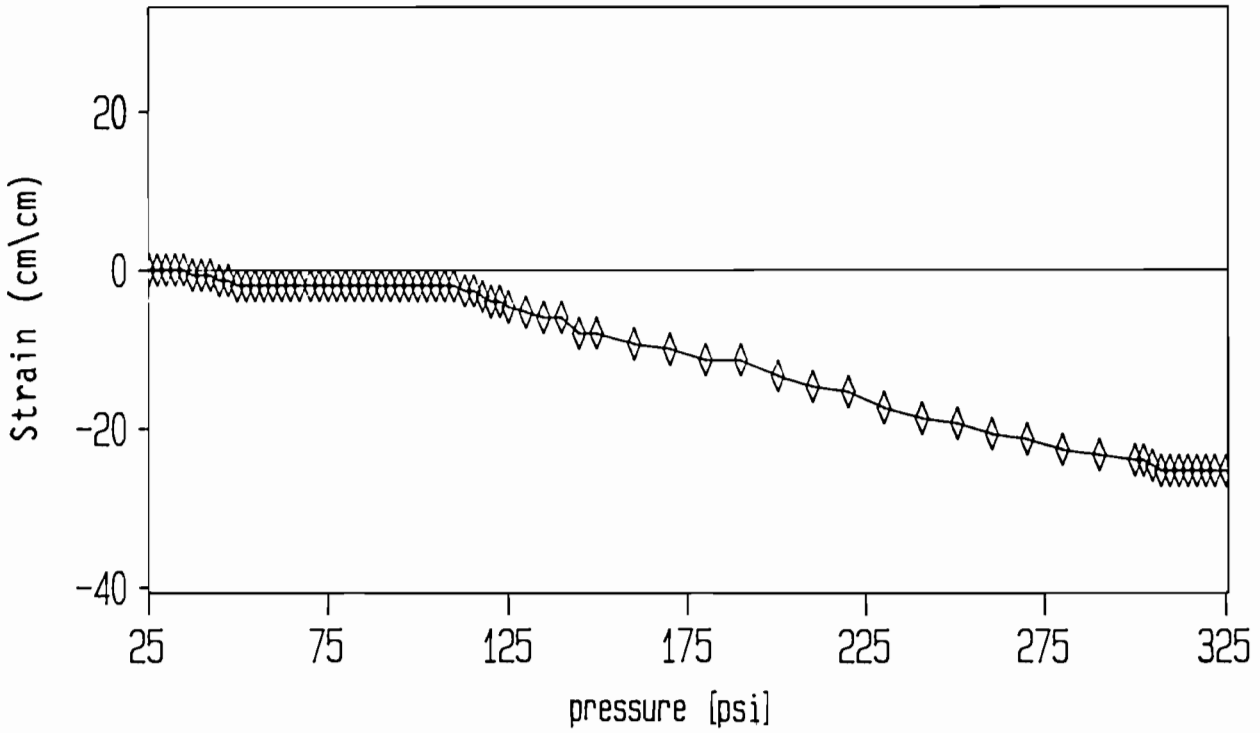


Figure B-17. Tank #410A Strain Gauge #12.